UNIVERSITY OF CALIFORNIA SAN DIEGO

Boron Chemistry in High Voltage Cathodes for Lithium-Ion Batteries

A Dissertation submitted in partial satisfaction of the requirements
for the degree Doctor of Philosophy

in

Chemical Engineering

by

Na Ri Park

Committee in charge:

Professor Ying Shirley Meng, Chair
Professor Zheng Chen
Professor Eric Fullerton
Professor Ping Liu

2024

The Dissertation of Na Ri Park is approved, and it is acceptable in quality and form for publication on microfilm and electronically.

University of California San Diego

2024

DEDICATION

All glory is given solely to God.

TABLE OF CONTENTS

LIST OF FIGURES

LIST OF TABLES

ACKNOWLEDGEMENTS

All glory be to the Lord alone.

I would like to express my heartfelt gratitude to Professor Shirley Meng for allowing me to continue my cathode career. Your honesty and forward-thinking research spirit will always inspire me. Thank you for having such a profound impact on my career. I am also deeply grateful to my committee members, Professor Eric Fullerton, Professor Zheng Chen, and Professor Ping Liu, for their unwavering support and invaluable feedback.

I would like to extend my heartfelt thanks to all my colleagues at LESC, with whom I shared both laughter and tears throughout this journey. Space here is limited; I couldn't mention everyone individually. However, what truly matters are that when each of us strives to do our best in our respective roles, I have no doubt that we will reunite in an even brighter light. I look forward to collaborating with everyone around the world to create sustainable energy future together.

I would like to express my deepest gratitude to Umicore for their unwavering support throughout this journey. Your consistent trust and encouragement have been instrumental in achieving meaningful results, and I am truly thankful for your support. I would also like to extend my gratitude to Cummins. It was a valuable opportunity to work with new cathode materials. Lastly, I would like to express my sincere gratitude to LG Chem for providing me with such a valuable opportunity, allowing me to grow further. I would especially like to thank Executive Director Dr. Youngmin Choi and Manager Dr. Dongjun Ahn once again.

I would like to take this opportunity to sincerely thank my beloved family, friends, and colleagues for their unwavering support. In particular, I am deeply grateful to my parents-in-law, who have loved me like their own daughter despite my shortcomings. I owe profound gratitude to my dad, Dr. Park, my role model and source of constant encouragement through the power of positivity. I also extend heartfelt thanks to my dear sister Du Ri, whose growth in faith. I offer my heartfelt thanks to my wonderful and loving husband, Dr. Eo, the most kind and amazing friend. I express boundless love and gratitude to my precious Sophia, more cherished than my own life. Lastly, I dedicate this doctoral thesis to my mom, who has selflessly given her all for me, without hesitation or change.

Chapter 2, in full, is a reprint of the material as it appears in "Park, N. R., Li, Y., Yao, W., Zhang, M., Han, B., Mejia, C., Sayahpour, B., Shimizu, R., Bhamwala, B., Dang, B., Kumakura, S., Li, W., & Meng, Y. S. (2023). Understanding the Role of Lithium Borate as the Surface Coating on High Voltage Single Crystal $LiNi_{0.5}Mn_{1.5}O_4$. *Advanced Functional Materials*." The dissertation author was the first author of this paper.

Chapter 3, in full, is a reprint of the material as it appears in "Park, N. R., Zhang, M., Han, B., Li, W., Qian, K., Nguyen, H., Kumakura, S., & Meng, Y. S. (2024). Understanding Boron Chemistry as the Surface Modification and Electrolyte Additive for Co-Free Lithium-Rich Layered Oxide. *Advanced Energy Materials*." The dissertation author was the first author of this paper.

VITA

2008 Bachelor of Science in Chemical Engineering, Sogang University

2010 Master of Science in Chemical Engineering, Sogang University

2024 Doctor of Philosophy in Chemical Engineering, University of California San Diego

ABSTRACT OF THE DISSERTATION

Boron Chemistry in High Voltage Cathodes for Lithium-Ion Batteries

by

Na Ri Park

Doctor of Philosophy in Chemical Engineering

University of California San Diego, 2024

Professor Ying Shirley Meng, Chair

Lithium-ion batteries are central to advancing energy storage solutions, and the high-voltage spinel lithium nickel manganese oxide (LNMO) and lithium-rich layered oxide (LRLO) stand out as two promising cathode materials for next-generation lithium-ion batteries.

The first half of this dissertation is on the study of LNMO for lithium-ion batteries. LNMO operates at 4.8 V and offers high energy density, yet LNMO/graphite (LNMO/Gr) full cells experience capacity fading, limiting practical applications. This work introduces a lithium metaborate (LBO) coating applied via a dry mixing method to enhance LNMO's cycling stability. The LBO-coated LNMO, with an areal capacity of 3 mAh cm^{-2}, exhibits superior long-term performance compared to uncoated LNMO. Characterization reveals that the 5 nm cathode electrolyte interphase (CEI) formed on LBO-coated LNMO mitigates phase transitions after extended cycling. Furthermore, the coating acts as a reservoir, dissolving into the electrolyte and reducing Nickel/Manganese dissolution and SEI formation on the anode side.

The second part of this dissertation is on the study of LRLO for Lithium-ion batteries. LBO is applied to LRLO cathodes to address their challenges, such as voltage decay and poor cycling performance. The LBO-coated LRLO forms a uniform 15 nm surface layer, and when combined with lithium bis(oxalato)borate (LiBOB) as an electrolyte additive, achieves capacity retention of 82% after 400 cycles. The boron species' interaction with PF_6^- anions generate BF_4^- and suppresses HF formation during high-voltage cycling, improving both cathode stability and electrolyte integrity.

Overall, this dissertation offers surface modification through LBO stabilizes LNMO and LRLO cathodes' surfaces and mitigates degradation mechanisms, paving the way for their practical use in advanced lithium-ion battery systems.

Chapter 1 INTRODUCTION

1.1 Advancements and Challenges in Lithium-Ion Battery Development

Efforts to develop advanced lithium-ion batteries (**Figure 1.1**) with enhanced energy density and extended cycle life are pivotal to meeting the increasing energy storage demands of the electric vehicle market and the broader integration of renewable energy sources into the global power grid [1]. As the world increasingly shifts toward electrification and sustainable energy, the importance of improving battery technology becomes even more pronounced. Notably, lithium-ion batteries have become the most widely used energy storage solution, recognized for their impressive ability to deliver high performance in terms of energy density, power density, and cost-effectiveness, which are critical for applications ranging from portable electronics to large-scale grid storage [2]. However, despite their widespread use, current generations of lithium-ion batteries, particularly those employing layered oxide cathode materials, face significant hurdles in meeting the ambitious energy storage goals needed to support a future dominated by electric mobility and renewable energy solutions [3].

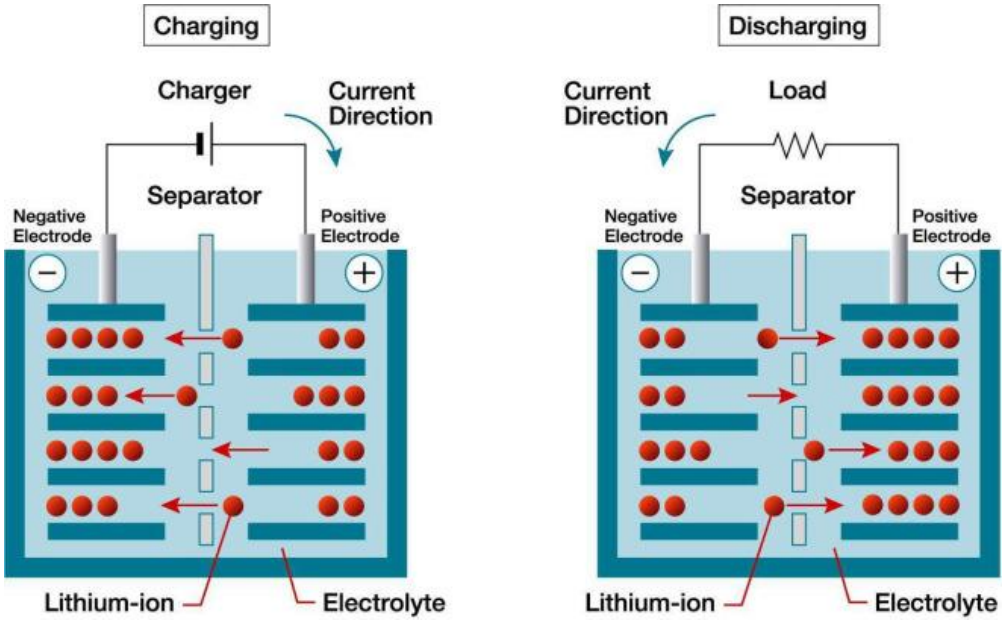

Figure 1.1: Illustration in diagrammatic form of lithium-ion battery structure.

Under existing operating conditions, today's cathode materials, such as nickel-rich layered oxides, high-voltage spinel lithium nickel manganese oxide, and lithium-rich layered oxides, struggle to meet the projected targets for energy density, particularly the target of 350 Wh/kg at the cell level, which is essential for advancing electric vehicle technology [1]. This translates to the need for over 800 Wh/kg at the cathode level, a substantial increase over current cathode material capacities. Meeting this challenge requires not only increasing the energy density but also improving the cycle life and safety of these materials to ensure their long-term viability. Additionally, the transition to higher voltage and capacity cathode materials introduces new complexities, such as the need for better electrolyte compatibility and enhanced thermal stability, which are essential for ensuring the safety and efficiency of lithium-ion batteries in various applications.

Moreover, as demand for lithium-ion batteries continues to rise, the sustainability of current battery production practices has become a pressing concern [4]. The high energy

consumption involved in extracting raw materials, coupled with the reliance on finite critical resources such as cobalt, lithium, and nickel, creates significant environmental and geopolitical challenges. The mining and refining of these materials, along with the low recycling rates for end-of-life batteries, exacerbate the environmental footprint of lithium-ion batteries. If these challenges are not addressed, the widespread adoption of lithium-ion batteries could have substantial environmental consequences, particularly as global demand for electric vehicles and energy storage systems increases. Additionally, the production of batteries remains highly energy-intensive, with much of the energy consumed coming from non-renewable sources, further contributing to their environmental impact [4].

Despite these challenges, research into next-generation battery technologies remains essential for advancing the adoption of electric vehicles, renewable energy systems, and other clean energy solutions. Breakthroughs in cathode materials and electrolyte compatibility hold the potential to enable batteries that meet—and even exceed—current energy density targets [5]. Such innovations could pave the way for batteries that not only deliver higher performance but are also more environmentally sustainable. For instance, almost every component of conventional lithium-ion batteries—ranging from the cathode and anode materials to the electrolytes and separators—could be replaced with more sustainable alternatives. However, achieving this transition while maintaining performance comparable to current lithium-ion batteries remains a significant hurdle. Greener alternatives, while promising, often face limitations in energy density, cycle life, and cost-effectiveness, which makes them less viable for high-performance applications like electric vehicles.

To ensure the sustainability of battery technology in the long term, the development of greener lithium-ion batteries will require addressing the inherent trade-offs between performance

and environmental impact [6]. For portable and mobile applications, such as consumer electronics, electric mobility, and aviation, the key priorities will remain high energy density, fast-charging capabilities, and safety. In these areas, lithium-ion batteries continue to excel due to their ability to store and deliver substantial energy in compact, lightweight packages. However, for larger-scale applications, such as grid storage and renewable energy integration, the focus will shift to improving material efficiency, reducing the environmental impact of production, and enhancing recyclability. The path forward for energy storage will likely involve a combination of improving the performance of existing lithium-ion battery technologies and developing entirely new materials and architectures that can meet the specific needs of various applications.

While lithium-ion batteries remain a cornerstone of modern energy storage, the challenges they face—from raw material sourcing to sustainability and performance—require ongoing innovation [7]. The continued development of cathode materials that can increase energy density, improve cycle life, and reduce environmental impact will be essential in meeting the future demands of electrification and renewable energy storage. As the field of battery research advances, it is clear that next-generation cathode materials, alongside improvements in other components of lithium-ion batteries, will play a crucial role in overcoming these challenges and enabling the widespread adoption of clean, sustainable energy solutions.

1.2 Increasing Energy Density Through Higher Voltage and Capacity

Enhancing the energy density of lithium-ion batteries is a critical goal in advancing battery technology, especially for applications such as electric vehicles and large-scale renewable energy storage. Two key strategies for increasing energy density are improving the battery's capacity and

increasing its voltage range. These approaches are often pursued together, as they complement each other in boosting overall energy storage [8].

Increasing battery capacity is essential for extending runtime in applications that require sustained energy output. Battery capacity refers to the total amount of energy a battery can store, and increasing this capacity primarily involves improving the materials used in the electrodes, especially the cathode materials, which are responsible for most of the energy storage. Nickel-rich layered oxides ($LiNi_{1-x}M_xO_2$, where M can be Co, Mn, or Al) have gained significant attention due to their superior specific capacity and energy density, particularly when high nickel content is incorporated [9]. This higher nickel content enables more lithium ions to be stored, making these materials particularly advantageous for applications that require both high energy density and extended runtime, such as electric vehicles and renewable energy storage systems.

In addition to capacity, increasing the battery's average operating voltage is another effective way to enhance energy density. Higher average operating voltage raises the energy stored per unit mass and volume, leading to a direct increase in overall energy density [9]. This enables the storage of more energy in a given battery pack without a proportional increase in size or weight, which is especially beneficial for compact and lightweight battery solutions used in electric vehicles and portable electronics. However, achieving higher voltages introduces challenges, primarily related to the stability of the electrolyte at elevated voltages. Conventional carbonate-based liquid electrolytes, commonly used in commercial lithium-ion batteries, offer high ionic conductivity and moderate electrochemical stability within the standard operating voltage range of 3.0 to 4.2 V [10]. However, when exposed to voltages exceeding 4.4 V, these electrolytes begin to degrade significantly, compromising battery performance and safety. The decomposition of electrolyte solvents at high voltages produces reactive species that interact with lithium salts,

generating corrosive byproducts such as HF (hydrofluoric acid), which damage both the cathode and the anode side. This degradation leads to increased impedance, diminished capacity retention, and ultimately, a reduction in overall battery performance.

Another concern with high-voltage operation is the generation of gaseous byproducts, such as CO_2, CO, and hydrocarbons, which accumulate inside the battery, causing pressure buildup and physical swelling. This compromises the mechanical integrity of the battery casing, reducing cycle performance and presenting safety risks, especially under prolonged high-voltage cycling or thermal stress. These challenges make it difficult to achieve the long-term reliability and safety needed for demanding applications [11].

Despite the challenges associated with high-voltage operation and structural stability in lithium-ion batteries, several promising solutions are being actively explored to address these limitations and enable the advancement of high-energy-density batteries [12]. One of the most effective and widely studied approaches involves the surface modification of cathode materials. By coating the surface of cathode materials with protective layers, it is possible to significantly enhance their structural stability, mitigate oxygen release, and reduce issues such as capacity fade and voltage degradation, which are common in high-voltage operations [13]. These coatings typically consist of materials such as metal oxides (e.g., Al_2O_3 [14], TiO_2 [15]), conductive polymers (e.g., polyaniline), or ceramics, which form a physical barrier between the cathode material and the electrolyte, preventing unwanted side reactions and helping to stabilize the cathode structure under high-voltage conditions.

The coatings help to prevent the degradation of the cathode material by acting as a shield against oxidation and the formation of harmful byproducts. For example, Al_2O_3 coatings are effective in reducing oxygen release from the cathode material, which is a common issue when

operating at high voltages [14]. Oxygen release can lead to a rapid loss of capacity and performance degradation, especially in nickel-rich or lithium-rich cathodes. TiO_2 coatings, on the other hand, have been shown to improve the structural integrity of the cathode and prevent the growth of cracks or microfractures during cycling [15]. Additionally, these coatings (**Figure 1.2**, [16]) can also suppress thermal instability, which is critical for maintaining the safety of LIBs during high-voltage operation. The surface coating approach also prevents direct contact between the electrolyte and the cathode material, minimizing the possibility of side reactions and enhancing the overall cycling stability of the battery [16].

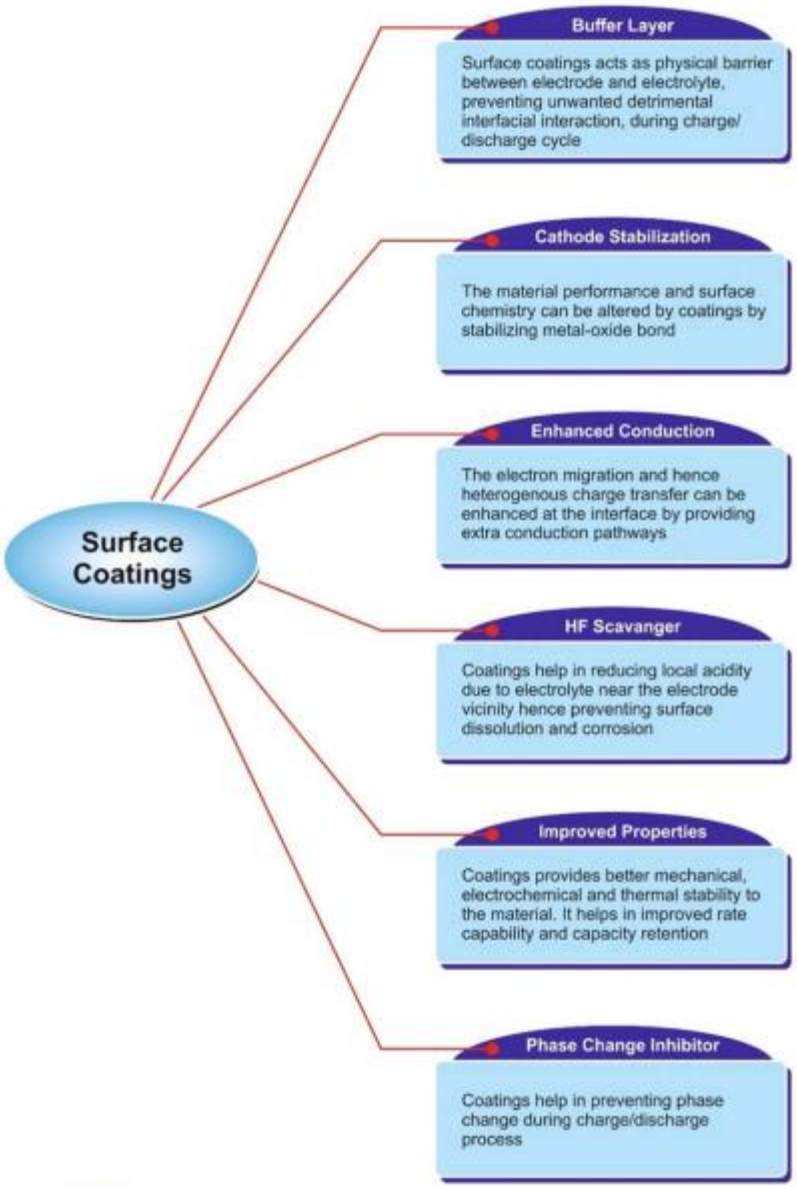

Figure 1.2: Roles of surface coatings on cathode materials.

Alongside surface modification, the development of electrolytes with enhanced stability at higher voltages is another crucial strategy to improve the performance of high-voltage LIBs. Conventional carbonate-based electrolytes, while widely used in LIBs, start to decompose at voltages above 4.4 V [17], leading to the generation of reactive species and corrosive byproducts that degrade the performance of both the electrolyte and the cathode material. To overcome this

limitation, researchers are focusing on developing electrolytes that can withstand higher voltages without undergoing oxidative decomposition. One promising approach involves the use of fluorinated solvents, which are more stable at high voltages and can form stable passivation layers on the cathode surface [18]. Lithium salts with enhanced oxidative stability, such as LiBOB (lithium bis(oxalato)borate) [19], have also shown potential in improving the electrochemical stability of the electrolyte. These salts help to minimize the formation of harmful byproducts and ensure stable ion transport at high voltages. By improving the stability of the electrolyte at high voltages, these additives can enhance the overall energy density and long-term cycling performance of LIBs, particularly in demanding applications like electric vehicles and large-scale renewable energy storage systems [20].

Ultimately, advancing the performance of high-energy LIBs requires a careful balance of increased capacity, higher voltage, and stability. By addressing the limitations of conventional electrolytes and improving the structural resilience of high-capacity cathodes, researchers aim to unlock the full potential of LIBs, resulting in batteries with greater energy density, longer cycling performance, and improved safety. These advancements will be crucial for meeting the energy storage demands of applications such as electric vehicles, portable electronics, and renewable energy storage systems [21].

1.3 Advancements in High-Voltage Cathode Materials for LIBs

The energy density of a battery has a direct impact on its driving range, operating time, and overall performance, making energy density improvement crucial for increasing energy storage capacity while reducing the size and weight of the battery. High-voltage cathode materials

represent one of the most promising strategies to achieve this goal, as they enable batteries to operate at higher voltages, significantly enhancing the overall energy storage capacity [22].

Among the most promising candidates (**Figure 1.3**) for high-voltage cathodes are nickel-rich layered oxides ($LiNi_{1-x}M_xO_2$, where M typically includes cobalt, manganese, or aluminum), high-voltage spinel lithium nickel manganese oxide such as $LiNi_{0.5}Mn_{1.5}O_4$ (LNMO), and lithium-rich layered oxides ($Li_{1+x}M_{1-x}O_2$, where M can be Mn, Ni, or Co). These materials have the potential to extend the voltage operating range, thereby enhancing energy storage capacity and overall energy density [23].

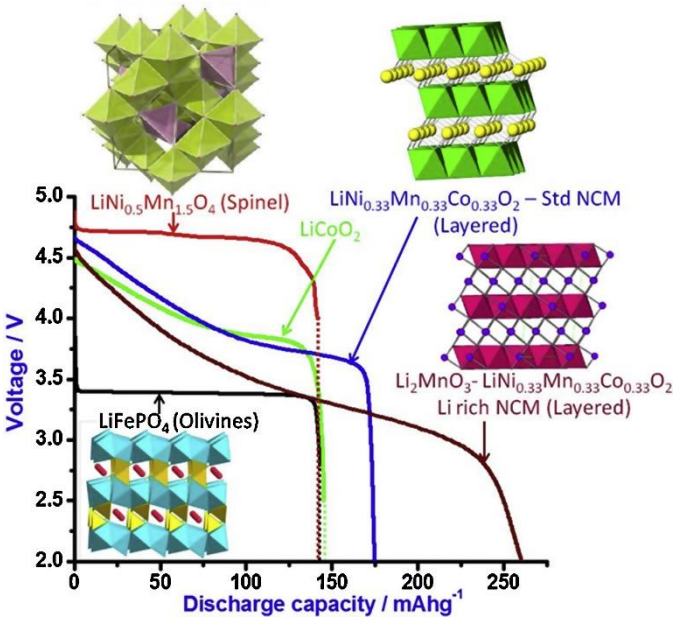

Figure 1.3: Li-ion battery cathodes: important formulae, structures, and voltage profiles during discharge. The potentials are versus Li reference electrodes.

1.3.1 Nickel-Rich Layered Oxide

Nickel-rich layered oxides have garnered significant attention for their ability to offer high specific capacity due to their ability to incorporate more lithium ions into the structure. As a result, they are highly attractive for high-energy applications, such as electric vehicles and large-scale

energy storage systems, where longer runtimes are crucial. Increasing the nickel content in the cathode material raises the lithium storage capacity, improving both the specific capacity and the energy density of the battery (**Figure 1.4**). This makes nickel-rich cathodes particularly desirable for applications requiring higher energy outputs. However, despite their high capacity, there are several critical challenges associated with their use, particularly under high-voltage cycling conditions [24].

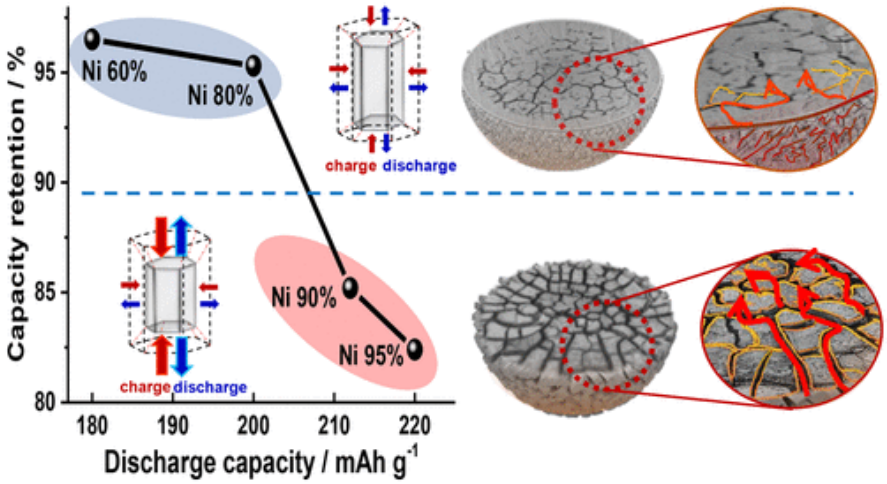

Figure 1.4: Capacity fading scheme of Ni-rich $Li[Ni_xCo_yMn_{1-x-y}]O_2$ cathodes.

At voltages above 4.4V, nickel-rich layered oxides tend to undergo a series of detrimental phase transitions, particularly between hexagonal and monoclinic phases. These phase changes generate significant internal mechanical stress, leading to the formation of microcracks (**Figure 1.4**) that weaken the material's lattice structure. Over time, such structural degradation results in irreversible capacity loss and poor cycling stability. The mechanical stress from these phase transitions, coupled with high-voltage cycling, undermines the material's structural integrity, which directly impacts battery performance and safety [25].

Moreover, at elevated voltages, the electrolyte is more likely to undergo undesirable oxidative decomposition reactions at the electrode/electrolyte interface. In commercially available

carbonate-based liquid electrolytes, the stable operating voltage is generally limited to 4.3–4.4V. Surpassing this threshold leads to aggressive oxidative reactions that result in the formation of a SEI layer, which impedes lithium-ion transport, causes gas generation, and can lead to transition metal dissolution. These processes significantly degrade the overall battery performance, making high-voltage operation a significant challenge for practical applications.

Another major issue with high-voltage cycling of nickel-rich cathodes is oxygen release, which becomes more pronounced under both high-voltage and high-temperature conditions (**Figure 1.5**). Oxygen evolution disrupts the structural integrity of the material by generating oxygen vacancies, which can lead to further destabilization of the lattice and compromise the overall safety of the system. The loss of oxygen from the lattice, particularly during high-temperature cycling or material synthesis, exacerbates these issues and can contribute to thermal runaway, a significant safety risk in battery systems [25].

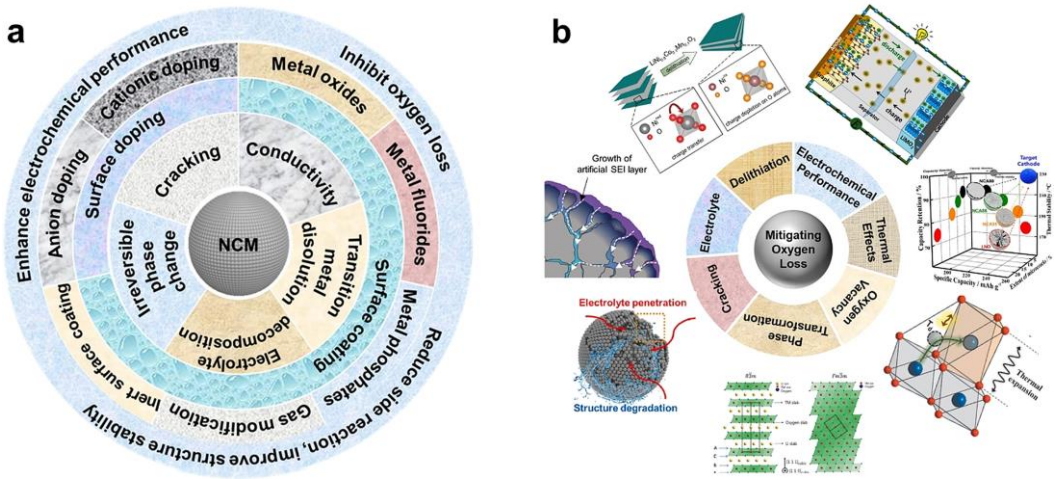

Figure 1.5: (a) Schematic illustration of the issues and methods of Ni-rich material. (b) Causality between the delithiation, electrolyte, cracking, phase transformation, oxygen vacancy, thermal effect, and electrochemical performance associated with the oxygen loss, and examples of each topic are illustrated.

The thermal treatment of these materials during synthesis or cycling further destabilizes the crystal structure, particularly through the loss of lattice oxygen (**Figure 1.6**). This process not only accelerates material degradation but also emphasizes the need for comprehensive structural characterization of nickel-rich layered oxides during various charge/discharge stages to better understand and mitigate these failure mechanisms [26]. Researchers must develop advanced techniques to monitor and control these structural changes in real-time, which will be critical for developing more stable and durable materials.

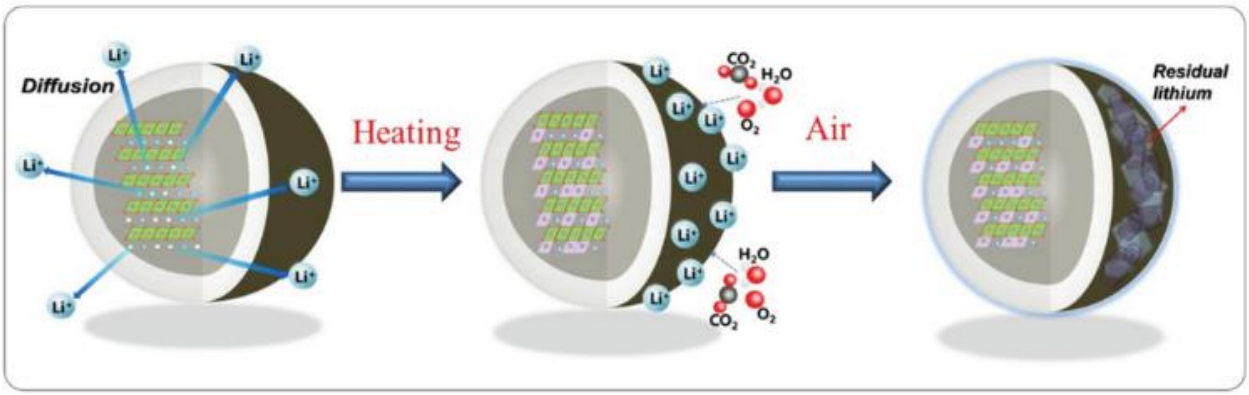

Figure 1.6: Schematic representation of the formation process of LiOH and Li_2CO_3 at a $LiNi_{0.7}Mn_{0.3}O_2$ cathode surface.

In recent years, various strategies have been developed to address these challenges and stabilize nickel-rich layered oxides. One promising approach is heterogeneous ion doping, where elements such as magnesium [27], aluminum [28], or titanium [29] are substituted into the structure. These dopants help to alleviate internal stresses by modifying the electronic environment, thus stabilizing the lattice and reducing the risk of phase transitions. Additionally, surface coating techniques—such as applying materials like aluminum oxide (Al_2O_3) [30] or lithium phosphate (Li_3PO_4) [31] —can form protective layers that minimize direct contact between the cathode material and the electrolyte, reducing surface degradation and mitigating oxygen release [28], [30].

Another key strategy is controlling the morphology of the cathode material (**Figure 1.7**). By using spherical or core-shell structures (**Figure 1.7 (b)**), researchers can optimize the distribution of mechanical stresses, preventing the development of microcracks and enhancing the overall mechanical stability of the material [32]. Moreover, concentration gradient designs—where the composition of nickel and other elements is varied from the core to the surface of the particles—can further improve the resistance to cracking and phase transitions, enhancing both the electrochemical and mechanical stability of the material (**Figure 1.7 (a)**).

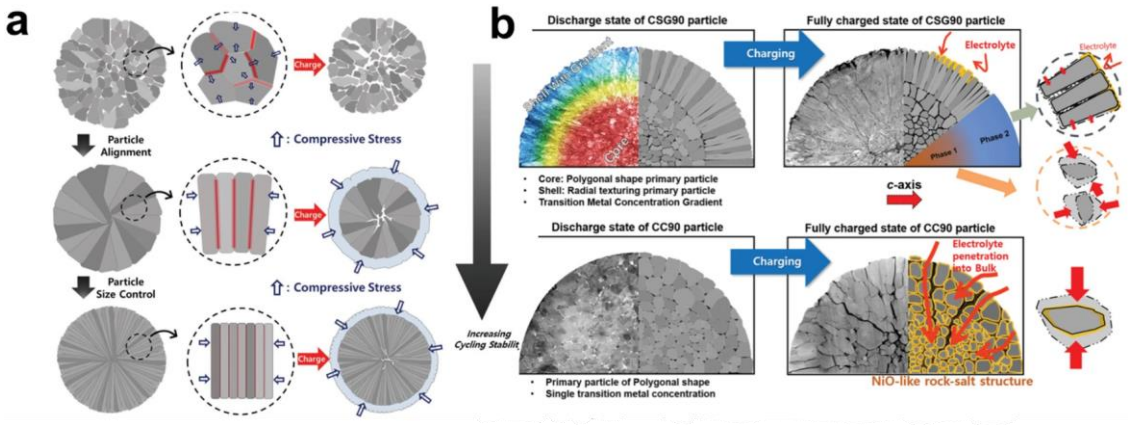

Figure 1.7: (a) The schematic of a build-up of local stress concentrations and stress distribution during charging depending on primary particle morphology. (b) The schematic of different degrees of sustained damage because of the different morphology.

A critical challenge in developing nickel-rich cathodes is the high cost and limited availability of cobalt. Cobalt is expensive (around $20,000 per ton ($11.02/lb) as of late 2024, https://www.dailymetalprice.com/) and relatively scarce in the Earth's crust, leading to concerns about the long-term sustainability of its use in battery materials. As a result, researchers have been exploring various ways to reduce or eliminate cobalt from these materials while maintaining their stability and performance [33]. However, stabilizing the layered structure of these cobalt-free or low-cobalt materials remains a significant challenge. Furthermore, the infrastructure changes

required to accommodate new materials and processing methods may incur high costs, potentially offsetting the benefits of reducing cobalt usage.

While nickel-rich layered oxides hold significant promise for high-energy applications, their long-term viability is contingent upon overcoming the structural and electrochemical challenges discussed above. The high nickel content, while boosting energy density, also contributes to instability under high-voltage cycling, which negatively affects the long-term performance and safety of the battery [34]. Further research into stabilizing these materials through advanced material design and process optimization will be essential to enable their practical and widespread use (**Figure 1.8**).

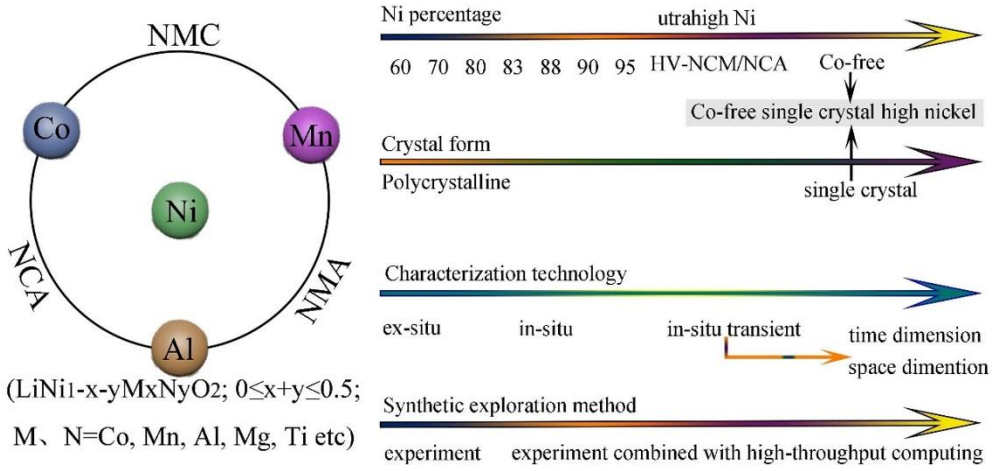

Figure 1.8: Further applications and development trends of nickel-rich cathodes in the future.

As a result, the development of high-energy cathode materials, particularly those that utilize nickel-rich layered oxides, holds significant promise for improving the energy density of lithium-ion batteries, especially for demanding applications such as electric vehicles and large-scale energy storage systems. However, to fully realize their potential, ongoing research must address the inherent challenges of structural degradation, oxygen release, and electrolyte stability under high-voltage cycling conditions [32], [34]. Through innovative material design strategies—

such as ion doping, surface coatings, and morphological control—it is possible to stabilize these materials, enhancing their performance and safety (**Figure 1.5**). As the demand for high-energy batteries grows, particularly in the automotive and renewable energy sectors, overcoming these challenges will be critical to advancing next-generation battery technologies and ensuring their long-term viability in commercial applications [35].

1.3.2 High-Voltage Spinel Lithium Nickel Manganese Oxide

High-voltage spinel lithium nickel manganese oxide, such as $LiNi_{0.5}Mn_{1.5}O_4$ (LNMO), have attracted significant attention as promising cathode materials for high-energy lithium-ion batteries due to their stable crystal structure and ability to operate at voltages up to 4.7 V [36]. This high-voltage tolerance is one of their key advantages, as it allows for increased energy density without significantly expanding the size or weight of the battery, making them particularly attractive for applications such as electric vehicles and large-scale energy storage systems. Furthermore, spinel lithium nickel manganese oxide exhibits good thermal stability, which enables it to maintain performance even under elevated temperatures, an essential characteristic for high-power applications [37].

Unlike nickel-rich layered oxides, prone to structural instability and phase transitions at high voltages, spinel lithium nickel manganese oxide materials are more resilient to mechanical stress, reducing the risk of microcracks and lattice degradation [38]. However, while their ability to withstand higher voltages gives them an edge in energy density, spinel lithium nickel manganese oxide oxides suffer from a lower specific capacity compared to nickel-rich materials. This means they store less energy for the same volume or weight, limiting their overall energy storage potential [37].

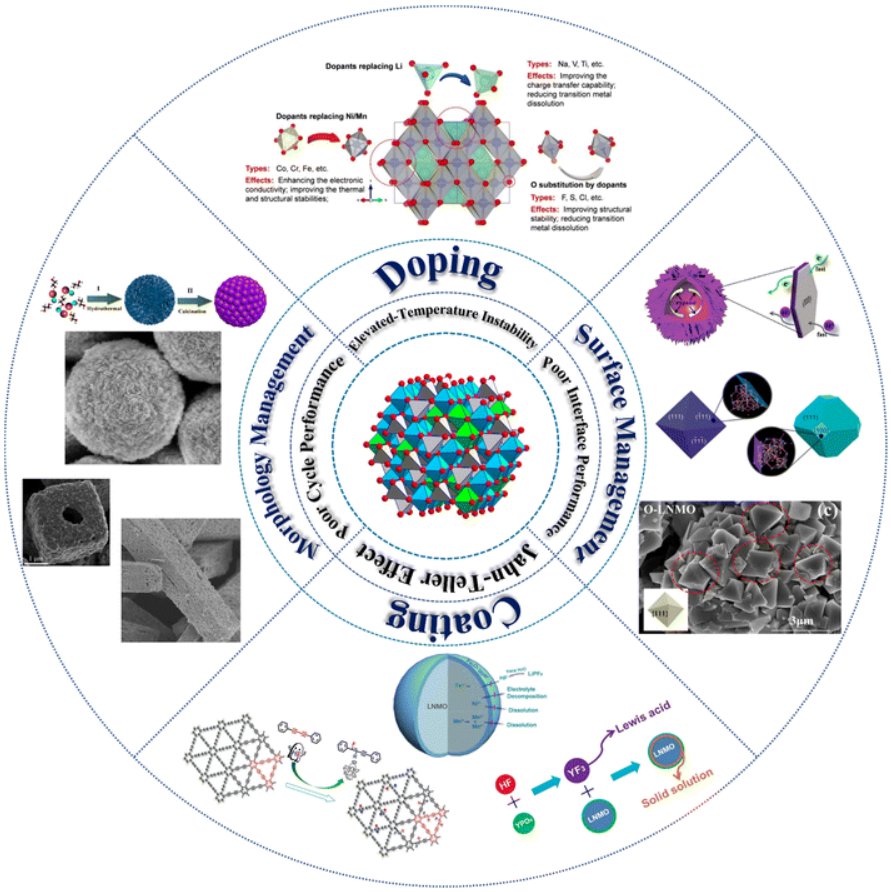

Figure 1.9: Schematic illustration of the current publications on LNMO cathodes according to modified methods.

Figure 1.9 highlights the key strategies for enhancing the performance of cathode materials in lithium-ion batteries through doping, surface management, and coating techniques, all within a comprehensive technology management framework [39]. Doping involves incorporating various elements into the crystal lattice to stabilize the structure, reduce degradation, and improve electrochemical performance. Surface management focuses on optimizing particle morphology and surface characteristics to mitigate side reactions and improve compatibility with electrolytes. Coating techniques apply protective layers to prevent electrolyte decomposition and enhance thermal and structural stability, especially under high-voltage conditions. Together, these

approaches synergistically improve energy density, cycle life, and thermal stability, as depicted through detailed illustrations of nanoscale modifications, particle engineering, and lattice stabilization mechanisms. This integrative framework emphasizes the importance of combining these strategies to achieve efficient, durable, and high-performance battery systems.

1.3.3 Lithium-rich Layered Oxides

Lithium-rich layered oxides offer exceptionally high theoretical capacity and the potential for very high energy density, making them attractive for next-generation batteries [40]. However, they face significant challenges such as voltage fade and poor cycle stability. **Figure 1.10** illustrates key strategies and challenges associated with LRLO as advanced cathode materials for lithium-ion batteries [41]. The central wheel highlights the primary issues: voltage decay, capacity loss, poor cycle life, lattice oxygen loss, and size control. Surrounding this are various solutions, including surface coating to enhance structural stability, morphology design for improved electronic pathways and reduced grain boundary resistance, element doping to stabilize the layered structure and suppress undesired reactions, and electrolyte modification to mitigate chemical degradation. This phenomenon is often linked to the formation of unstable phases and side reactions at the electrode-electrolyte interface, which degrade electrochemical performance and shorten battery lifespan [44]. Despite these challenges, lithium-rich oxides exhibit capacities exceeding the traditional theoretical limits due to anion redox activity, such as oxygen oxidation, which adds reversible capacity during electrochemical cycling [43]. Research advancements have steadily improved the capacity of these materials from around 200 mAh/g to nearly 350 mAh/g over the past decade [44]. To achieve commercial viability, ongoing efforts are focusing on mitigating issues like voltage fade, structural instability, and slow reaction kinetics while

harnessing the unique anion redox properties for further capacity enhancement. These developments highlight the material's potential to meet the demands of high-energy applications while addressing critical limitations [43].

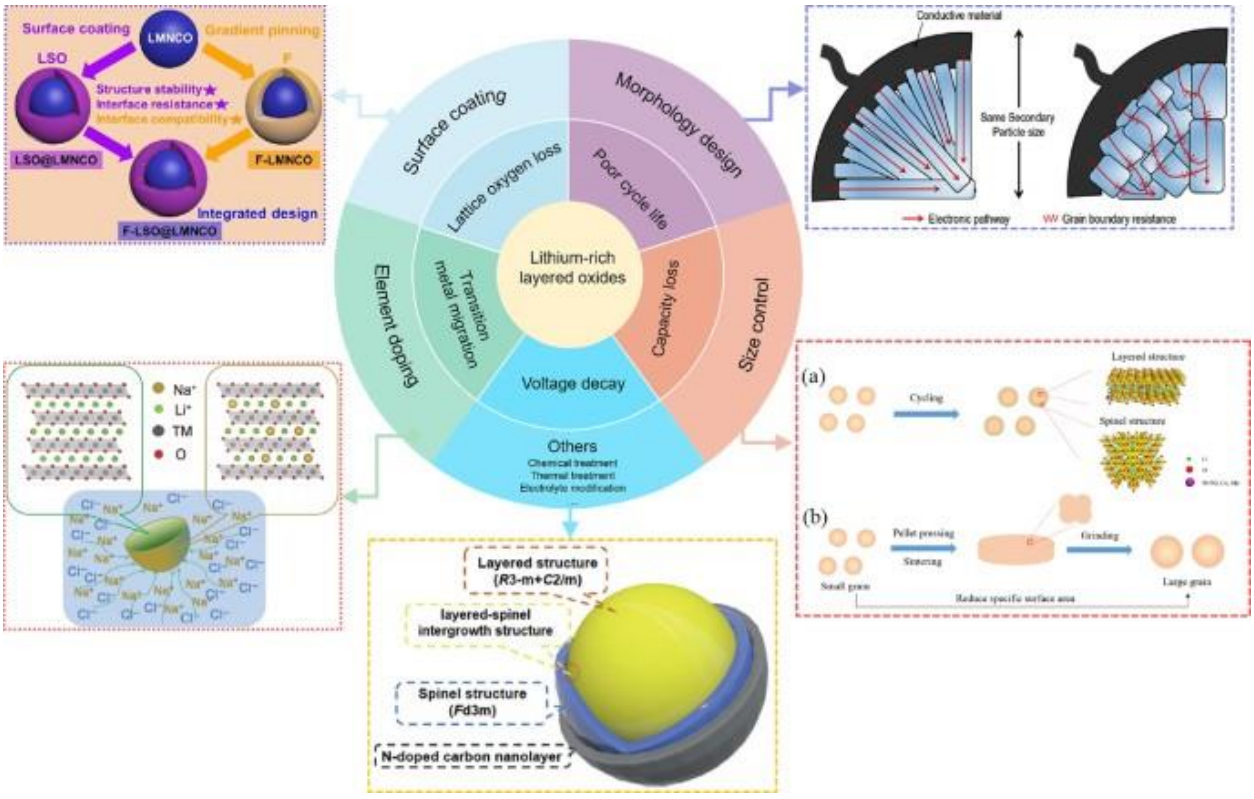

Figure 1.10: Schematic illustration of various challenges and corresponding strategies of LRLO.

The illustrations emphasize the interplay between structural engineering, chemical modifications, and interface stabilization in addressing LRLO's inherent limitations, paving the way for better performance and practical application in next-generation batteries [41].

1.4 References

[1] Lithium-ion battery separator film SETELATM | TORAY FILMS | TORAY. (n.d.). https://www.films.toray/en/products/setela/.

[2] Amir, M., Deshmukh, R. G., Khalid, H. M., Said, Z., Raza, A., Muyeen, S. M., Nizami, A. S., Elavarasan, R. M., Saidur, R., & Sopian, K. (2023). Energy storage technologies: An integrated survey of developments, global economical/environmental effects, optimal scheduling model, and sustainable adaption policies. In *Journal of Energy Storage* (Vol. 72). Elsevier Ltd. https://doi.org/10.1016/j.est.2023.108694

[3] Yang, Z., Huang, H., & Lin, F. (2022). Sustainable Electric Vehicle Batteries for a Sustainable World: Perspectives on Battery Cathodes, Environment, Supply Chain, Manufacturing, Life Cycle, and Policy. *Advanced Energy Materials*, *12*(26). https://doi.org/10.1002/aenm.202200383

[4] Tan, S., Ji, Y. J., Zhang, Z. R., & Yang, Y. (2014). Recent progress in research on high-voltage electrolytes for lithium-ion batteries. In *ChemPhysChem* (Vol. 15, Issue 10, pp. 1956–1969). Wiley-VCH Verlag. https://doi.org/10.1002/cphc.201402175

[5] Koech, A. K., Mwandila, G., Mulolani, F., & Mwaanga, P. (2024). Lithium-ion battery fundamentals and exploration of cathode materials: A review. In *South African Journal of Chemical Engineering* (Vol. 50, pp. 321–339). Elsevier B.V. https://doi.org/10.1016/j.sajce.2024.09.008

[6] Molaiyan, P., Bhattacharyya, S., dos Reis, G. S., Sliz, R., Paolella, A., & Lassi, U. (2024). Towards greener batteries: sustainable components and materials for next-generation batteries. In *Green Chemistry* (Vol. 26, Issue 13, pp. 7508–7531). Royal Society of Chemistry. https://doi.org/10.1039/d3gc05027k

[7] Rostami, F., Kis, Z., Koppelaar, R., Jiménez, L., & Pozo, C. (2022). Comparative sustainability study of energy storage technologies using data envelopment analysis. *Energy Storage Materials*, *48*, 412–438. https://doi.org/10.1016/j.ensm.2022.03.026

[8] Lu, C., Wu, W., Wang, L., Tian, R., & Du, F. (2024). Thick electrode for energy storage systems: A facile strategy towards high energy density Li ion batteries. *Next Materials*, *4*, 100170. https://doi.org/10.1016/j.nxmate.2024.100170

[9] Kim, Y., Seong, W. M., & Manthiram, A. (2021). Cobalt-free, high-nickel layered oxide cathodes for lithium-ion batteries: Progress, challenges, and perspectives. In *Energy Storage Materials* (Vol. 34, pp. 250–259). Elsevier B.V. https://doi.org/10.1016/j.ensm.2020.09.020

[10] Li, Q., Chen, J., Fan, L., Kong, X., & Lu, Y. (2016). Progress in electrolytes for rechargeable Li-based batteries and beyond. In *Green Energy and Environment* (Vol. 1, Issue 1, pp. 18–42). KeAi Publishing Communications Ltd. https://doi.org/10.1016/j.gee.2016.04.006

[11] Pender, J. P., Jha, G., Youn, D. H., Ziegler, J. M., Andoni, I., Choi, E. J., Heller, A., Dunn, B. S., Weiss, P. S., Penner, R. M., & Mullins, C. B. (2020). Electrode Degradation in Lithium-Ion Batteries. In *ACS Nano* (Vol. 14, Issue 2, pp. 1243–1295). American Chemical Society. https://doi.org/10.1021/acsnano.9b04365

[12] Masias, A., Marcicki, J., & Paxton, W. A. (2021). Opportunities and Challenges of Lithium Ion Batteries in Automotive Applications. In *ACS Energy Letters* (Vol. 6, Issue 2, pp. 621–630). American Chemical Society. https://doi.org/10.1021/acsenergylett.0c02584

[13] Kim, J. M., Zhang, X., Zhang, J. G., Manthiram, A., Meng, Y. S., & Xu, W. (2021). A review on the stability and surface modification of layered transition-metal oxide cathodes. In *Materials Today* (Vol. 46, pp. 155–182). Elsevier B.V. https://doi.org/10.1016/j.mattod.2020.12.017

[14] Ø stli, E. R., Tesfamhret, Y., Wenner, S., Lacey, M. J., Brandell, D., Svensson, A. M., Selbach, S. M., & Wagner, N. P. (2021). Limitations of Ultrathin Al_2O_3Coatings on LNMO Cathodes. *ACS Omega*, *6*(45), 30644–30655. https://doi.org/10.1021/acsomega.1c04457

[15] Zhang, X., Belharouak, I., Li, L., Lei, Y., Elam, J. W., Nie, A., Chen, X., Yassar, R. S., & Axelbaum, R. L. (2013). Structural and electrochemical study of Al_2O_3 and TiO_2 Coated $Li_{1.2}Ni_{0.13}Mn_{0.54}Co_{0.13}O_2$ cathode material using ALD. *Advanced Energy Materials*, *3*(10), 1299–1307. https://doi.org/10.1002/aenm.201300269

[16] Kaur, G., & Gates, B. D. (2022). Review—Surface Coatings for Cathodes in Lithium Ion Batteries: From Crystal Structures to Electrochemical Performance. *Journal of The Electrochemical Society*, *169*(4), 043504. https://doi.org/10.1149/1945-7111/ac60f3

[17] Xu, K. (2014). Electrolytes and interphases in Li-ion batteries and beyond. In *Chemical Reviews* (Vol. 114, Issue 23, pp. 11503–11618). American Chemical Society. https://doi.org/10.1021/cr500003w

[18] Rao, Y., Li, X., Zhao, S., Liu, P., Wu, F., Liu, X., Zhou, N., Fang, S., & Passerini, S. (2024). Fluorinated electrolyte formulations design enabling high-voltage and long-life lithium metal batteries. *Nano Energy*, *123*. https://doi.org/10.1016/j.nanoen.2024.109362

[19] Li, Y., Li, W., Shimizu, R., Cheng, D., Nguyen, H. N., Paulsen, J., Kumakura, S., Zhang, M., & Meng, Y. S. (2022). Elucidating the Effect of Borate Additive in High-Voltage Electrolyte for Li-Rich Layered Oxide Materials. *Advanced Energy Materials*, *12*(11). https://doi.org/10.1002/aenm.202103033

[20] Wuamprakhon, P., Songthan, R., Sangsanit, T., Santiyuk, K., Phojaroen, J., Homlamai, K., Tejangkura, W., & Sawangphruk, M. (2024). Designing electrolytes for enhancing stability and performance of lithium-ion capacitors at large-scale cylindrical cells. *Journal of Power Sources*, *622*. https://doi.org/10.1016/j.jpowsour.2024.235331

[21] Njema, G. G., Ouma, R. B. O., & Kibet, J. K. (2024). A Review on the Recent Advances in Battery Development and Energy Storage Technologies. *Journal of Renewable Energy*, *2024*, 1–35. https://doi.org/10.1155/2024/2329261

[22] Khan, F. M. N. U., Rasul, M. G., Sayem, A. S. M., & Mandal, N. (2023). Maximizing energy density of lithium-ion batteries for electric vehicles: A critical review. *Energy Reports*, *9*, 11–21. https://doi.org/10.1016/j.egyr.2023.08.069

[23] Yoo, H. D., Markevich, E., Salitra, G., Sharon, D., & Aurbach, D. (2014). On the challenge of developing advanced technologies for electrochemical energy storage and conversion. In *Materials Today* (Vol. 17, Issue 3, pp. 110–121). Elsevier B.V. https://doi.org/10.1016/j.mattod.2014.02.014

[24] Flores, E., Novák, P., Aschauer, U., & Berg, E. J. (2020). Cation Ordering and Redox Chemistry of Layered Ni-Rich $Li_xNi_{1-2y}Co_yMn_yO_2$: An Operando Raman Spectroscopy Study. *Chemistry of Materials*, *32*(1), 186–194. https://doi.org/10.1021/acs.chemmater.9b03202

[25] Ryu, H. H., Park, K. J., Yoon, C. S., & Sun, Y. K. (2018). Capacity fading of ni-rich $Li[Ni_xCo_yMn_{1-x-y}]O_2$ ($0.6 \leq x \leq 0.95$) Cathodes for High-Energy-Density Lithium-Ion Batteries: Bulk or Surface Degradation? *Chemistry of Materials*, *30*(3), 1155–1163. https://doi.org/10.1021/acs.chemmater.7b05269

[26] Jiang, M., Danilov, D. L., Eichel, R. A., & Notten, P. H. L. (2021). A Review of Degradation Mechanisms and Recent Achievements for Ni-Rich Cathode-Based Li-Ion Batteries. In *Advanced Energy Materials* (Vol. 11, Issue 48). John Wiley and Sons Inc. https://doi.org/10.1002/aenm.202103005

[27] Ma, F., Wu, Y., Wei, G., Qiu, S., & Qu, J. (2019). Enhanced electrochemical performance of $LiNi_{0.8}Co_{0.1}Mn_{0.1}O_2$ cathode via wet-chemical coating of MgO. *Journal of Solid State Electrochemistry*, *23*(7), 2213–2224. https://doi.org/10.1007/s10008-019-04308-3

[28] Lee, Y. S., Shin, W. K., Kannan, A. G., Koo, S. M., & Kim, D. W. (2015). Improvement of the Cycling Performance and Thermal Stability of Lithium-Ion Cells by Double-Layer Coating of Cathode Materials with Al_2O_3 Nanoparticles and Conductive Polymer. *ACS Applied Materials and Interfaces*, *7*(25), 13944–13951. https://doi.org/10.1021/acsami.5b02690

[29] Tao, S., Kong, F., Wu, C., Su, X., Xiang, T., Chen, S., Hou, H., Zhang, L., Fang, Y., Wang, Z., Chu, W., Qian, B., & Song, L. (2017). Nanoscale TiO_2 membrane coating spinel $LiNi_{0.5}Mn_{1.5}O$ cathode material for advanced lithium-ion batteries. *Journal of Alloys and Compounds*, *705*, 413–419. https://doi.org/10.1016/j.jallcom.2017.02.139

[30] Yin, H., Yu, X. X., Zhao, H., Li, C., & Zhu, M. Q. (2018). Towards high-performance cathode materials for lithium-ion batteries: Al_2O_3-coated $LiNi_{0.8}Co_{0.15}Zn_{0.05}O_2$. *Journal of Solid State Electrochemistry*, *22*(8), 2395–2403. https://doi.org/10.1007/s10008-018-3904-4

[31] Zhao, Q. fang, Yu, Y. hui, Ouyang, Q. sheng, Hu, M. yi, Wang, C., Ge, J. hua, Zhang, S. qiong, & Jiang, G. hui. (2022). Surface modification of $LiFePO_4$ by Coatings for Improving of Lithium-ion Battery Properties. *International Journal of Electrochemical Science*, *17*. https://doi.org/10.20964/2022.11.31

[32] Meng, Z., Ma, X., Azhari, L., Hou, J., & Wang, Y. (2023). Morphology controlled performance of ternary layered oxide cathodes. In *Communications Materials* (Vol. 4, Issue 1). Springer Nature. https://doi.org/10.1038/s43246-023-00418-8

[33] William Gourley, S. D., Or, T., & Chen, Z. (2020). *iScience Breaking Free from Cobalt Reliance in Lithium-Ion Batteries*. https://doi.org/10.1016/j.isci

[34] Lv, Y., Huang, S., Zhao, Y., Roy, S., Lu, X., Hou, Y., & Zhang, J. (2022). A review of nickel-rich layered oxide cathodes: synthetic strategies, structural characteristics, failure mechanism, improvement approaches and prospects. *Applied Energy*, *305*. https://doi.org/10.1016/j.apenergy.2021.117849

[35] Jannesar Niri, A., Poelzer, G. A., Zhang, S. E., Rosenkranz, J., Pettersson, M., & Ghorbani, Y. (2024). Sustainability challenges throughout the electric vehicle battery value chain. In *Renewable and Sustainable Energy Reviews* (Vol. 191). Elsevier Ltd. https://doi.org/10.1016/j.rser.2023.114176

[36] Ohzuku, T., Takeda, S., & Iwanaga, M. (1999). Solid-state redox potentials for Li $[Me_{1/2}Mn_{3/2}]O_4$ (Me: 3d-transition metal) having spinel-framework structures: a series of 5 volt materials for advanced lithium-ion batteries. In *Journal of Power Sources* (Vol. 81). https://doi.org/10.1016/S0378-7753(99)00246-3

[37] Park, N. R., Li, Y., Yao, W., Zhang, M., Han, B., Mejia, C., Sayahpour, B., Shimizu, R., Bhamwala, B., Dang, B., Kumakura, S., Li, W., & Meng, Y. S. (2023). Understanding the Role of Lithium Borate as the Surface Coating on High Voltage Single Crystal $LiNi_{0.5}Mn_{1.5}O_4$. *Advanced Functional Materials*. https://doi.org/10.1002/adfm.202312091

[38] Ghosh, S., charjee, U. B., Bhowmik, S., & Martha, S. K. (2021). A Review on High-Capacity and High-Voltage Cathodes for Next-Generation Lithium-ion Batteries. *Journal of Energy and Power Technology*, *4*(1), 1–1. https://doi.org/10.21926/jept.2201002

[39] Fu, T., Lu, D., Yao, Z., Li, Y., Luo, C., Yang, T., Liu, S., Chen, Y., Guo, Q., Zheng, C., & Sun, W. (2023). Advances in modification methods and the future prospects of high-voltage spinel $LiNi_{0.5}Mn_{1.5}O_4$ — a review. In *Journal of Materials Chemistry A* (Vol. 11, Issue 26, pp. 13889–13915). Royal Society of Chemistry. https://doi.org/10.1039/d3ta01777j

[40] Armand, M., Axmann, P., Bresser, D., Copley, M., Edström, K., Ekberg, C., Guyomard, D., Lestriez, B., Novák, P., Petranikova, M., Porcher, W., Trabesinger, S., Wohlfahrt-Mehrens, M., & Zhang, H. (2020). Lithium-ion batteries – Current state of the art and anticipated developments. *Journal of Power Sources*, *479*. https://doi.org/10.1016/j.jpowsour.2020.228708

[41] Nie, L., Chen, S., & Liu, W. (2023). Challenges and strategies of lithium-rich layered oxides for Li-ion batteries. In *Nano Research* (Vol. 16, Issue 1, pp. 391–402). Tsinghua University. https://doi.org/10.1007/s12274-022-4707-6

[42] Radin, M. D., Hy, S., Sina, M., Fang, C., Liu, H., Vinckeviciute, J., Zhang, M., Whittingham, M. S., Meng, Y. S., & van der Ven, A. (2017). Narrowing the Gap between Theoretical and Practical Capacities in Li-Ion Layered Oxide Cathode Materials. In *Advanced Energy Materials* (Vol. 7, Issue 20). Wiley-VCH Verlag. https://doi.org/10.1002/aenm.201602888

[43] Park, N. R., Zhang, M., Han, B., Li, W., Qian, K., Nguyen, H., Kumakura, S., & Meng, Y. S. (2024). Understanding Boron Chemistry as the Surface Modification and Electrolyte Additive for Co-Free Lithium-Rich Layered Oxide. *Advanced Energy Materials*. https://doi.org/10.1002/aenm.202401968

[44] Wu, F., Kim, G. T., Diemant, T., Kuenzel, M., Schür, A. R., Gao, X., Qin, B., Alwast, D., Jusys, Z., Behm, R. J., Geiger, D., Kaiser, U., & Passerini, S. (2020). Reducing Capacity and Voltage Decay of Co-Free $Li_{1.2}Ni_{0.2}Mn_{0.6}O_2$ as Positive Electrode Material for Lithium Batteries Employing an Ionic Liquid-Based Electrolyte. *Advanced Energy Materials*, *10*(34). https://doi.org/10.1002/aenm.202001830

Chapter 2 Understanding the Role of Lithium Borate as the Surface Coating on High Voltage Single Crystal $LiNi_{0.5}Mn_{1.5}O_4$

2.1 Introduction

The demand for electric vehicles has increased significantly due to extensive regulations on CO_2 emissions and the rising price of gasoline. However, charging electric vehicles can be inconvenient for customers due to the short mileage per charge and long charging time. To address this issue, many researchers are working on increasing the energy density and fast charging capability of lithium-ion batteries. For energy density improvement, increasing the operating voltage of cathode active material is one of the most effective ways, but challenging. First, regular battery electrolyte suffers severe decomposition during high-voltage operation. Second, cathode active materials such as high nickel $LiNi_xCo_yMn_zO_2$ (x+y+z=1, NCM) are unstable when charged to more than 4.5V, resulting in fast capacity decay and safety issues. Third, the choice of cathode transition metal composition is important. Cobalt is commonly used to improve the stability of cathodes, but its price has risen significantly in recent years. As a result, high voltage cobalt-free spinel material $LiNi_{0.5}Mn_{1.5}O_4$ (LNMO) has attracted attention [1], considering its three-dimensional spinel structure for fast charge/discharge, a high working potential of 4.8 V, and a theoretical capacity of 147 mAh/g [2]. All these advantages enable a significant chance for LNMO to be the cathode active material for next-generation high-voltage lithium-ion batteries.

However, the practical application of LNMO in full cells is yet to be achieved because of the intrinsic high-voltage operation, which results in fast capacity decay during cycling. Several hypotheses have been proposed to explain the fast degradation: 1) When operating at high voltage, the structure change of the cathode itself is intensified. Mn_3O_4-like spinel and rock-salt structures are known to form on and below the surface of LNMO particles due to the migration of transition

metals to tetrahedral (8a sites) and octahedral sites (16c sites). This irreversible structure change initiated transition metals migration/dissolution, increased charge transfer impedance, and severely degraded battery performance [3]. 2) Choi et al. reported that aging of the LNMO electrode was accelerated at high temperature (i.e., 60 ℃) or high voltage due to continuous SEI growth following transition metals redeposition in LNMO/Gr full cell, increasing the surface impedance of the electrode [4]. 3) The capacity fade of the LNMO/Gr full cell resulted from lithium inventory loss. Since active lithium is used to continuously form an interphase in the LNMO/Gr full-cell system, the amount is continuously depleted, which eventually affects the long-term cycle [5]. 4) Moreover, the standard electrolyte consisting of organic carbonate solvent and $LiPF_6$ salt is unstable at operating potentials above 4.5 V. The electrolyte decomposition severely triggered the degradation of LNMO/Gr full cell [6].

Several methods have been verified to improve the cycling performance of LNMO/Gr full cells. First, many strategies have been explored in designing high-voltage electrolytes, including different electrolyte additives. These additives could facilitate stable CEI and SEI, which helped stabilize active materials and prevent dramatic capacity degradation. Cho et al. successfully demonstrated succinic anhydride (SA) and 1,3-propane sultone (PS) additives for improving the electrochemical performance of LNMO/Gr full cells [7]. They proposed that SA and PS could control the swelling behavior of LNMO/Gr cells because of the increased stability against oxidation on the cathode side and robust SEI on graphite. High salt concentration electrolytes (HCE) [8] and ionic liquids [9] have also been explored for high-voltage systems, but both suffer from high viscosity and poor wettability with thick electrodes. The replacement of carbonate-based solvents with fluorinated-based [10], sulfone-based [11], or nitrile-based [12] solvents has also been demonstrated, as these solvents typically have very high oxidation stability. However, the

practical implementation is challenging due to their expensive price, high viscosity, and low ionic conductivity, which make them difficult to use in practical cells. Second, different LNMO cathode modification methods, including doping and particle size optimization. It was proposed that the dopants could stabilize the LNMO structure, therefore decreasing transition metal dissolution and surface phase change. Okudur et al. doped the LNMO surface with Ti and annealed it in an oxygen atmosphere, resulting in an increase in the Ni-Mn ordering degree of doped LNMO with increasing annealing temperature [13]. Interface stability can be improved with developed intrinsic properties by changing the chemical composition design material of the cathode. Chen et al. synthesized $LiNi_xMn_{2-x}O_4$ ($0.3 \leq x \leq 0.5$) single-crystal samples using molten salt and changed the chemical composition. As a result, the ordering/disordering transition of spinel is affected by the chemical composition. The change in Mn^{3+} content can be induced by optimizing the Ni/Mn ratio through various chemical compositions [14]. Liang et al. used a nickel-manganese compound with a low Mn^{3+} and impurity content as a precursor for the synthesis of LNMO due to the compound's highly crystalline spinel structure [15]. Last, the surface coating has been applied to improve the electrochemical performance of LNMO/Gr full cells. Different coating chemistries have been verified, such as oxides (Al_2O [16], ZnO [17], and Bi_2O_3 [18]), phosphate [19,20], and borate [21,22] on the cathode. With all these surface coatings, different improvement mechanisms have been proposed. Gong et al. [21] reported that electrolyte corrosion could be prevented by coating Li_3BO_3 on LNMO using the wet-chemistry method. They claim that the structural stability increases because of the low Mn^{3+} and O vacancy after coating. Roh et al. [22] reported that the Li_2O-$2B_2O_3$ coating is effective for high-temperature cycling. They mentioned that the coating layer could control the organic CEI layer growth even at high temperatures. Sheen et al. [23] reported that coating the surface of spinel lithium manganese oxide with LBO glass through the

solid-state method resulted in good cycle performance. They stated that the improvement was due to reducing the contact with the electrolyte through the physical coating. A literature summary of surface modification on LNMO with different coating materials or methods is shown in **Table 2.1**, along with the proposed mechanism and results.

Table 2.1: Literature summary of coating layer stature after cycling using surface-modified LNMO for LIBs.

Author (Year)	Material	Synthesis method	Improving mechanism	Coating status after cycling	Ref.
Oh et al. (2003)	ZnO	Sol-gel	Formation of the graphitic surface phase, hindering the Li migration	X	[31]
Sun et al. (2011)	Carbon	Sol-gel	Mechanically surface protection	Not mentioned	[32]
Xiao et al. (2014)	CuO	Co-precipitation	Mitigating lithium inventory loss	Not mentioned	[33]
Cabana et al. (2014)	$LiAlO_2$	Atomic layer deposition	Physical barriers against side reactions at the electrode-electrolyte interface	Not mentioned	[34]
Cabana et al. (2014)	MgO	Solid-state	Controlling cathode structure change	Not mentioned	[35]
Kim et al. (2014)	SiO_2	Co-precipitation	Graphite SEI growth control	Not mentioned	[36]
Zhang et al. (2015)	Carbon	Solid-state	Mitigating surface phase change	Not mentioned	[37]
Meng et al. (2015)	TiO_2 and Al_2O_3	Atomic layer deposition	Prevention of electrolyte side reactions	TiO_2-50Cy Al_2O_3-15Cy	[38]
Choi et al. (2016)	Carbon	Mechanofusion	Graphite SEI growth control	Not mentioned	[39]
Jung et al. (2017)	RuO_2	Wet-chemical route	Controlling cathode structure change	Not mentioned	[40]
Lin et al. (2020)	AlF_3	Sol-gel	Protecting from corrosion or suppressing the electrolyte decomposition	Not mentioned	[41]
Lethien et al. (2021)	Li_3PO_4	Atomic layer deposition	Mechanically surface protection	X	[42]
Meng et al. (2022)	Al_2O_3	Atomic layer deposition	Controlling cathode dissolution	After 300cy	[43]
This work	$LiBO_2$	Solid-state	Acting as an LBO reservoir to control cycle degradation via HF scavenging	X	

However, several questions must be tackled regarding the surface-coated LNMO: 1) How can the surface coating uniformity be evaluated? 2) is there any change in the surface coating after long-term cycling, and would the change influence the components such as the cathode, electrolyte, and anode? 3) how would the surface coating correlate to improved performance?

This study modified the LNMO surface by dry mixing the material with an organic nano-sized boron precursor. The surface coating quality was systematically checked using backscattered scanning electron microscopy (BSE-SEM) and electron energy loss spectra (EELS) from scanning transmission electron microscopy (STEM). It was found that $LiBO_2$ was uniformly distributed on the single-crystal LNMO particle surface, which remarkably improved the cycle stability of LNMO/Gr full cells with 3 mAh/cm^2 areal capacity. The mechanism was thoroughly investigated using advanced characterizations including SEM, XRD, X-ray photoelectron spectroscopy (XPS), ^{19}F-Nuclear magnetic resonance spectroscopy (NMR), Inductively coupled plasma mass spectrometry (ICP-MS), STEM-EELS. We found that the coating acts as an LBO reservoir to mitigate capacity degradation via HF scavenging rather than physically protecting the surface of the cathode during cycling. These results may facilitate the design of the surface coating layer for high-voltage cathode materials and the application of electrolyte additives.

2.2 Material and Methods

2.2.1 Sample Preparation

A pristine LNMO sample was provided by Umicore. For coating material synthesis, we added 0.03 mol of Polyvinylpyrrolidone (PVP) (MW=50,000) to 100 mL of Tetraethylene Glycol (TTEG). The remaining PVP in the solution was properly dissolved. We added 0.015 mol of LiOH H_2O and waited until it dissolved and added 0.015 mol of H_3BO_3 and then raised the heat to 80

℃. After 2 hours of reaction, let it naturally cool, then wash it in ethanol 7 times. After removing moisture in an 80 ℃ vacuum oven for a day, grind it finely using a mortar and pestle, and finally, use a ball mill to make it small at 500 rpm for 5 hours with ethanol. Dry again in a vacuum oven at 80 ℃ for a day and grind with a mortar and pestle. Measure $LiBO_2$ suitable for 2wt% in a weight ratio of cathode and physically mix the cathode with a Thinky Mixer (Thinky Corporation) at 2000 rpm for 10 minutes. Put the well-mixed powder into the furnace, set the temperature raising condition to 600 ℃ at 5 ℃ per hour, and maintain it at 600 ℃ for 10 hours, and the same temperature condition as raising the temperature to lower the temperature to room temperature (20 ℃). After calcination, the powder is evenly ground using a mortar and pestle for about 10 minutes. FEI Apreo® was applied with 5 kV as the accelerating voltage and 0.1 nA as the beam current for the SEM analysis. We applied a backscattered electron imaging technique to verify the uniformity of the $LiBO_2$ surface coating layer on single-crystal LNMO, especially for large-area coating uniformity evaluation. The microscope detector was first changed to backscattered mode, which was extremely sensitive to backscattered electrons. Then, the accelerated voltage was lowered to detect the surface information well. The contrast gradually appeared when lowering the accelerated voltage from 5 kV to 200 V, while the optimized voltage was 500 V to 1000 V to acquire clear images.

2.2.2 Electrode Preparation

To evaluate the electrochemical performance of LBO-coated LNMO, electrodes using uncoated and LBO-coated LNMO were prepared, with SPC65 (carbon black, TIMCAL Ltd.) as the conductive agent and HSV900 (PVDF, Arkema Inc.) as the binder, in a mass ratio of 90:5:5 and a cathode loading of 3 mAh/cm^2. The mix was then well dissolved in a proper amount of N-

methyl-2-pyrrolidone (NMP, ≥ 99%, Sigma-Aldrich) and mixed with a Thinky Mixer to form the slurry. The slurry was cast onto Al foil and dried at 80 ℃ in a vacuum oven overnight, followed by 1 h of 120 ℃ drying at elevated temperature. The electrode was punched into cathode discs with a 12.7 mm diameter and a loading of active mass around 24 mg/cm^2. For LNMO/Gr full cells, both CR2032 and pouch cells were assembled. The graphite electrode used in this work is provided by NIMTE with an active mass ratio of 94%. For CR2032 full cells, the graphite electrode was punched into anode discs with a 13 mm diameter, and the designed N/P ratio was around 1.1. For pouch-type full cells, the cathode size was 44 × 30 mm, and the anode size was 45 × 32 mm. For all the cells, Celgard 2325 was used as the separator. 1M $LiPF_6$ in EC: EMC = 3:7 (vol%) was obtained from Gotion, USA, and is denoted as baseline electrolyte in the following sessions. All the coin cells were assembled in the Ar-filled glovebox with moisture control (H_2O < 0.5 ppm), and 50 μl of electrolyte was used for each coin cell. The pouch cells were first assembled in the atmosphere without electrolytes. Afterward, the pouch cell was moved to a heating tray inside the glovebox antechamber and dried at 80 ℃ overnight under vacuum before the electrolyte injection. After drying, the dry pouches were moved inside the Ar-filled glovebox without air exposure, and 500 μl of electrolyte was injected into each cell. The pouch cells with electrolytes were vacuum-sealed inside the glovebox and moved out for further testing.

2.2.3 Electrochemical Performance Evaluation

After assembling, the coin cell(CR2032) and pouch cell full cells were evaluated by cycling them at a rate of C/3 (where 1C is 147 mA/g) after two formation cycles at C/10. The electrochemical performances of all the cells were tested at room temperature either by Neware

Battery Test System (Neware Technology Ltd., China) or Arbin BT2000 instruments (Arbin instrument, USA).

2.2.4 Characterization

The cycled cells were disassembled in the glovebox to prevent air exposure. After long-term cycling, the cycled glass fiber became sticky to graphite, so a surgical blade separated most of them and scratched the residual fiber from the graphite side. XPS analysis was performed using a Kratos AXIS Supra. All the cycled electrodes were prepared without washing, and the transfer process was air-tight to avoid any possible degradation. The XPS was operated using an Al anode source at 15 kV with a 10^{-8} Torr vacuum level. All XPS measurements were collected using an auto-neutralizer during acquisition. Survey scans were collected with a 1.0 eV step size, followed by high-resolution scans with a step size of 0.1 eV. All the data were calibrated using a C 1s peak at 284.6 eV. ICP-MS analysis was performed with a Thermo iCAP RQ ICP-MS to analyze the elemental concentration in fresh and cycled electrolytes. ^{19}F-NMRs were conducted on electrolytes to analyze the salt species in the electrolyte. The ^{19}F-NMR measurements of the electrolyte samples were performed with a Jeol ECA 500 spectrometer. Liquid NMR samples were prepared by adding 10 µL of electrolyte to 600 µL of DMSO-D6 solution, and 50 µl of α, α, α-Trifluorotoluene was added to each sample as the reference and sealed in an NMR tube inside the Ar-filled glovebox for further measurement. The NMR spectrums were analyzed with MestReNova. All spectrums were calibrated with α, α, α-Trifluorotoluene at −63.72 ppm. TEM analysis was performed on a field emission gun JEOL2800 at 200 kV with Gatan OneView Camera (full 4k × 4k resolution). STEM and EELS were performed on primary particles at the annular dark-field (ADF) mode using a JEOL JEM-ARM300CF at 300 kV, equipped with double

correctors. EELS spectra presented in this work were acquired from areas without pre-beam irradiation to minimize possible electron beam irradiation effects.

2.3 Results and Discussion

2.3.1 Optimization and Characterization of LBO Surface Coating

To better image the surface coating substances, the accelerating voltage in BSE mode was tuned, and the related results are shown in **Figure 2.1**. Backscattered mode detects the backscattered electrons, sensitive to atomic mass. The minimal voltage is 200 V (**Figure 2.1(f)**), but it is not suitable for more accurate observation of the surface. The optimized voltage is 500V (**Figure 2.1(e)**) for the surface coating layer differentiation from the LNMO.

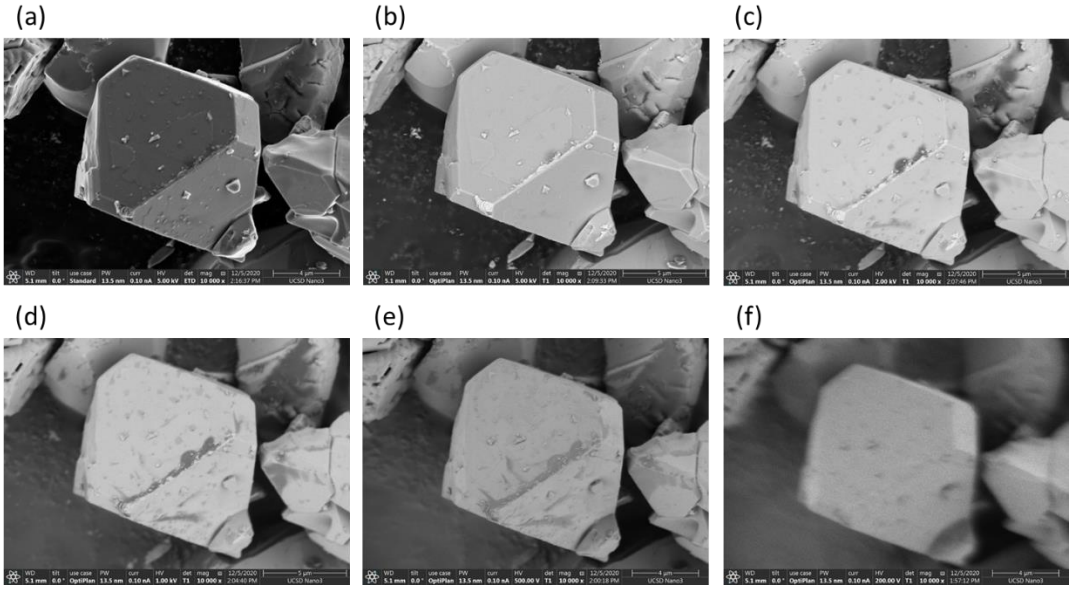

Figure 2.1: Optimization of the voltage with BSE mode: (a) standard mode/5kV (b) backscattered mode/5kV (c) backscattered mode/2kV (d) backscattered mode/1kV (e) backscattered mode/500V (f) backscattered mode/200V.

Then, the surface coating process was optimized based on coverage and uniformity. The mixing time and sintering conditions were identified as influencing factors, and the results are listed in **Figure 2.2.** The coating process and calcination conditions are described in detail in the experiment session. Nano-sized black dots are uniformly distributed around the single crystal at 450 ℃ but the black dot amount was reduced at 600 ℃. When the temperature rises to 700 ℃, large black dots are generated on the surface. So, 600 ℃ is the optimized temperature for LBO coating on the LNMO surface. For checking the coating uniformity according to the dwell time, the minimum contrast is shown when the temperature is maintained for 10 hours (**Figure 2.2(f)**).

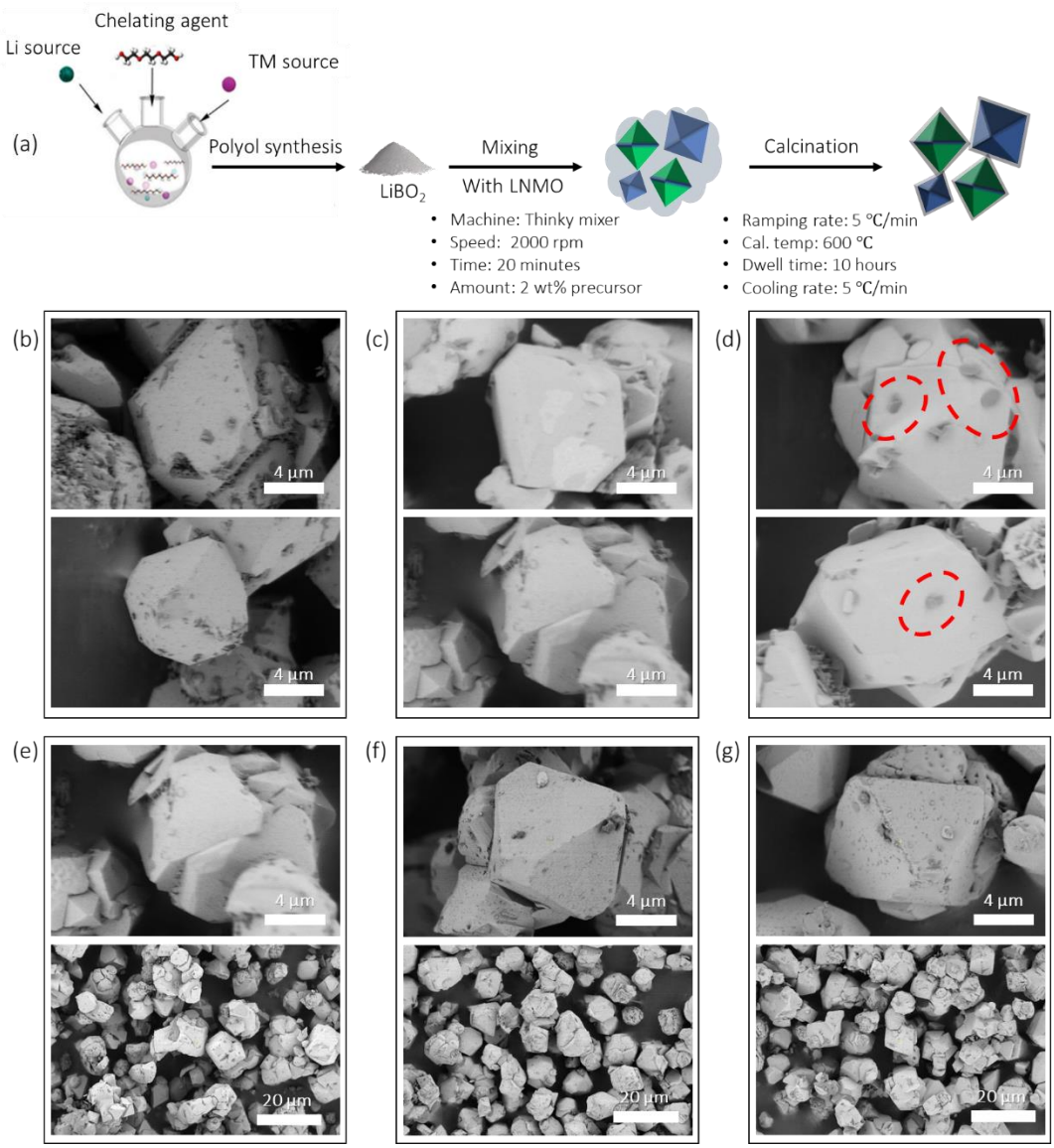

Figure 2.2: (a) Material preparation process, LBO-coated LNMO after calcination with different temperatures: (b) 450 ℃ (c) 600 ℃ (d) 750 ℃ (dwell time: 5h) and with different dwell time: (e) 5h, (f) 10h, and (g) 20h (dwell temperature: 600 ℃).

After optimization, the LBO-coated LNMO sample was synthesized with 10 g per batch for subsequent evaluation.

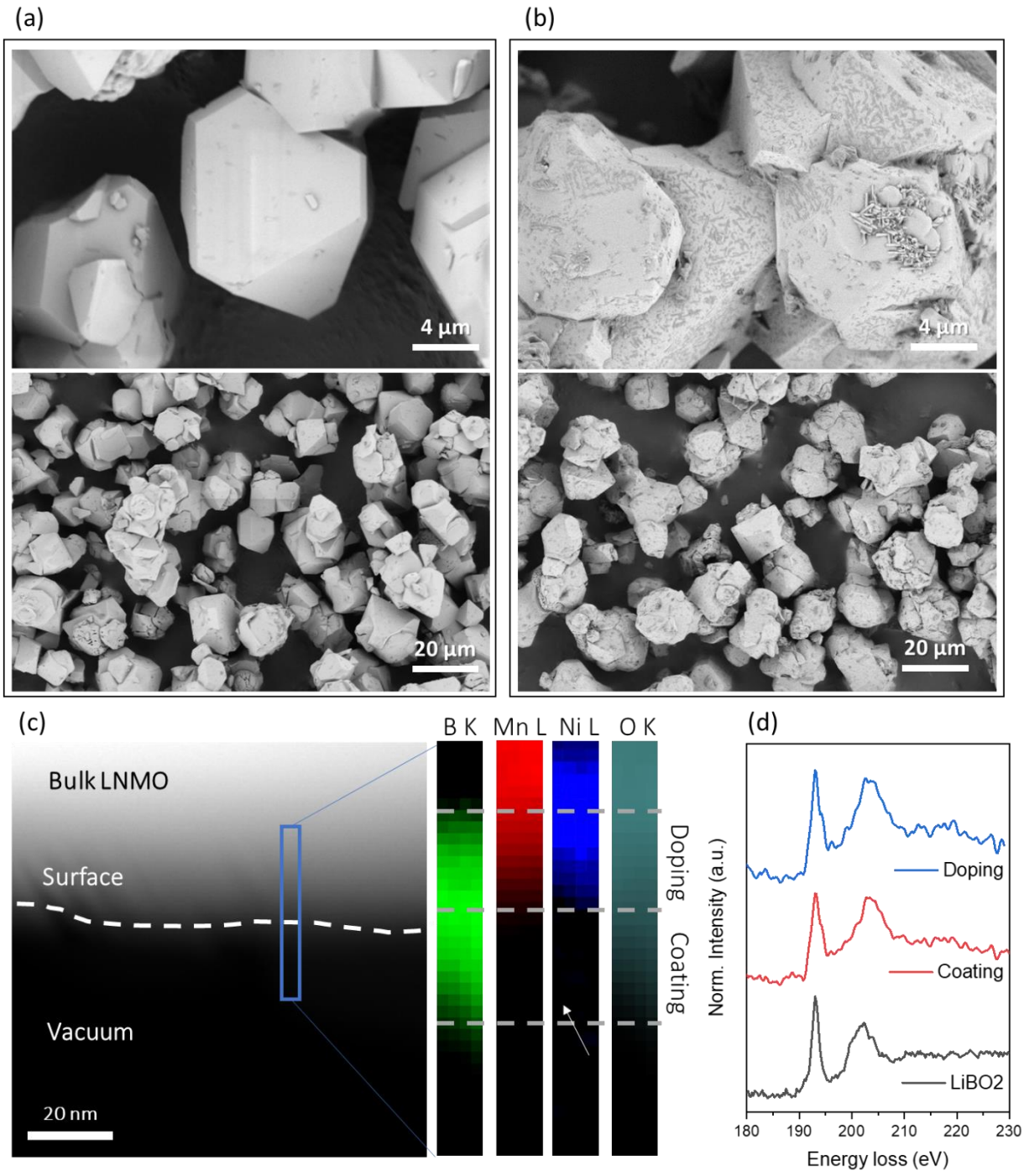

Figure 2.3 BSE images of (a) uncoated and (b) LBO-coated LNMO with the corresponding large views; (c) STEM-EELS mapping results of LBO-coated LNMO sample; (d) EELS spectra of boron corresponded to different locations.

As shown in **Figure 2.3,** the uncoated LNMO showed uniform light grey color under BSE mode, and the particle size is ~6-8 microns with typical single-crystal morphology. The uniform black dots can be observed from the LBO-coated LNMO powder in **Figure 2.3(b)** due to the surface coating substances with low atomic mass (borate species). We took low-magnification images with the same BSE mode and low accelerating voltage for large-scale coating uniformity evaluation. No dark agglomeration areas were observed, showing that low atomic mass species were well dispersed during the surface coating process.

We used STEM coupled with EELS mapping and spectra analysis to identify the chemical information of the boron coating, as shown in **Figure 2.3(c) and (d).** The boron layer distribution was comprehensive. For the surface part, the boron layer without Nickel/Manganese on the LNMO surface was identified, suggesting that it was a coating layer. At the same time, the boron overlap area with Nickel and Manganese was observed, suggesting that surface doping also occurred. The results indicate that boron coating can coexist with transition metal ions and act as a surface dopant. The Nickel signal is attenuated by the atomic ratio, and the thickness of the sample would additionally diminish the Nickel signal. **Figure 2.3(d)** indicates that the $LiBO_2$ surface dopant creates boron sites in a tetrahedral oxygen environment, as the energy loss peak position and shape are consistent with those of LBO coating materials. This suggests that $LiBO_2$ maintains its own phase without phase transition for coating and doping. Note that STEM-EELS was performed rather than EDS since boron is a light element that could hardly be excited with enough X-ray through the EDS detector. More results are shown in **Figure 2.4**. The consistent results showed that the boron element can be detected at a surface region like positions 1 and 2 but disappears at position 3 as the sub-surface. As for Mn and Ni chemical environment, the EELS spectra indicated

negligible changes. Therefore, the $LiBO_2$ surface coating layer on the LNMO was physically and chemically identified.

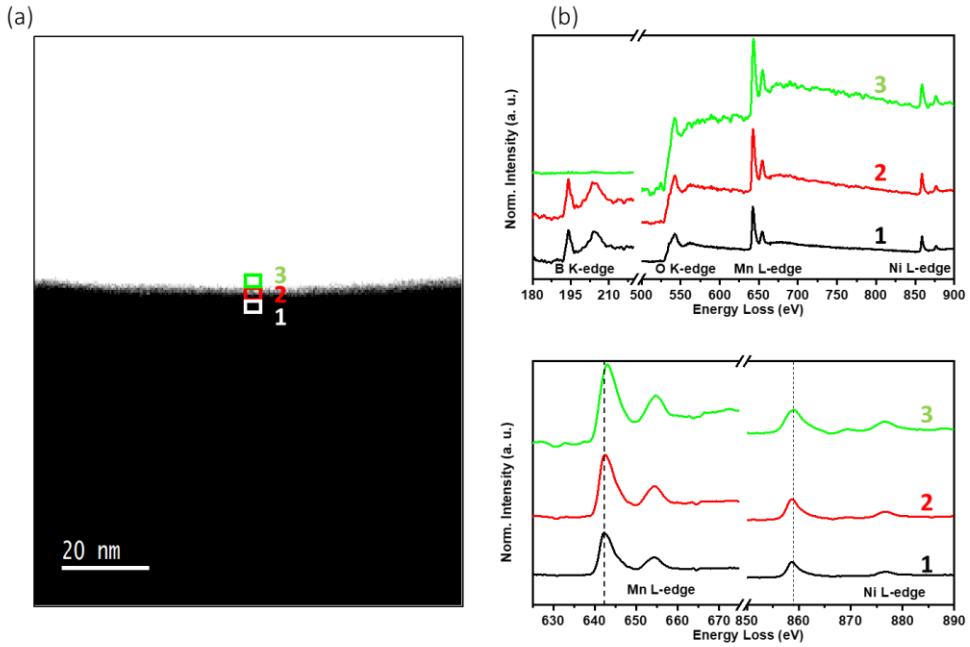

Figure 2.4: (a) Different EELS regions from one particle surface; (b) Related EELS spectra from regions in (a).

2.3.2 Enhanced Cycling Stability of LBO-Coated LNMO in Full Cells

Full cells were assembled using uncoated LNMO and LBO-coated LNMO, and graphite was used as the anode. As shown in **Figure 2.5**, the capacity retention after 1000 cycles is 18.1% for the uncoated LNMO and 46.1% for the LBO-coated LNMO. The uncoated LNMO shows a steep cycle slope up to around 70 cycles in the beginning, followed by a large capacity drop in this interval and then an abrupt cycle degradation up to around 300 cycles. In contrast, the LBO-coated LNMO shows slower degradation at the beginning, followed by a stable cycle slope after 100 cycles and a stable 99.9% coulombic efficiency. It can be inferred that the side reaction with the electrolyte is minimized due to the borate coating layer. However, even LBO-coated LNMO

experiences a drop in capacity retention within the initial 100 cycles. This phenomenon is primarily attributed to two main reasons. First, the full cells exhibit an initial phase stabilizing both the cathode and anode interphase. An early cycle retention drop is commonly observed in the full cell cycle performance. Secondly, this behavior is also attributed to the inherent characteristics of LNMO. LNMO is known to have poor long-term cycling performance, starting with a low initial coulombic efficiency and a continuous degradation in efficiency. LBO-coated LNMO, while releasing LBO during cell operation, experiences ongoing degradation due to side reactions initiated by the electrochemical reaction of the carbonate baseline electrolyte at high voltage. Nevertheless, the dissolved LBO serves to alleviate the extent of degradation as cycling progresses. **Figure 2.5 (b)** also shows that the LBO-coated LNMO has a more stable charge/discharge voltage from the beginning, demonstrating its improved performance.

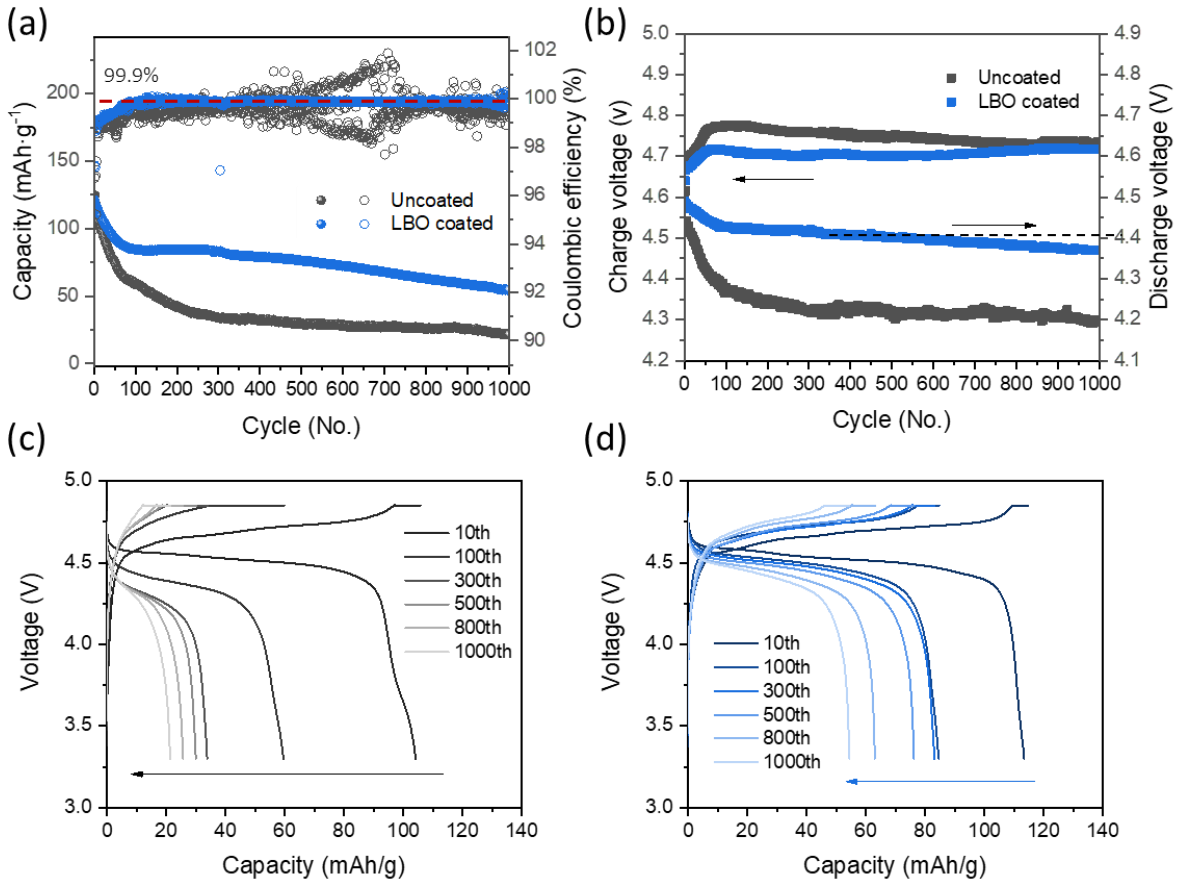

Figure 2.5: (a)Full cells cycling performances with (b) the corresponding average charge/discharge voltage; the charge/discharge profiles of different cycles from (c) uncoated and (d) LBO-coated LNMO full cell.

The results of cycling at room temperature, as well as at elevated temperatures (45 ℃), demonstrate that LBO-coated LNMO exhibits a consistently stable initial slope even at higher temperatures (**Figure 2.6 (a)**). This is further corroborated by the remarkably stable average discharge voltage plot (**Figure 2.6 (b)**). **Figure 2.5 (c) and (d)** show the charge-discharge profiles of uncoated and LBO-coated LNMO full cells. The charge plateau of uncoated LNMO cells shifts to a higher voltage region while the discharge plateau shifts to a lower region, suggesting an increase in internal impedance, while both the charge and discharge capacity drop quickly, which implies fast active lithium inventory loss.

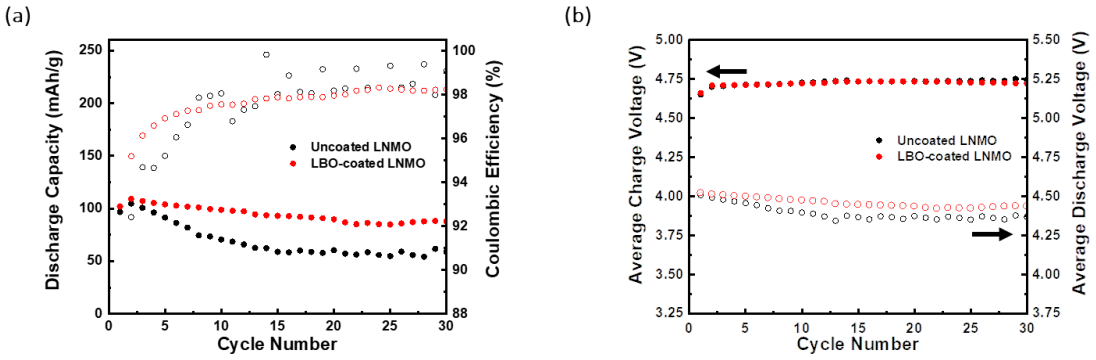

Figure 2.6: (a) Full cell cycling performances with (b) the corresponding average charge/discharge voltage.

The charge and discharge plateau of LBO-coated LNMO shifts much less than the uncoated sample, meaning the LBO coating plays a significant role in controlling the internal impedance. As for the length of the constant voltage (CV) section at 4.85 V, LBO-coated LNMO remained the same with the cycling, while the uncoated LNMO CV section stretched from 100 cycles. The escalation observed in the CV section signifies an elevation in internal impedance. In the context of V=IR, a prolonged CV segment under consistent current cut-off conditions suggests a proportional rise in resistance [24]. This suggests that lithium from the cathode was not sufficiently de-intercalated during charging, resulting in low and unstable coulombic efficiency.

2.3.3 Impact of Boron Surface Coating and Electrochemical Performance

To understand the mechanism of LiF the LBO surface coating can dramatically improve the cycling stability of LNMO/Gr full cells, different characterizations were performed to track boron inside the cells. First, soaking tests were performed with the uncycled electrodes for boron dissolution. The uncoated LNMO and LBO-coated LNMO electrodes were soaked in the fresh electrolyte for 24 hours, and the supernatant was fetched and diluted for the ICP-MS test. The

detailed experiment setup can be found in **Figure 2.6**. As shown in **Figure 2.7**, the $LiBO_2$ coating layer can be partially dissolved by the baseline electrolyte before cycling, resulting in the loss of about 60 wt.% of the total coating mass. The cycled electrodes were also investigated. The soluble boron species are uniformly distributed in the cathode and anode after long-term cycling, as shown in **Figure 2.7 (a)**. Meanwhile, no floating Nickel/Manganese from cycled graphite with LBO-coated LNMO was detected (**Figure 2.7 (b)**). This implies that the boron species mitigated the cross-talk issues between the LNMO cathode and graphite anode.

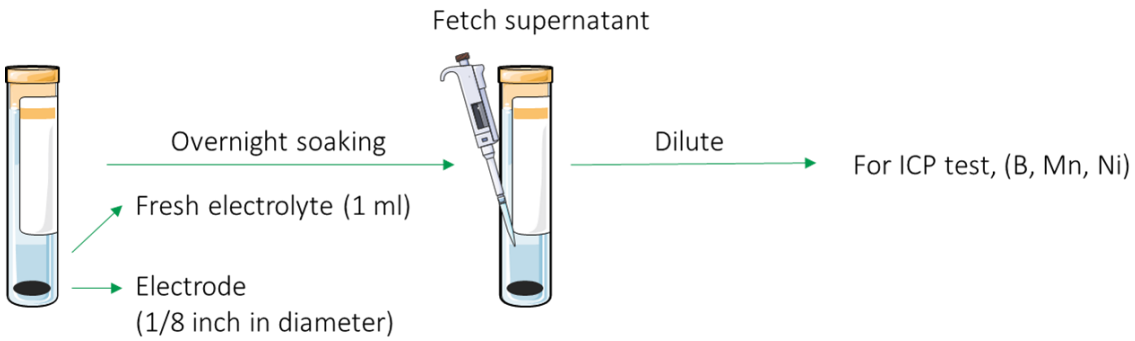

Figure 2.7: Scheme of ICP-MS soaking test.

Second, XPS was performed to understand the chemical status of the interphase, and the results are shown in **오류! 참조 원본을 찾을 수 없습니다.**. After long-term cycling, cathode interphase components were almost the same for both the uncoated and LBO-coated LNMO, except for the minor difference from the P 2p signal. Both samples showed a lattice oxygen peak around 684.5 eV in O 1s spectra, implying a thin cathode electrolyte interphase. The uncoated sample showed an obvious P-F signal, while the LBO-coated sample did not, which may be related to salt residual on the sample surface. 오류! 참조 원본을 찾을 수 없습니다. **(b)** shows the SEI information on the anode, and several distinctive features have been detected. The first one is the

Li-O peak in O 1s spectra, which remained in the graphite paired with the LBO-coated LNMO while not appearing in the uncoated case. This implies that the electrode corrosion is stronger in the uncoated LNMO cell than in the LBO-coated LNMO cell.

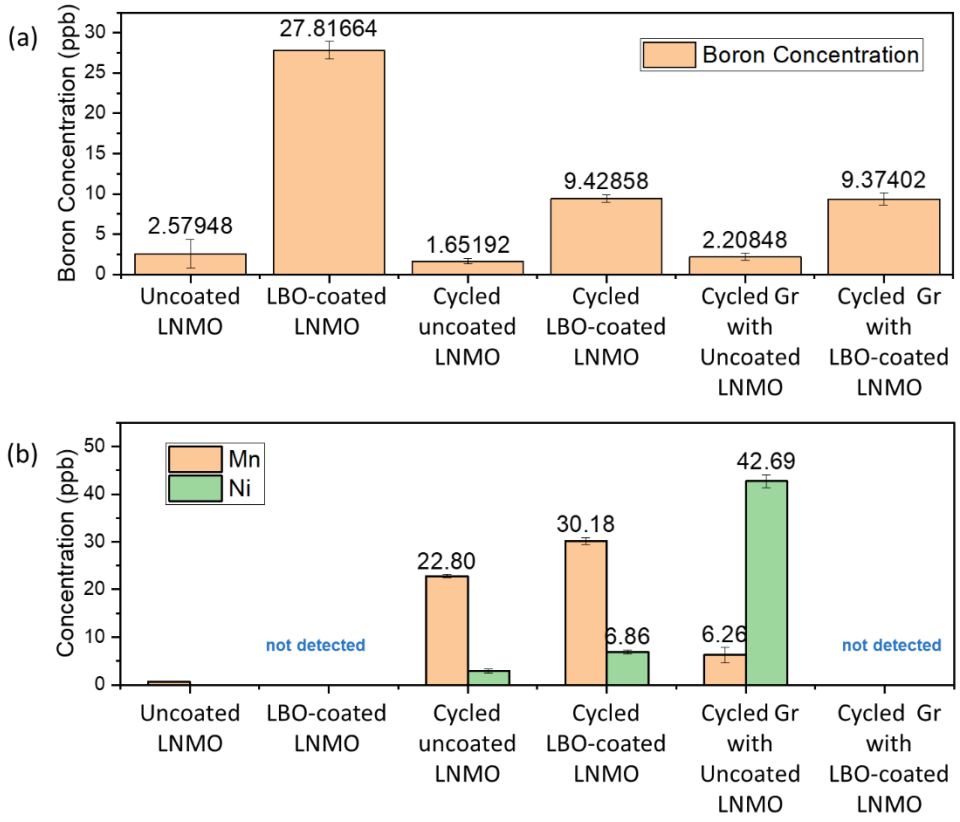

Figure 2.8: ICP-MS analysis: (a) Boron concentration and (b) Transition metal concentration.

The second is the metal-F peak around 684.5 eV in F 1s spectra. The graphite paired with uncoated LNMO showed a stronger peak, which refers to a higher metal fluoride content than the graphite pared with LBO-coated LNMO. The third is the Mn 2p spectra; the graphite with uncoated LNMO has an obvious Manganese signal, while the graphite paired with LBO-coated

LNMO does not, suggesting the cross-talk between cathode and anode in the uncoated cell was stronger than the LBO coated cell. The XPS results are consistent with ICP-MS results.

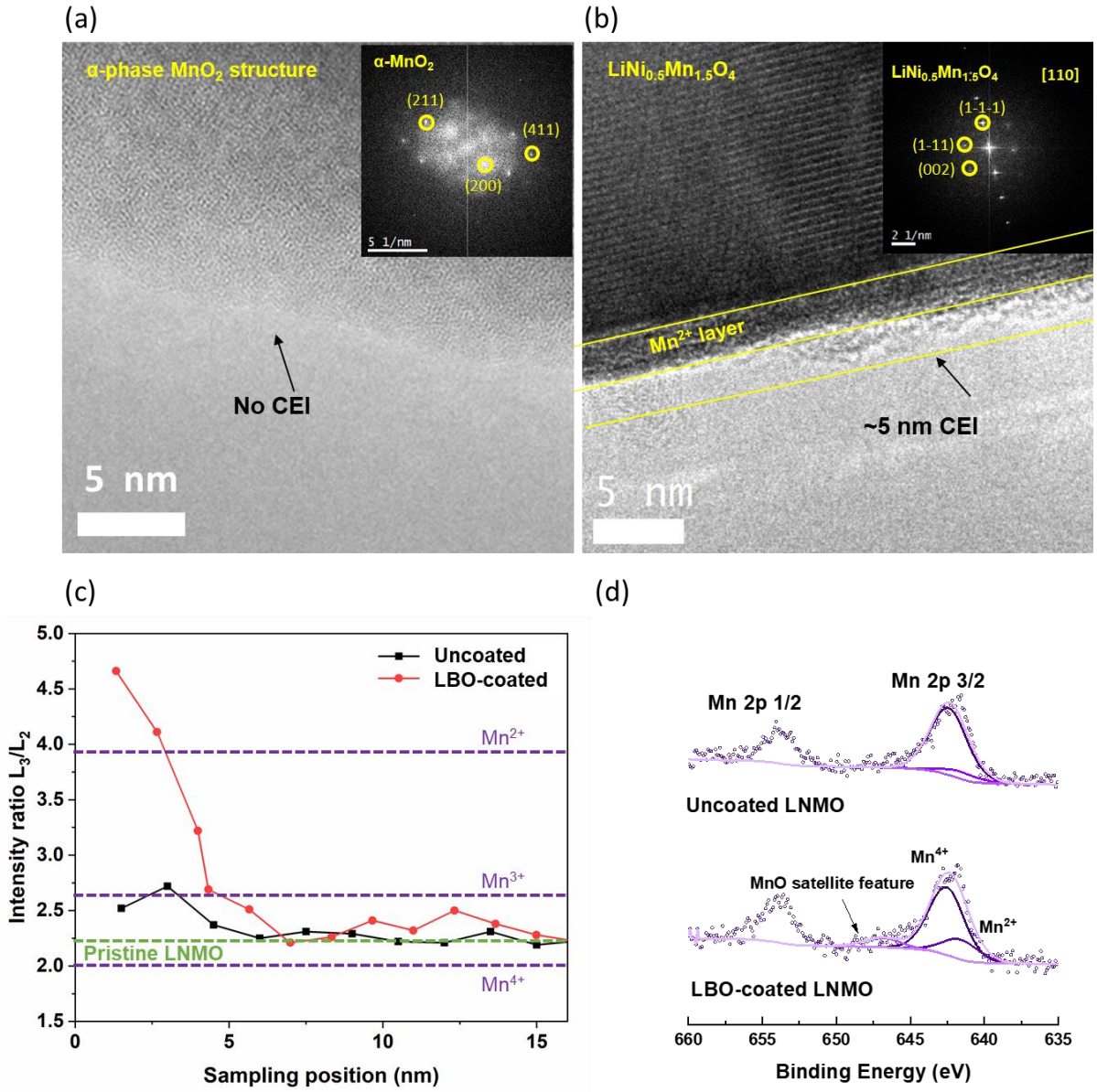

Figure 2.9 TEM with SAED results of (a) uncoated and (b) LBO-coated LNMO after 1000 cycles. (c) EELS Mn Spectra and (d) XPS spectra of Mn 2p of uncoated and LBO-coated LNMO after 1000 cycles.

TEM was performed on the cathode surface to compare the uncoated and LBO-coated LNMO. As shown in **Figure 2.9**, both samples showed degradation on the surface after 1000 cycles. While the uncoated LNMO shows no CEI with severe phase change (**Figure 2.9 (a)**), the LBO-coated LNMO had limited phase change with CEI, and no boron was detected (**Figure 2.9 (b)**). In the case of the uncoated LNMO, the cathode surface was found to be in the disordered MnO_2, as confirmed by both lattice fringe and selected area electron diffraction (SAED), as the [200], [211], and [411] diffraction patterns corresponding to the α-phase MnO_2 structure [25], [26] and the disordered phase were identified. The absence of CEI may indicate severe corrosion from the degraded electrolyte. However, in the case of the LBO-coated LNMO, the bulk structure slightly changed into a more disordered phase but maintained the spinel feature at a thickness of 5 nm, as the [110] diffraction pattern was still observed. This suggests that surface coating with boron can improve long-term cycling by controlling the outermost phase transition and helping to mitigate corrosion from the electrolyte. To further verify the Mn valence on the surface, EELS were performed and the related data are shown in **Figure 2.10**, the intensity ratio of L3 and L2 peaks were calculated as shown in **Figure 2.9 (c)**. After 1000 cycles, Mn^{2+} still exists up to about 3 nm from the surface of LBO-coated LNMO, but no more Mn^{2+} exists in uncoated LNMO. This implies that the transition metal including Mn was dissolved into the electrolyte and induced obvious cross-talk phenomena, further redeposited on the surface of the anode. XPS shown in **Figure 2.9 (d)** confirmed the different Mn valences from uncoated and LBO-coated LNMO surface. For the LBO-coated LNMO sample, a MnO satellite feature (~647 eV) as well as the high Mn^{2+} ratio proved the Mn^{2+} existence [27] as consistent with the TEM and EELS spectra results.

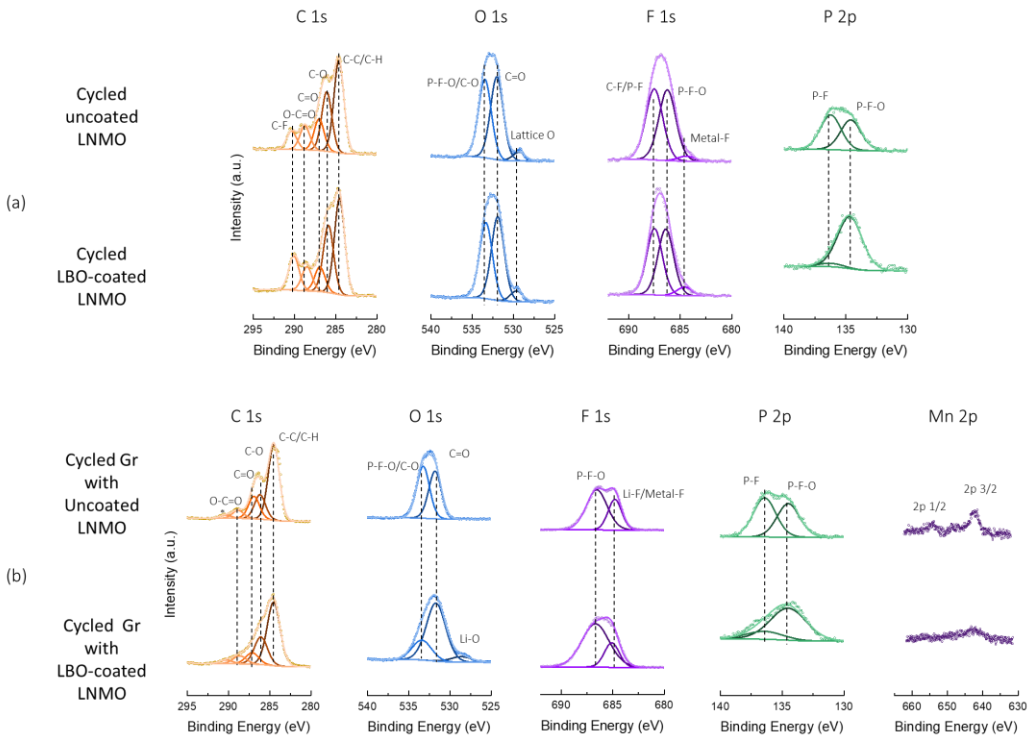

Figure 2.10: XPS spectra of C 1s, O 1s, F 1s, P 2p, and Mn 2p of (a) uncoated and LBO-coated LNMO and (b) graphite anode paired with different cathode after cycling.

Further investigations on the chemical information of boron from the LBO-coated LNMO after 1000 cycles were performed via EELS spectra, as shown in **Figure 2.11**. It could be confirmed that there was no boron signal on the particle, which means that the borate surface coating was completely dissolved/detached from the LNMO surface. The results align well with the previous results, where half of the boron elements would be dissolved into the electrolyte only by soaking overnight. This indicates that the physical separation between LNMO and degraded electrolyte by borate coating needs additional explanations.

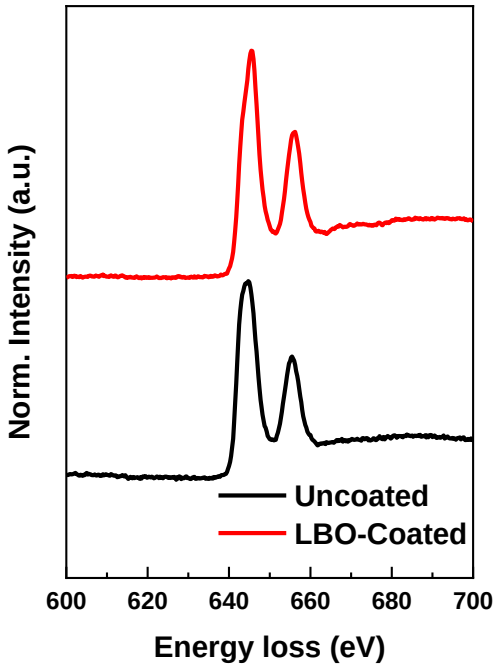

Figure 2.11: EELS spectra of Mn from uncoated and LBO-coated LNMO after cycles.

2.3.4 Effect of Cathode Coating on Anode Surface Reactions and SEI Formation

The presence or absence of coating on the cathode side significantly impacts the chemical reactions occurring in the full cell through the anode. To investigate the cross-talk effect between the cathode and anode, we performed post-mortem SEM and XRD analysis, as shown in **Figure 2.12**.

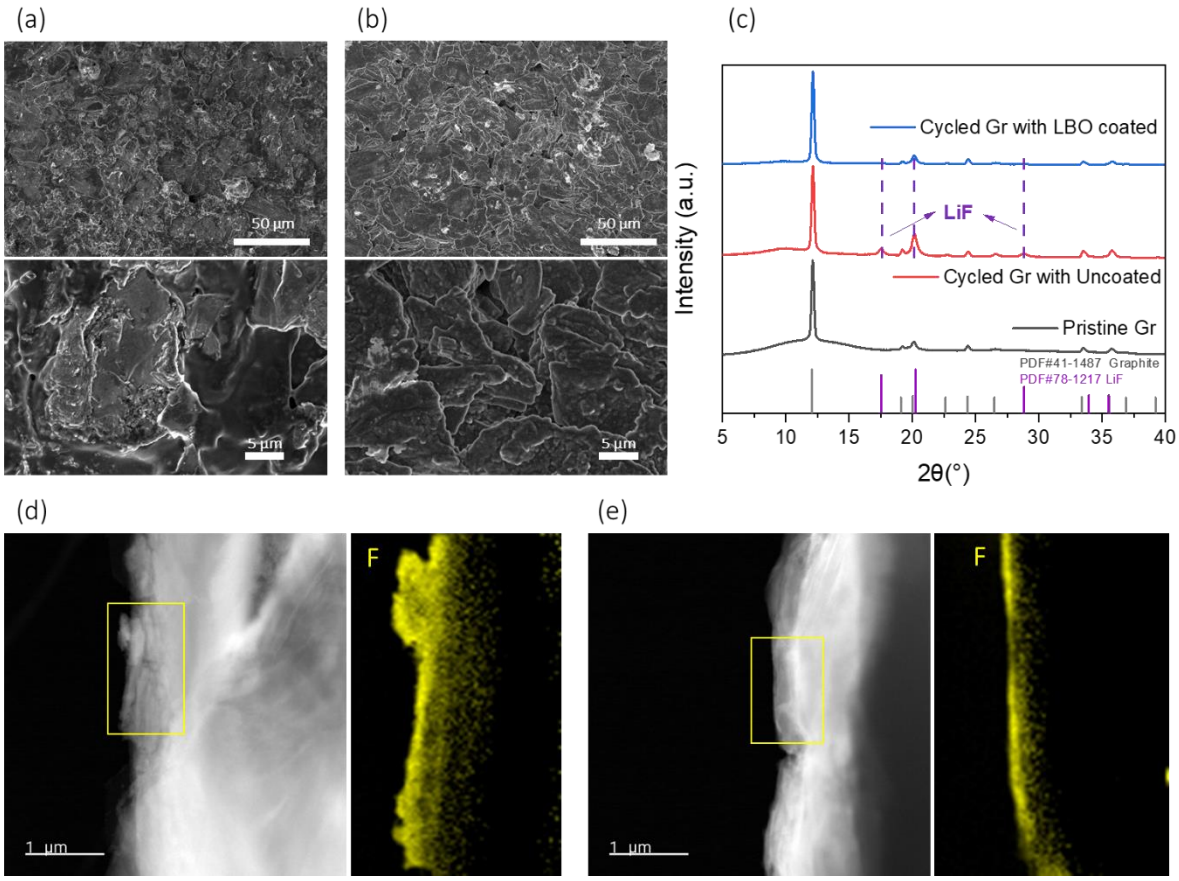

Figure 2.12: SEM images of graphite surface paired with (a) uncoated and (b) LBO-coated LNMO; (c) XRD results of different graphite powders. EELS fluorine (F) mapping graphite paired with (d) uncoated LNMO (after 1000 cycles) and (e) LBO-coated LNMO (after 1000 cycles).

The presence or absence of coating on the cathode side significantly impacts the chemical reactions occurring in the full cell through the anode. To investigate the cross-talk effect between the cathode and anode, we performed post-mortem SEM and XRD analysis, as shown in **Figure 2.12**. The graphite paired with the uncoated LNMO has a larger number of by-products on its surface, covering the graphite particles (**Figure 2.12 (a)**), while the graphite paired with the LBO-coated LNMO has little by-product (**Figure 2.12 (b)**). We further conducted XRD on the collected graphite powder to identify the chemical composition of the by-products. The XRD results identified the presence of crystal LiF with the graphite, as peaks corresponding to LiF are observed

(**Figure 2.12 (c)**). Such a large amount of LiF may result from severe anode SEI corrosion, which consumes active Li and degrades the cycling performance [28], [29]. LiF itself does not induce corrosion in the electrode; rather, the adverse consequences stem from chemical reactions leading to LiF formation, warranting concern. To expound, the high-voltage decomposition reaction between $LiPF_6$ and carbonate-based electrolytes swiftly produces HF and H_2O, culminating in LiF formation. Thus, the substantial presence of LiF within the SEI layer substantiates the heightened activity of the electrolyte decomposition reaction in the full-cell system, signifying a more robust progression of electrode corrosion. EELS fluorine elemental mapping was performed. Graphite paired with uncoated LNMO showed much thicker fluorine layers on the surface than the graphite paired with LBO-coated LNMO, with obvious particle shape (**Figure 2.12 (d)** and **(e)**). Additional images can be found in the supplementary information (**Figure 2.13**). This result is consistent with SEM and XRD results that boron surface coating can alleviate the continuous growth of SEI.

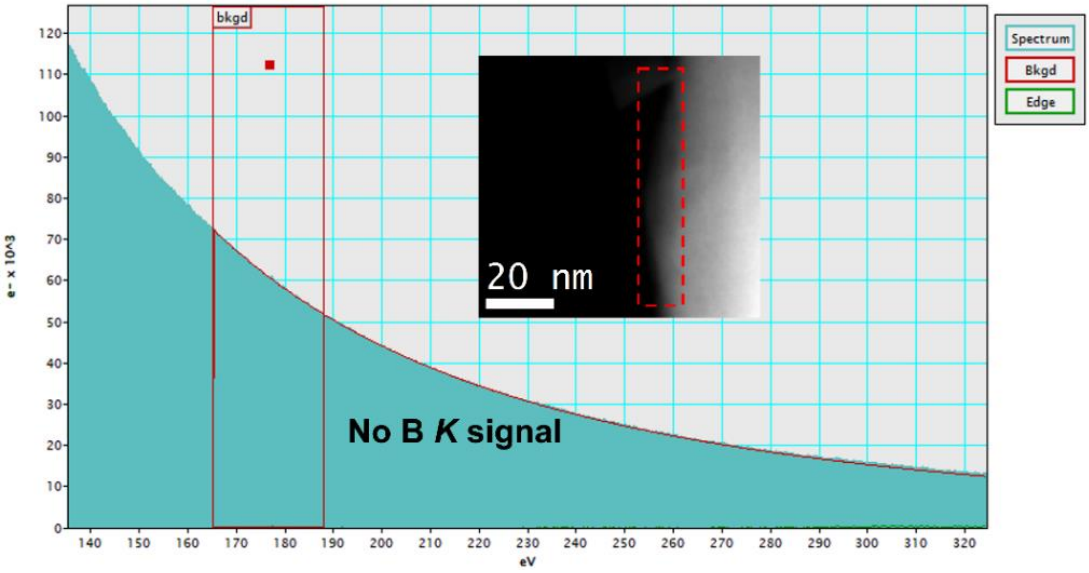

Figure 2.13: EELS of boron from LBO-coated LNMO after 1000 cycles.

2.3.5 Electrolyte Degradation and Transition Metal Dissolution in Pouch Cells

Such obvious differences induced by different cathodes bring up the necessity for electrolyte investigations because the electrolyte is the only media for the cross-talk phenomenon. Therefore, single-layer pouch cells were assembled using the uncoated and LBO-coated LNMO, and the specifications are listed in **Table 2.2**.

Table 2.2: Full cell – pouch cell type specification

	Specification
Material	Cathode: LNMO Anode: NEI Graphite, (BE-200E, NEI Corporation, USA)
N/P ratio	1.15
Voltage range	3.3-4.85 V
Test protocols	Rest for 48 hours after assembling, then C/20 (1C= 147mA/g) for the initial three cycles, then degassing and resealing are performed, then switch to C/10 for one cycle and C/3 for the subsequent cycles.
Separator	Celgard®
Electrolyte amount	1 mL
Pouch bag type	EQ-alf-100-210 (MTI Corporation, USA)
Electrode tab	Cathode tab: EQ-PLiB-ATC4 (MTI Corporation, USA) Anode tab: EQ-PLiB-NTA4 (MTI Corporation, USA)
Fixture	Insulating Plate: polycarbonate Pressure sensor: DYHW-116 Mini Compression Force Sensor Load Cell Indicator: TOKY® accurate micro digital differential pressure gauge

The electrochemical performances of pouch cells are shown in **Figure 2.14 (a)**. LBO-coated LNMO pouch cells showed better cycling performance than uncoated LNMO pouch cells,

which is consistent with coin cells. The pouch cells were disassembled in the glovebox after 50 cycles and then placed into the sealed centrifuge tube for electrolyte collection.

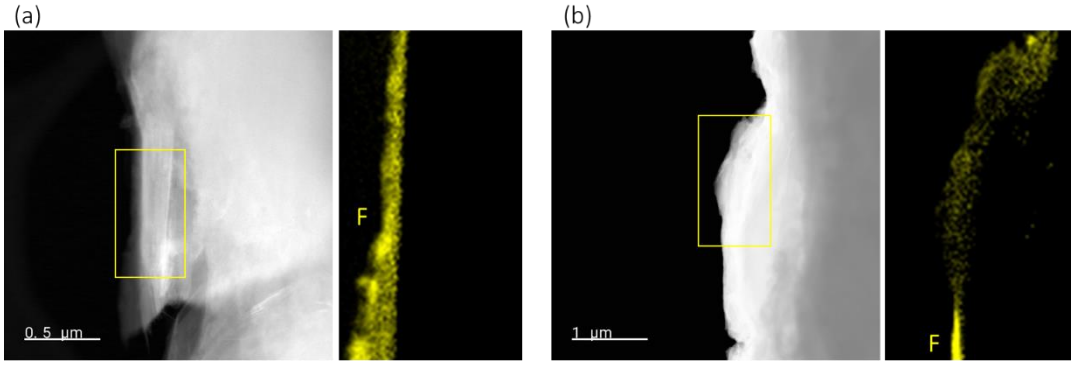

Figure 2.14: EELS fluorine mapping graphite paired with (a) uncoated LNMO (after 1000 cycles) and (b) LBO-coated LNMO (after 1000 cycles).

Another set of identical pouch cells cycled 1 time was prepared as the reference sample, and the electrolytes from these two cells were also collected. The collected electrolytes from different cells are shown in **Figure 2.14 (b)**. The uncoated LNMO consumed more electrolytes than the LBO-coated LNMO, and the color was also much darker, indicating severe decomposition. The collected electrolytes were diluted for ICP-MS and ^{19}F-NMR analysis.

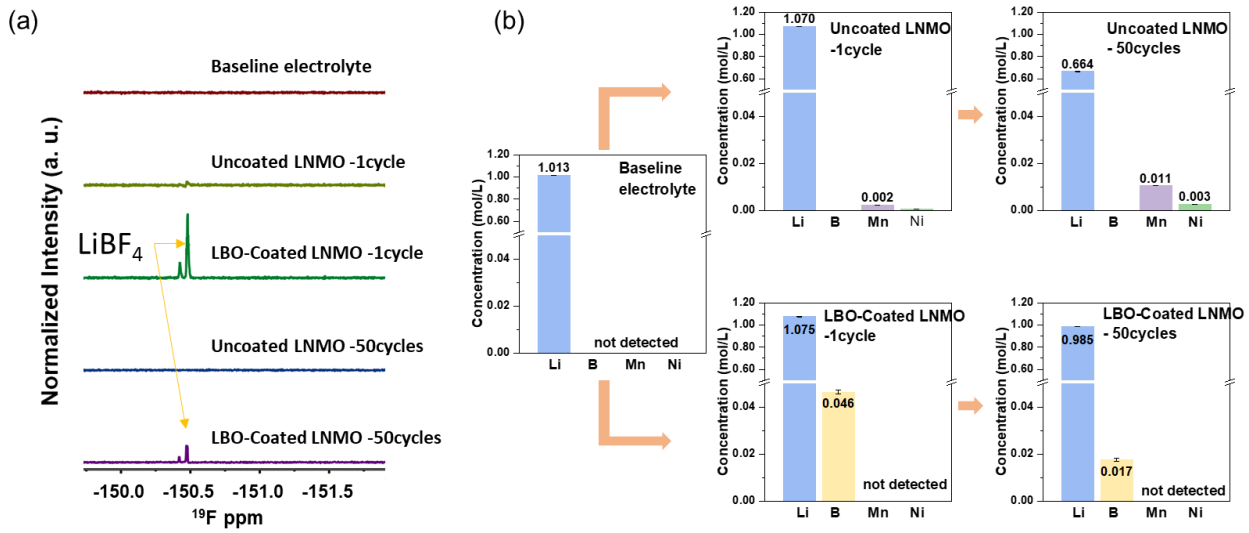

Figure 2.15 (a) ^{19}F-NMR and (b) ICP-MS from different electrolyte samples, including pristine baseline and cycled electrolytes from uncoated/LBO-coated LNMO after 1 cycle and 50 cycles.

To understand the mechanism behind the improved cycling performance of the LBO-coated LNMO, we focused on the dissolution of transition metals and the behavior of boron-related species. Pouch cells were assembled and the electrolyte solutions were collected from the opened cells after different numbers of cycles. The cell's electrolyte was collected after the first formation cycle to identify the degradation mechanism at the beginning of the cycle, and the cells were disassembled after 50 cycles to observe the changes in species over time. The results of ^{19}F-NMR and ICP-MS analysis are shown in **Figure 2.15**.

In the ^{19}F-NMR analysis (**Figure 2.16**), the LBO-coated LNMO is found to contain $LiBF_4$ peaks around -150 ppm after just one cycle at C/3, indicating that the $LiBO_2$ coating layer can be partially dissolved and converted into BF_4^- during cycling. The concentration of boron in the form of BF_4^- decreased after cycling (**Figure 2.15 (a)**) and was uniformly deposited on both the cathode and anode. This suggests that B-F bonding had already been formed even after just one charge/discharge cycle. It is also confirmed that this forms the CEI/SEI layer and is involved in

the cycle degradation mechanism by being dissolved in the electrolyte. If B-F bonding is not formed, the decomposed fluorine will form HF or LiF and accelerate cycle degradation.

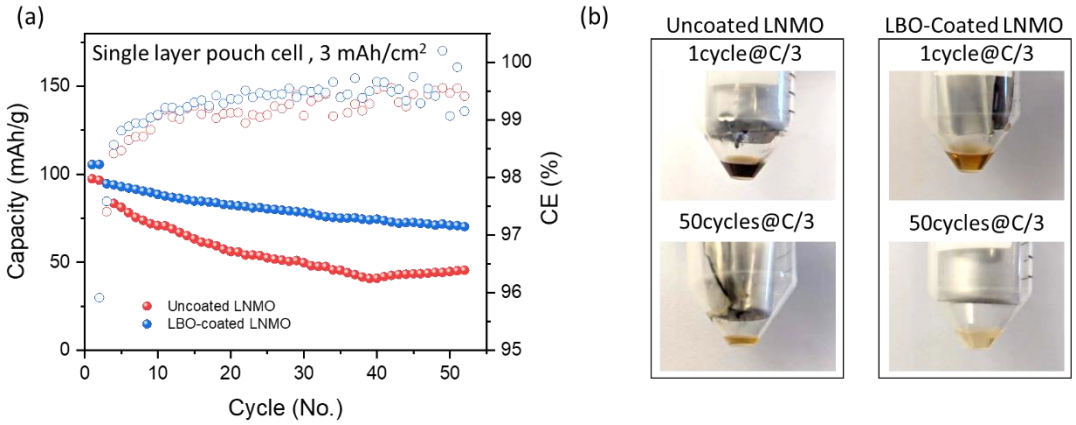

Figure 2.16: (a) Single layer pouch cell electrochemical performance. (b) Electrolyte collected by Centrifuge method.

In the ICP-MS analysis, the uncoated LNMO cell showed significant dissolution of Ni and Mn even after the first cycle at C/3, with concentrations of 12 ppb Ni and 48 ppb Mn after 50 cycles. The lithium concentration in the electrolyte also decreased significantly from the original ~580 ppb to 378 ppb. This indicates a loss of lithium inventory in the electrolyte. In contrast, the LBO-coated LNMO showed Nickel and Manganese concentrations below the detection limit, and the lithium concentration in the electrolyte remained relatively stable after 50 cycles. The boron concentration was also monitored via ICP-MS analysis, and no transition metals were dissolved in the electrolyte of the LBO-coated LNMO pouch cell as the lithium concentration. The amount of lithium after the first formation is almost the same. However, after 50 cycles, it was confirmed that the concentration decreased as more lithium was used for cycle degradation. The boron increased to 41 ppb after 1 cycle at C/3 and dropped to 15 ppb after 50 cycles, showing that the concentration

became lower along with more cycles. The boron species in the electrolyte would be consumed along with the cycling.

2.3.6 Mitigating Cross-Talk and Enhancing CEI/SEI Integrity

The detailed mechanism of boron species helps improve the high voltage cell as shown in **Figure 2.17**. $LiPF_6$ and the solvent are constantly decomposed during high-voltage cycling, generating by-products such as water and HF [6]. The acid will corrode the cathode material as transition metal ions are dissolved and deposited on the anode simultaneously. The degraded electrolyte will also lead to the overgrowth of SEI layers that consume active lithium. However, in the case of the LBO-coated LNMO, borate radicals from the coating layer decomposition can effectively prevent salt decomposition by forming $LiBF_4$ species. The bonding related to boron and fluorine appeared only in the LBO-coated LNMO. The formation energy of BF_4^- (-1710 kJ/mol) is much lower than that of HF (-273 kJ/mol), making this reaction thermodynamically favorable. In addition, the B–F bond (613 kJ/mol) has a higher bond energy than the H–F (565 kJ/mol) and P–F (490 kJ/mol) bonds, meaning that the B-F bond is more stable [30]. As a result, less HF corrosion occurs in the LBO-coated LNMO cell, leading to uniform CEI/SEI. The well-preserved CEI/SEI layers then lead to reduced transition metal dissolution and deposition in the cell, all of which contribute to improved cell cycling stability.

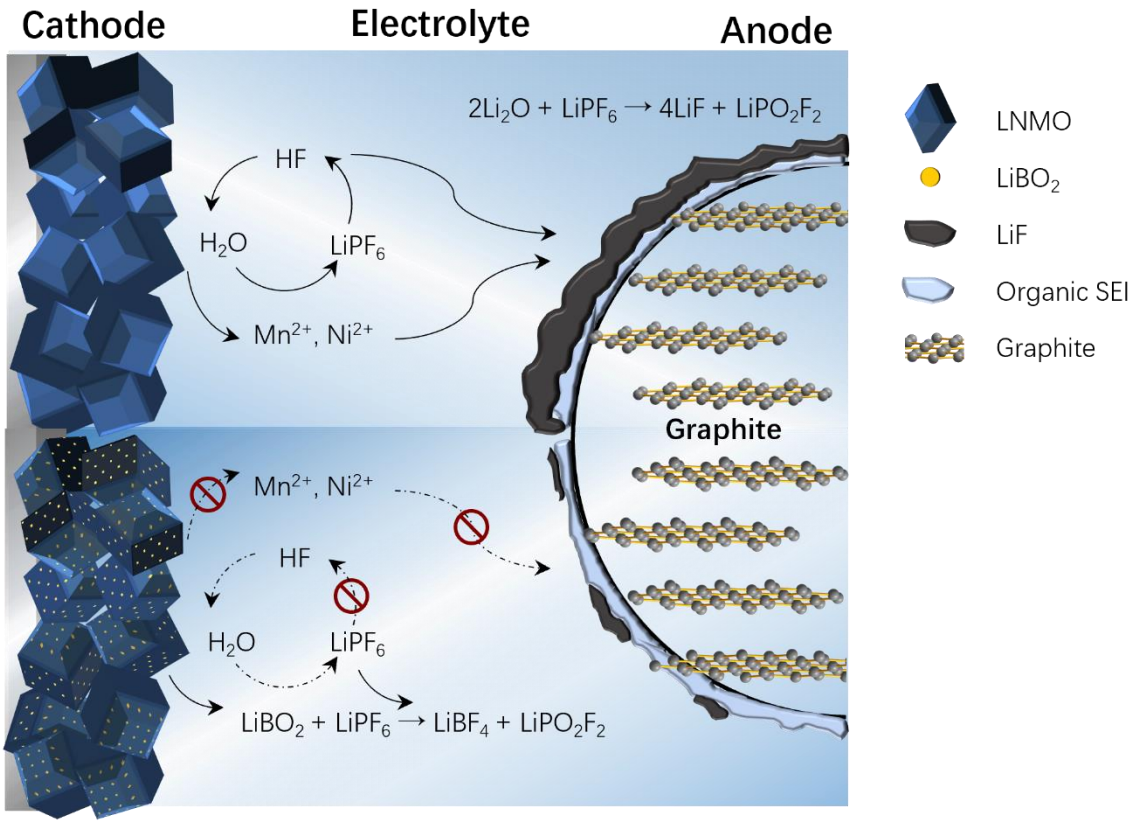

Figure 2.17: Schematics of performance improvement by LBO-coated LNMO in LNMO/Gr full cell.

This process can dramatically prevent salt decomposition. Consequently, the cross-talk phenomena between the cathode and anode were mitigated, and both CEI/SEI were well preserved. We believe these findings can be applied to other high-voltage cathode materials and contribute to the commercialization of next-generation high-voltage LIBs. This work may also inspire future research to stabilize the $LiPF_6$-carbonate-based electrolytes through cathode surface coating and electrolyte additive design.

2.4 Conclusions

LiBO was successfully coated on the surface of single-crystal LNMO cathode materials. The surface coating uniformity was evaluated via BSE-SEM methods, and the related chemical environment of boron species was characterized via STEM-EELS. It was identified that the surface boron species were in nano-sized particles and well distributed on the LNMO surface. Furthermore, the boron elements existed both as surface doping and coating. The electrochemical performances of LBO-coated LNMO were compared with the uncoated sample in full cells for 1000 cycles, and the coated sample outperformed the uncoated one. The surface boron species fully dissolved into electrolytes after long-term cycling. ^{19}F-NMR and ICP-MS results from electrolyte showed that LiBO started to dissolve and turned into $LiBF_4$. This process can dramatically prevent salt decomposition. Consequently, the cross-talk phenomena between the cathode and anode were mitigated, and both CEI/SEI were well preserved. We believe these findings can be applied to other high-voltage cathode materials and contribute to the commercialization of next-generation high-voltage LIBs. This work may also inspire future research to stabilize the $LiPF_6$-carbonate-based electrolytes through cathode surface coating and electrolyte additive design.

2.5 Acknowledgements

Chapter 2, in full, is a reprint of the material as it appears in "Park, N. R., Li, Y., Yao, W., Zhang, M., Han, B., Mejia, C., Sayahpour, B., Shimizu, R., Bhamwala, B., Dang, B., Kumakura, S., Li, W., & Meng, Y. S. (2023). Understanding the Role of Lithium Borate as the Surface Coating on High Voltage Single Crystal $LiNi_{0.5}Mn_{1.5}O_4$. *Advanced Functional Materials*." The dissertation author was the first author of this paper.

2.6 References

[1] Schmuch, R., Wagner, R., Hörpel, G., Placke, T., & Winter, M. (2018). Performance and cost of materials for lithium-based rechargeable automotive batteries. In Nature Energy (Vol. 3, Issue 4, pp. 267–278). Nature Publishing Group. https://doi.org/10.1038/s41560-018-0107-2

[2] Ohzuku, T., Takeda, S., & Iwanaga, M. (1999). Solid-state redox potentials for Li $[Me_{1/2}Mn_{3/2}]O_4$ (Me: 3d-transition metal) having spinel-framework structures: a series of 5 volt materials for advanced lithium-ion batteries. In *Journal of Power Sources* (Vol. 81). https://doi.org/10.1016/S0378-7753(99)00246-3

[3] Liang, G., Wu, Z., Didier, C., Zhang, W., Cuan, J., Li, B., Ko, K. Y., Hung, P. Y., Lu, C. Z., Chen, Y., Leniec, G., Kaczmarek, S. M., Johannessen, B., Thomsen, L., Peterson, V. K., Pang, W. K., & Guo, Z. (2020). A Long Cycle-Life High-Voltage Spinel Lithium-Ion Battery Electrode Achieved by Site-Selective Doping. *Angewandte Chemie - International Edition*, *59*(26), 10594–10602. https://doi.org/10.1002/anie.202001454

[4] Aurbach, D., Markovsky, B., Talyossef, Y., Salitra, G., Kim, H. J., & Choi, S. (2006). Studies of cycling behavior, ageing, and interfacial reactions of $LiNi_{0.5}Mn_{1.5}O_4$ and carbon electrodes for lithium-ion 5-V cells. *Journal of Power Sources*, *162*(2 SPEC. ISS.), 780–789. https://doi.org/10.1016/j.jpowsour.2005.07.009

[5] Li, W., Cho, Y. G., Yao, W., Li, Y., Cronk, A., Shimizu, R., Schroeder, M. A., Fu, Y., Zou, F., Battaglia, V., Manthiram, A., Zhang, M., & Meng, Y. S. (2020). Enabling high areal capacity for Co-free high voltage spinel materials in next-generation Li-ion batteries. *Journal of Power Sources*, *473*. https://doi.org/10.1016/j.jpowsour.2020.228579

[6] Xu, K. (2014). Electrolytes and interphases in Li-ion batteries and beyond. In *Chemical Reviews* (Vol. 114, Issue 23, pp. 11503–11618). American Chemical Society. https://doi.org/10.1021/cr500003w

[7] Lee, H., Choi, S., Choi, S., Kim, H. J., Choi, Y., Yoon, S., & Cho, J. J. (2007). SEI layer-forming additives for $LiNi_{0.5}Mn_{1.5}O_4$/graphite 5 V Li-ion batteries. *Electrochemistry Communications*, *9*(4), 801–806. https://doi.org/10.1016/j.elecom.2006.11.008

[8] Liu, W., Li, J., Li, W., Xu, H., Zhang, C., & Qiu, X. (2020). Inhibition of transition metals dissolution in cobalt-free cathode with ultrathin robust interphase in concentrated electrolyte. *Nature Communications*, *11*(1). https://doi.org/10.1038/s41467-020-17396-x

[9] Cimini, A., Palumbo, O., Simonetti, E., de Francesco, M., Appetecchi, G. B., Fantini, S., Lin, R., Falgayrat, A., & Paolone, A. (2020). Decomposition temperatures and vapour pressures of selected ionic liquids for electrochemical applications. *Journal of Thermal Analysis and Calorimetry*, *142*(5), 1791–1797. https://doi.org/10.1007/s10973-020-10334-5

[10] Im, J., Lee, J., Ryou, M.-H., Lee, Y. M., & Cho, K. Y. (2017). Fluorinated Carbonate-Based Electrolyte for High-Voltage Li($Ni_{0.5}$ $Mn_{0.3}$ $Co_{0.2}$)O_2 /Graphite Lithium-Ion Battery. *Journal of The Electrochemical Society*, *164*(1), A6381–A6385. https://doi.org/10.1149/2.0591701jes

[11] Noguchi, T., Hasegawa, T., Yamauchi, H., Yamazaki, I., & Utsugi, K. (2017). Effect of Using Fluorinated Ether and Sulfone as Electrolyte Solvents for Lithium Ion Batteries with Lithium-Rich Layered Cathodes and Silicon Oxide Anodes. *ECS Transactions*, *80*(10), 291–303. https://doi.org/10.1149/08010.0291ecst

[12] Ehteshami, N., & Paillard, E. (2017). Ethylene Carbonate-Free, Adiponitrile-Based Electrolytes Compatible with Graphite Anodes. *ECS Transactions*, *77*(1), 11–20. https://doi.org/10.1149/07701.0011ecst

[13] Ulu Okudur, F., D'Haen, J., Vranken, T., de Sloovere, D., Verheijen, M., Karakulina, O. M., Abakumov, A. M., Hadermann, J., van Bael, M. K., & Hardy, A. (2018). Ti surface doping of $LiNi_{0.5}Mn_{1.5}O_4$-: δ positive electrodes for lithium ion batteries. *RSC Advances*, *8*(13), 7287–7300. https://doi.org/10.1039/c7ra12932g

[14] Duncan, H., Hai, B., Leskes, M., Grey, C. P., & Chen, G. (2014). Relationships between Mn^{3+} content, structural ordering, phase transformation, and kinetic properties in $LiNi_xMn_{2-x}O_4$ cathode materials. *Chemistry of Materials*, *26*(18), 5374–5382. https://doi.org/10.1021/cm502607v

[15] Liang, Z. J., Liang, R., Wang, Z. B., Xue, Y., Yu, F. da, Liu, D., & Zhou, Y. X. (2017). Investigation on $LiNi_{0.5}Mn_{1.5}O_4$ cathode material based on the precursor of nickel-manganese compound for lithium-ion battery. *Ionics*, *23*(1), 35–41. https://doi.org/10.1007/s11581-016-1789-8

[16] Ø stli, E. R., Tesfamhret, Y., Wenner, S., Lacey, M. J., Brandell, D., Svensson, A. M., Selbach, S. M., & Wagner, N. P. (2021). Limitations of Ultrathin Al_2O_3Coatings on LNMO Cathodes. *ACS Omega*, *6*(45), 30644–30655. https://doi.org/10.1021/acsomega.1c04457

[17] Piao, J. Y., Gu, L., Wei, Z., Ma, J., Wu, J., Yang, W., Gong, Y., Sun, Y. G., Duan, S. Y., Tao, X. sen, Bin, D. S., Cao, A. M., & Wan, L. J. (2019). Phase Control on Surface for the Stabilization of High Energy Cathode Materials of Lithium Ion Batteries. *Journal of the American Chemical Society*, *141*(12), 4900–4907. https://doi.org/10.1021/jacs.8b13438

[18] Noguchi, T., Yamazaki, I., Numata, T., & Shirakata, M. (2007). Effect of Bi oxide surface treatment on 5 V spinel $LiNi_{0.5}Mn_{1.5-x}Ti_xO_4$. *Journal of Power Sources*, *174*(2), 359–365. https://doi.org/10.1016/j.jpowsour.2007.06.139

[19] Chong, J., Xun, S., Song, X., Liu, G., & Battaglia, V. S. (2013). Surface stabilized $LiNi_{0.5}Mn_{1.5}O_4$ cathode materials with high-rate capability and long cycle life for lithium ion batteries. *Nano Energy*, *2*(2), 283–293. https://doi.org/10.1016/j.nanoen.2012.09.013

[20] Shi, J. Y., Yi, C. W., & Kim, K. (2010). Improved electrochemical performance of $AlPO_4$-coated $LiMn_{1.5}Ni_{0.5}O_4$ electrode for lithium-ion batteries. *Journal of Power Sources*, *195*(19), 6860–6866. https://doi.org/10.1016/j.jpowsour.2010.02.063

[21] Zhu, R., Zhang, S., Guo, Q., Zhou, Y., Li, J., Wang, P., & Gong, Z. (2020). More than just a protection layer: Inducing chemical interaction between Li_3BO_3 and $LiNi_{0·5}Mn_{1·5}O_4$ to achieve stable high-rate cycling cathode materials. *Electrochimica Acta*, *342*. https://doi.org/10.1016/j.electacta.2020.136074

[22] Chae, J. S., Yoon, S. B., Yoon, W. S., Kang, Y. M., Park, S. M., Lee, J. W., & Roh, K. C. (2014). Enhanced high-temperature cycling of Li_2O-$2B_2O_3$-coated spinel-structured $LiNi_{0.5}Mn_{1.5}O_4$ cathode material for application to lithium-ion batteries. *Journal of Alloys and Compounds*, *601*, 217–222. https://doi.org/10.1016/j.jallcom.2014.02.154

[23] Chan, H. W., Duh, J. G., & Sheen, S. R. (2004). Electrochemical performance of LBO-coated spinel lithium manganese oxide as cathode material for Li-ion battery. *Surface and Coatings Technology*, *188–189*(1-3 SPEC.ISS.), 116–119. https://doi.org/10.1016/j.surfcoat.2004.08.065

[24] Liu, K., Zou, C., Li, K., & Wik, T. (2018). Charging pattern optimization for lithium-ion batteries with an electrothermal-aging model. *IEEE Transactions on Industrial Informatics*, *14*(12), 5463–5474. https://doi.org/10.1109/TII.2018.2866493

[25] Davoglio, R. A., Cabello, G., Marco, J. F., & Biaggio, S. R. (2018). Synthesis and characterization of α-MnO_2 nanoneedles for electrochemical supercapacitors. In *Electrochimica Acta* (Vol. 261, pp. 428–435). Elsevier Ltd. https://doi.org/10.1016/j.electacta.2017.12.118

[26] Lin, H. Y., Sun, Y. P., Weng, B. J., Yang, C. T., Suen, N. T., Liao, K. H., Huang, Y. C., Ho, J. Y., Chong, N. S., & Tang, H. Y. (2007). Factors influencing the structure of electrochemically prepared α-MnO_2 and γ-MnO_2 phases. *Electrochimica Acta*, *52*(23), 6548–6553. https://doi.org/10.1016/j.electacta.2007.04.095

[27] Biesinger, M. C., Payne, B. P., Grosvenor, A. P., Lau, L. W. M., Gerson, A. R., & Smart, R. S. C. (2011). Resolving surface chemical states in XPS analysis of first row transition metals, oxides and hydroxides: Cr, Mn, Fe, Co and Ni. *Applied Surface Science*, *257*(7), 2717–2730. https://doi.org/10.1016/j.apsusc.2010.10.051

[28] Choi, N. S., Han, J. G., Ha, S. Y., Park, I., & Back, C. K. (2015). Recent advances in the electrolytes for interfacial stability of high-voltage cathodes in lithium-ion batteries. In *RSC Advances* (Vol. 5, Issue 4, pp. 2732–2748). Royal Society of Chemistry. https://doi.org/10.1039/c4ra11575a

[29] Wang, H., Xie, X., Wei, X., Zhang, X., Zhang, J., Huang, Y., & Li, Q. (2017). A New Strategy to Stabilize Capacity and Insight into the Interface Behavior in Electrochemical Reaction of $LiNi_{0.5}Mn_{1.5}O_4$/Graphite System for High-Voltage Lithium-Ion Batteries. *ACS*

Applied Materials and Interfaces, *9*(38), 33274–33287. https://doi.org/10.1021/acsami.7b08828

[30] Li, Y., Li, W., Shimizu, R., Cheng, D., Nguyen, H. N., Paulsen, J., Kumakura, S., Zhang, M., & Meng, Y. S. (2022). Elucidating the Effect of Borate Additive in High-Voltage Electrolyte for Li-Rich Layered Oxide Materials. *Advanced Energy Materials*, *12*(11). https://doi.org/10.1002/aenm.202103033

[31] Sun, Y.-K., Yoon, C. S., & Oh, I.-H. (2003). Surface structural change of ZnO-coated $LiNi_{0.5}Mn_{1.5}O_4$ spinel as 5 V cathode materials at elevated temperatures. *Electrochimica Acta*, 48, 503-506. https://doi.org/10.1016/S0013-4686(02)00717-X

[32] Zhang, N., Yang, T., Lang, Y., & Sun, K. (2011). A facile method to prepare hybrid $LiNi_{0.5}Mn_{1.5}O_4$/C with enhanced rate performance. *Journal of Alloys and Compounds*, *509*(9), 3783–3786. https://doi.org/10.1016/j.jallcom.2010.12.188

[33] Li, X., Guo, W., Liu, Y., He, W., & Xiao, Z. (2014). Spinel $LiNi_{0.5}Mn_{1.5}O_4$ as superior electrode materials for lithium-ion batteries: Ionic liquid assisted synthesis and the effect of CuO coating. *Electrochimica Acta*, *116*, 278–283. https://doi.org/10.1016/j.electacta.2013.11.055

[34] Park, J. S., Meng, X., Elam, J. W., Hao, S., Wolverton, C., Kim, C., & Cabana, J. (2014). Ultrathin lithium-ion conducting coatings for increased interfacial stability in high voltage lithium-ion batteries. *Chemistry of Materials*, *26*(10), 3128–3134. https://doi.org/10.1021/cm500512n

[35] Alva, G., Kim, C., Yi, T., Cook, J. B., Xu, L., Nolis, G. M., & Cabana, J. (2014). Surface chemistry consequences of Mg-based coatings on $LiNi_{0.5}Mn_{1.5}O_4$ electrode materials upon operation at high voltage. *Journal of Physical Chemistry C*, *118*(20), 10596–10605. https://doi.org/10.1021/jp5003148

[36] Shin, W. K., Lee, Y. S., & Kim, D. W. (2014). Study on the cycling performance of $LiNi_{0.5}Mn_{1.5}O_4$ electrodes modified by reactive SiO_2 nanoparticles. *Journal of Materials Chemistry A*, *2*(19), 6863–6869. https://doi.org/10.1039/c3ta14558a

[37] Wang, H., Shi, Z., Li, J., Yang, S., Ren, R., Cui, J., Xiao, J., & Zhang, B. (2015). Direct carbon coating at high temperature on $LiNi_{0.5}Mn_{1.5}O_4$ cathode: Unexpected influence on crystal structure and electrochemical performances. *Journal of Power Sources*, *288*, 206–213. https://doi.org/10.1016/j.jpowsour.2015.04.137

[38] Cho, H. M., Chen, M. V., MacRae, A. C., & Meng, Y. S. (2015). Effect of Surface Modification on Nano-Structured $LiNi_{0.5}Mn_{1.5}O_4$ Spinel Materials. *ACS Applied Materials and Interfaces*, *7*(30), 16231–16239. https://doi.org/10.1021/acsami.5b01392

[39] Hwang, T., Lee, J. K., Mun, J., & Choi, W. (2016). Surface-modified carbon nanotube coating on high-voltage $LiNi_{0.5}Mn_{1.5}O_4$ cathodes for lithium ion batteries. *Journal of Power Sources*, *322*, 40–48. https://doi.org/10.1016/j.jpowsour.2016.04.118

[40] Jung, S. H., Kim, D. H., Brüner, P., Lee, H., Hah, H. J., Kim, S. K., & Jung, Y. S. (2017). Extremely conductive RuO_2-coated $LiNi_{0.5}Mn_{1.5}O_4$ for lithium-ion batteries. *Electrochimica Acta*, *232*, 236–243. https://doi.org/10.1016/j.electacta.2017.02.109

[41] Chu, C. T., Mondal, A., Kosova, N. v., & Lin, J. Y. (2020). Improved high-temperature cyclability of AlF_3 modified spinel $LiNi_{0.5}Mn_{1.5}O_4$ cathode for lithium-ion batteries. *Applied Surface Science*, *530*. https://doi.org/10.1016/j.apsusc.2020.147169

[42] Hallot, M., Caja-Munoz, B., Leviel, C., Lebedev, O. I., Retoux, R., Avila, J., Roussel, P., Asensio, M. C., & Lethien, C. (2021). Atomic Layer Deposition of a Nanometer-Thick Li_3PO_4 Protective Layer on $LiNi_{0.5}Mn_{1.5}O_4$ Films: Dream or Reality for Long-Term Cycling? *ACS Applied Materials and Interfaces*, *13*(13), 15761–15773. https://doi.org/10.1021/acsami.0c21961

[43] Li, W., Cheng, D., Shimizu, R., Li, Y., Yao, W., Raghavendran, G., Zhang, M., & Meng, Y. S. (2022). Artificial cathode electrolyte interphase for improving high voltage cycling stability of thick electrode with Co-free 5 V spinel oxides. *Energy Storage Materials*, *49*, 77–84. https://doi.org/10.1016/j.ensm.2022.04.002

[44] Hua, W., Wang, S., Knapp, M., Leake, S. J., Senyshyn, A., Richter, C., Yavuz, M., Binder, J. R., Grey, C. P., Ehrenberg, H., Indris, S., & Schwarz, B. (2019). Structural insights into the formation and voltage degradation of lithium- and manganese-rich layered oxides. *Nature Communications*, *10*(1). https://doi.org/10.1038/s41467-019-13240-z

[45] Hua, W., Zhang, J., Wang, S., Cheng, Y., Li, H., Tseng, J., Wu, Z., Shen, C. H., Dolotko, O., Liu, H., Hung, S. F., Tang, W., Li, M., Knapp, M., Ehrenberg, H., Indris, S., & Guo, X. (2023). Long-Range Cationic Disordering Induces two Distinct Degradation Pathways in Co-Free Ni-Rich Layered Cathodes. *Angewandte Chemie - International Edition*, *62*(12). https://doi.org/10.1002/anie.202214880

[46] Chen, J., Yang, Y., Tang, Y., Wang, Y., Li, H., Xiao, X., Wang, S., Darma, M. S. D., Etter, M., Missyul, A., Tayal, A., Knapp, M., Ehrenberg, H., Indris, S., & Hua, W. (2023). Constructing a Thin Disordered Self-Protective Layer on the $LiNiO_2$ Primary Particles Against Oxygen Release. *Advanced Functional Materials*, *33*(6). https://doi.org/10.1002/adfm.202211515

[47] Chryssikos, G. D., Duffy, J. A., Hutchinson, J. M., Ingram B', M. D., Kamitsos, E. I., & Pappin, A. J. (1994). Lithium borate glasses: a quantitative study of strength and fragility. In *Journal of Non-Crystalline Solids* (Vol. 172).

Chapter 3 Understanding Boron Chemistry as the Surface Modification and Electrolyte Additive for Co-free Lithium-Rich Layered Oxide

3.1 Introduction

Li-ion batteries have been extensively investigated, particularly in the context of emerging applications such as electric vehicles, hybrid electric vehicles, portable electronic devices, and energy storage systems. These applications require advanced lithium storage capacity, increased energy density (calculated as the product of specific capacity and average operating voltage), and prolonged battery cycle performance [1]. The ongoing progress in battery systems that meet these demanding requirements underscores the critical nature of cathode development, as the cathode is a key component in Li-ion batteries. In pursuit of this objective, LRLO emerges as a promising candidate for the cathode material [2]. A notable characteristic of the LRLO cathode material is the remarkable reversible capacity of 250 mAh/g within the voltage range of 2.0 to 4.7 V [3]. Importantly, the incorporation of cost-effective manganese as a substitute for the more expensive nickel and cobalt elements holds significant potential for reducing production costs [4].

The practical implementation of LRLO is hindered by capacity degradation and voltage decay observed in full-cell performance, particularly at high voltages [5]. The elevation of the operating voltage introduces undesirable outcomes, including cathode-electrolyte interfacial reactions, structural transformations, and the formation of lower-voltage redox couples [6]. These effects are posited to initiate at the cathode surface, progressively extending into the bulk over successive cycles [7]. It is acknowledged that the distinctive characteristic of LRLO is oxygen redox activation at high voltages (>4.5 V versus Li/Li^+) [8]. This activation gives rise to a cascade of issues during cycling: irreversible oxygen loss, the generation of oxygen vacancies on the

surface, migration and dissolution of transition metals, and the redeposition of transition metals on both cathode and anode surfaces [9].

Extensive efforts have been directed toward mitigating capacity and voltage decay in LRLO through the implementation of cathode surface modifications [10]. This strategic focus arises from the recognition that all pertinent parasitic reactions manifest most actively at the cathode's surface. Diverse methodologies for modifying the surface of LRLO cathode material have been explored, including the wet coating method [11], atomic layer deposition (ALD) [12], and solution-processable method [13]. A sol-gel based wet coating method, involving the dissolution of $Al(NO_3)_3 \cdot 9H_2O$ and NH_4F in deionized water, was employed by Zhao et al. to establish stable integrated layered-spinel structures [11]. However, the wet coating method utilizing water requires additional chemical infrastructure, including explosion-proof facilities, complicating the commercialization process. Furthermore, the rate capability reported needs to be verified in full cells. X. Zhang et al. utilized the spray pyrolysis process, employing the ALD method, to coat the cathode surface with a very thin layer of Al_2O_3, approximately 2-3 nm in thickness. This coating significantly improved the initial Coulombic efficiency and cycling performance of the coin half-cell. However, it also led to an approximately 10% decrease in the initial discharge capacity compared to the uncoated cathode, indicating a lithium inventory loss through the coating [12]. S. Kim et al. coated the surface of LRLO with polydopamine (PDA), an oxygen radical scavenger, to form a chemically protective layer, demonstrating an 82% retention in coin half-cell cycling after 200 cycles at room temperature. The use of a self-polymerizing solution impregnation technique for coating poses challenges for mass production due to the necessity of filtering powder during the coating process and subsequent washing with ethanol and deionized water [13].

Another approach employed for cathode surface treatment is the dry coating method, wherein a solid phase identical to that of the cathode material is utilized, thereby eliminating any heterogeneity between the cathode and the coating material [14]. Notably, the mass production of dry coating is streamlined, involving the straightforward addition of the coating material during the mixing process, without necessitating supplementary infrastructure for commercialization. Consequently, the present study endeavors to advance the properties of the cathode toward commercial viability through the implementation of the dry coating method for surface treatment.

Along with determining the surface modification method, the choice of an appropriate surface modification material is pivotal in achieving performance improvements. A large number of compounds have been investigated, such as fluorides [15], phosphates [16], and oxides [11, 12]. Fluorides involve the partial doping of F^- into the surface lattice of the oxide, enhancing surface conductivity. However, fluorides have traditionally been utilized in high-Ni cathode materials where excess lithium is prevalent on the surface [17]. Phosphates are also known for their ease of reaction with excess lithium and the absorption of water in the electrolyte [18]. While Li_3PO_4 is preferred due to its ionic conductivity, in the high working voltage range of LRLO, it can readily react with free protons. This reaction leads to the formation of H_3PO_4, consequently inducing a shift in the cell environment towards a deleterious acidic state. Oxides are electrochemically stable materials [19], generally exhibiting low electrical conductivity, thereby minimizing parasitic reactions of the cathode materials with the electrolyte. Moreover, the versatility in designing various oxides provides flexibility to tailor properties in accordance with specific requirements. Various oxides, such as Li_2ZrO_3 [20], Li_3PO_4 [21], AlF_3 [15], $MgPO_4$ [22], CeO_2 [23], and Al_2O_3 [24] have been applied for the surface modification of LRLO to improve cycling stability. Nevertheless, these published results encounter challenges in mitigating the initial irreversible

capacity loss, and the application of such inactive oxides as coatings may potentially diminish the reversible capacity.

In this work, we applied surface modification to Co-free LRLO ($Li_{1.222}Ni_{0.349}Mn_{0.651}O_2$) using a dry coating process with LBO based on an organic nano-sized boron precursor. LBO coating materials are introduced as (1) it protects the surface lattice oxygen of LRLO, reducing the exacerbated generation of H_2O and free protons at high voltage; (2) it also reacts with PF_6^- to form thermodynamically stable BF_4^-, mitigating the generation of HF acid in the electrolyte. The quality of surface modification was assessed through electron energy loss spectroscopy (EELS) obtained via scanning transmission electron microscopy (STEM). Our analysis revealed the 15 nm uniform distribution of LBO coating on the LRLO surface, resulting in a significant improvement in cycling stability and mitigation of voltage decay in LRLO/graphite full cells featuring a 3 mAh/cm^2 areal capacity. These findings have the potential to guide the design of surface modification layers for high-voltage cathode materials and inform the utilization of boron-based electrolyte additives in future applications.

3.2. Material and Methods

3.2.1 Sample Preparation

The pristine $Li_{1.222}Ni_{0.349}Mn_{0.651}O_2$ sample (denoted as LRLO) was provided by Umicore. SEM images of the pristine LRLO are presented in **Figure 3.1 (a-c)**, revealing oval-spherical secondary particles with an average size of approximately 9 μm. The X-ray diffraction (XRD) pattern was obtained for the structural analysis of the pristine LRLO. Rietveld refinement was applied to the collected XRD data to determine the lattice parameters and site occupancies of the pristine LRLO sample, as shown in **Figure 3.1 (d)** and **(e)**.

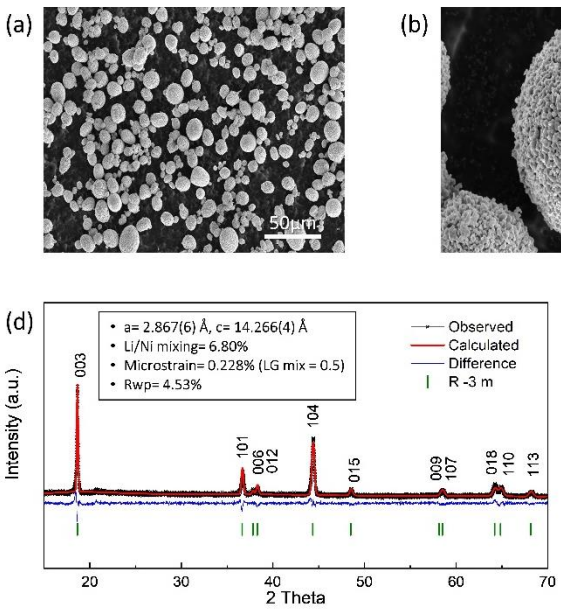

(e)

Atom	Wyckoff Position			Designed	Occupancy
Li1	0	0	0	1.000	0.961
Ni1	0	0	0	0	0.068
Li2	0	0	0.5	0.222	0.261
Ni2	0	0	0.5	0.349	0.281
Mn2	0	0	0.5	0.651	0.651
O	0	0	0.2435	1	1

Figure 3.1: (a-c) SEM image of pristine LRLO material. (d) XRD Rietveld refinement of the pristine LRLO material. (e) refined crystal structure parameters for the pristine LRLO.

The XRD pattern can be matched to the R-3m space group, with lattice parameters a = 2.867(6) Å and c = 14.266(4) Å. The refined occupancies reveal a 6.8% Li/Ni mixing between the Li and TM layers. In summary, the LRLO sample exhibits high material purity and a well-organized layered structure with low Li/Ni mixing, establishing it as a reliable baseline material for this study. For coating material synthesis, 0.03 mol of Polyvinylpyrrolidone (PVP) (MW=50,000) was added to 100 mL of Tetraethylene Glycol (TTEG). We then added 0.015 mol of $LiOH \cdot H_2O$ and 0.015 mol of H_3BO_3 into the solution. After 2 hours of heating the solution at 80 ℃, the products were naturally cooled down, followed by washing in ethanol 7 times. After removing moisture in an 80 ℃ vacuum oven for one day, the dried powder was ground finely using a mortar and pestle, and finally, using a ball mill at 500 rpm for 5 hours with ethanol to make the particle size smaller. The obtained LBO precursor (2% in a weight ratio) was then mixed with

the LRLO cathode in a Thinky Mixer (Thinky Corporation) at 2000 rpm for 10 minutes. The well-mixed powder was transferred into the furnace for calcination under different temperatures and dwell time. After calcination, the powder was ground using a mortar and pestle for about 10 minutes.

3.2.2 Electrode Preparation

To evaluate the electrochemical performance of LBO-coated LRLO, electrodes using uncoated and LBO-coated LRLO were prepared, with SPC65 (carbon black, TIMCAL Ltd.) as the conductive agent and HSV900 (PVDF, Arkema Inc.) as the binder, in a mass ratio of 80:10:10 and a cathode loading of 3 mAh/cm^2. The mixture was then dissolved in a proper amount of N-methyl-2-pyrrolidone (NMP, ≥ 99%, Sigma-Aldrich) in a Thinky Mixer to form the slurry. The slurry was cast onto Al foil and dried at 80 ℃ in a vacuum oven overnight, followed by 1 hour of drying at an elevated temperature of 120 ℃. The cathode was punched into discs with a 12.7 mm diameter and a loading of active mass around 14 mg/cm^2. For LRLO/graphite full cells, both CR2032 and pouch cells were assembled. The graphite electrode used in this work was provided by NIMTE with an active material ratio of 94%. For CR2032 full cells, the graphite electrode was punched into discs with a 13 mm diameter, and the designed N/P ratio was around 1.1. For single-layer pouch-type full cells, the cathode size was 44 × 30 mm, and the anode size was 45 × 32 mm. For all the cells, Celgard 2325 was used as the separator. 1M $LiPF_6$ in EC: DMC = 3:7 (vol%) was obtained from Gotion, USA, and is denoted as carbonate baseline electrolyte. All the coin cells were assembled in the Ar-filled glovebox with moisture control (H_2O < 0.5 ppm), and 50 μl of electrolyte was used for each coin cell. The single-layer pouch cells were first assembled in the atmosphere without electrolytes. The assembled pouch cells were moved to a heating tray inside

the glovebox antechamber and dried at 80 ℃ overnight under vacuum before the electrolyte injection. After drying, the dry pouches were moved inside the Ar-filled glovebox without air exposure, and 500 μl of electrolyte was injected into each cell. The pouch cells with electrolytes were vacuum-sealed inside the glovebox and transferred out for further testing.

3.2.3 Electrochemical Performance Evaluation

After assembling, the coin cell (CR2032) and pouch cell full cells were evaluated by cycling at a rate of C/10 (where 1C is 270 mAh/g) after the formation cycle at a current rate of C/20. The electrochemical performances of all the cells were tested either by Neware Battery Test System (Neware Technology Ltd., China) or Arbin BT2000 instruments (Arbin instrument, USA).

3.2.4 Characterizations

FEI Apreo® was applied with 5 kV as the accelerating voltage and 0.1 nA as the beam current for the SEM analysis. We applied a backscattered electron imaging technique to verify the uniformity of the LBO surface modification layer on LRLO, especially for large-area coating uniformity evaluation. The microscope detector was first changed to T1 mode, which was extremely sensitive to backscattered electrons. Then, the accelerated voltage was lowered to detect the surface information. The contrast gradually appeared when lowering the accelerated voltage from 5 kV to 200 V, while the optimized voltage was 500 V to 1000 V to acquire clear images. A Thermofisher Talos F200X G2 transmission electron microscope, equipped with a Ceta camera and operated at 200 kV, was used to acquire STEM-EELS and STEM-EDS data. EELS spectra presented in this work were acquired from areas without pre-beam irradiation to minimize possible electron beam irradiation effects. ICP-MS analysis was performed with a Thermo iCAP RQ ICP-

MS to analyze the elemental concentration in fresh and cycled electrolytes. The ^{11}B, ^{19}F, and ^{31}P-NMR measurements of the electrolyte samples were performed with a JEOL ECA 500 spectrometer. Liquid NMR samples were prepared by adding 10 μL of electrolyte to 600 μL of DMSO-D6 solution, and 50 μl of α, α, α-Trifluorotoluene was added to each sample as the reference and sealed in an NMR tube inside the Ar-filled glovebox for further measurement. The NMR spectrums were analyzed with MestReNova. All spectra were calibrated with α, α, α-Trifluorotoluene at −63.72 ppm. FT-IR spectra were collected using Nicolet 6700 Fourier transform infrared spectrometer. Approximately 5−10 mg of LRLO was dried at 80 °C for at least 12 hours before the FT-IR analysis. The electronic conductivity was determined using the direct current polarization method using a Biologic SP-200 impedance analyzer by applying a bias of 10 mV for 1 hour and extracting the steady-state leakage current.

3.3 Results and Discussion

3.3.1 LBO Dry Coating Optimization and Cycling Stability Improvement

The dry coating method involves physically mixing powder-form LBO precursors with LRLO in the desired weight percentage and calcination of the blended powder. The detailed LRLO sample information is provided in the Material and Method section. The LBO precursors were synthesized through a polyol process, as described in our previous work [14]. The synthesized precursors are organic soft materials featuring boron as a functional group along their C-H backbone (**Figure 3.2 (a)**).

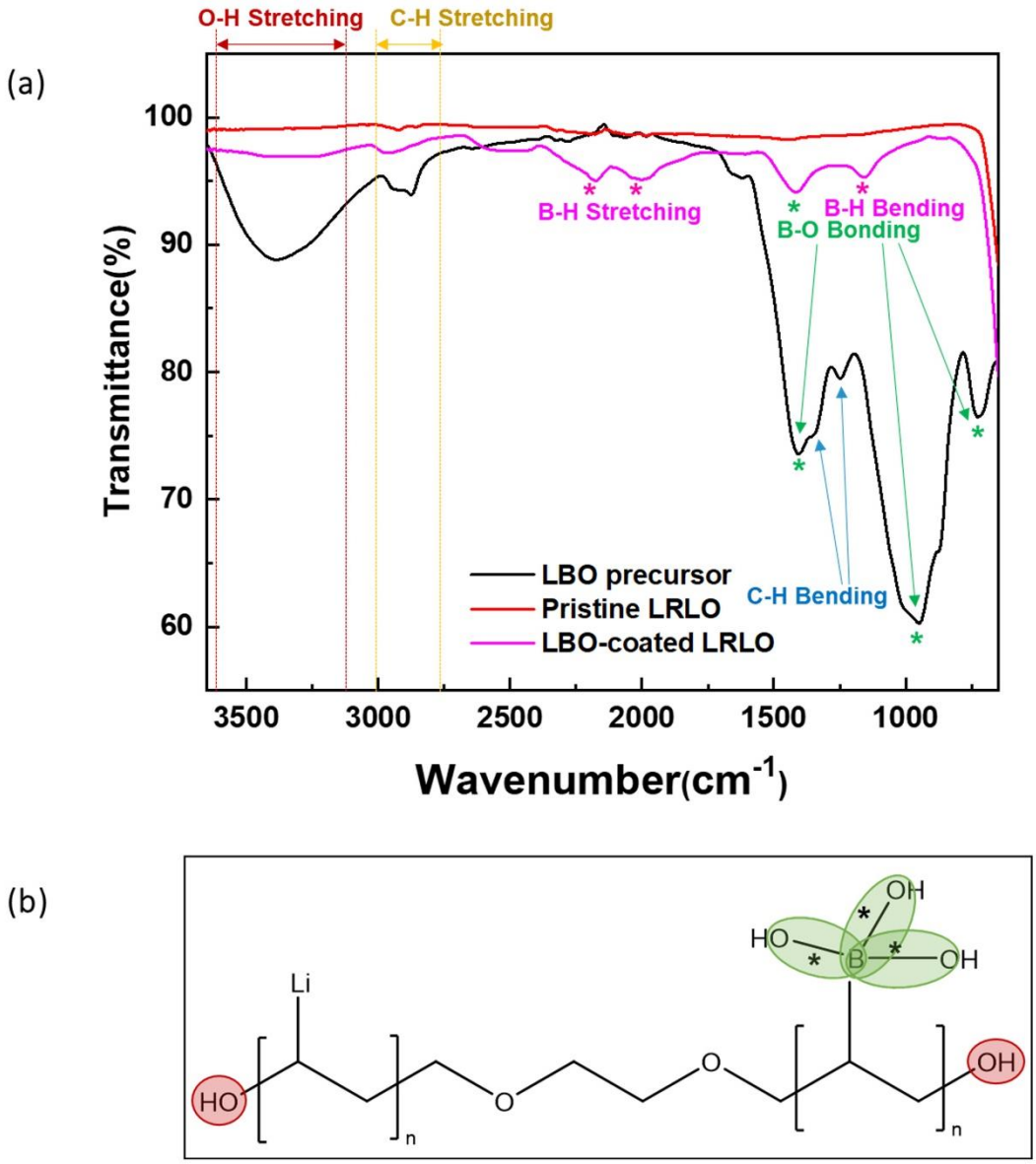

Figure 3.2: (a) FT-IR spectra of LBO precursor, pristine LRLO, and LBO-coated LRLO. (b) The anticipated structure of LBO precursor through FT-IR analysis.

Upon mixing, chemical bonding, such as B-H, O-H, and C-H, is established on the LRLO surface. After calcination, it is anticipated that most of the C-H backbone chains will be removed. However, the presence of boron bonding on the LRLO surface can be confirmed. This is evident as both the stretching and bending modes of B-H bonding, absent in pristine LRLO, become distinctly observable after calcination. The resulting chemical bonding, as illustrated in **Figure 3.2**

(b), plays a crucial role in facilitating conformal contact between the precursor and the core material. These attributes emphasize the unique advantages associated with employing polyol precursors for the dry coating process, including enhanced adhesion due to the functional group, as well as flexibility and plasticity. The critical variables for the mixing and calcination step were then optimized, as shown in **Figure 3.3**.

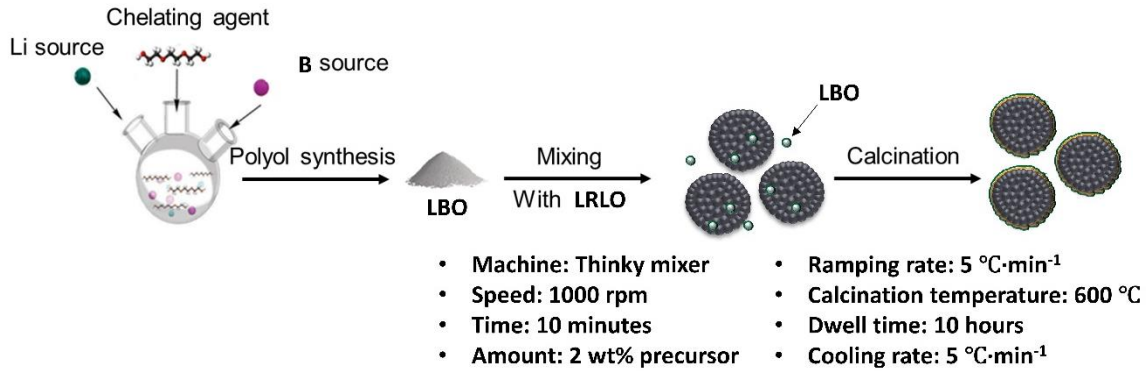

Figure 3.3: Scheme of the dry coating method for LRLO surface modification with LBO precursor synthesized through the polyol method.

When the mixing time exceeds 20 minutes (**Figure 3.4 (d)**), secondary particles break apart. Conversely, mixing for less than 5 minutes (**Figure 3.4 (a)** and **(b)**) reveals agglomeration of LBO precursors. Vigorous mixing for an extended period can impose stress on LRLO, necessitating appropriate mixing conditions. It was determined that mixing for 10 minutes at 1000 rpm induces the most uniform mixing while simultaneously maintaining the secondary particle of LRLO.

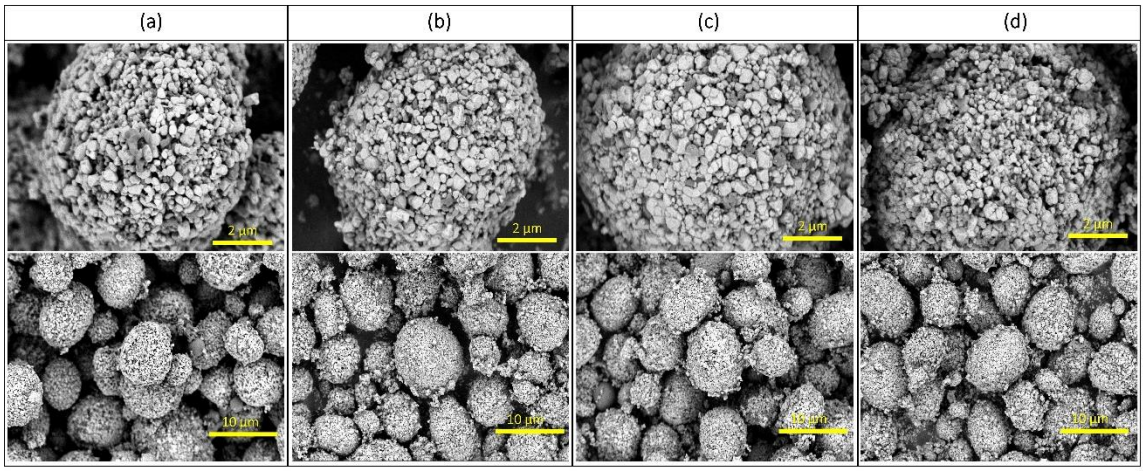

Figure 3.4: SEM/BSE images of LRLO after mixing with LBO at 1000 rpm for (a) 1 minute (b) 5 minutes (c) 10 minutes and (d) 20 minutes.

After blending the powder, calcination is carried out to decompose the organic functional group within the precursor, thereby yielding the LBO coating layer. As shown in **Figure 3.3**, optimal conditions for the calcination step are achieved when the surface modification appears uniformly, and LBO precursors are no longer visible. This optimal calcination condition with a dwell temperature of 600 ℃ and a dwell time of 10 hours is further verified through electrochemical evaluations (**Figure 3.5**).

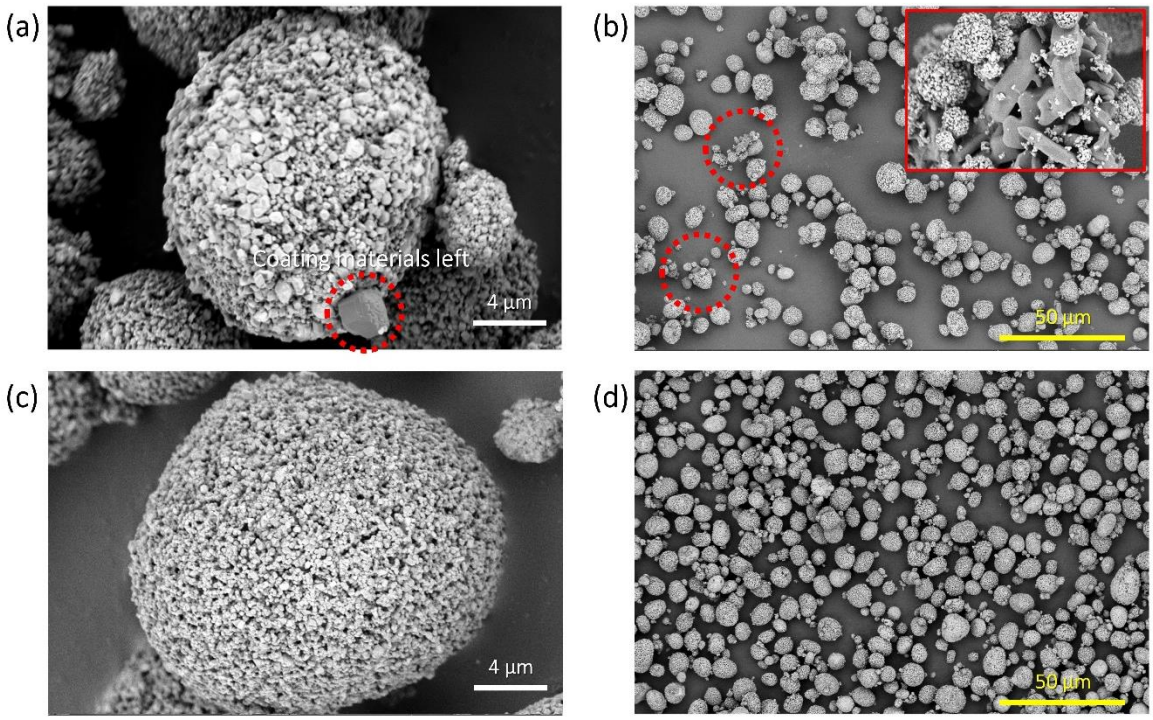

Figure 3.5: SEM/BSE images of LRLO after calcination at 600 ℃ for (a) 5 hours at high magnification (b) at low magnification (c) 10 hours at high magnification and (d) at low magnification.

Another critical variable in this study is the amount of LBO coating. STEM-EELS mapping (**Figure 3.6 (a)**) reveals a boron layer approximately 4 nm thick for the 1 wt% LBO surface modification, which is insufficient to fully cover the cathode surface. The 4 wt% LBO coating shows clustering of boron species on the cathode surface (**Figure 3.6 (b)**).

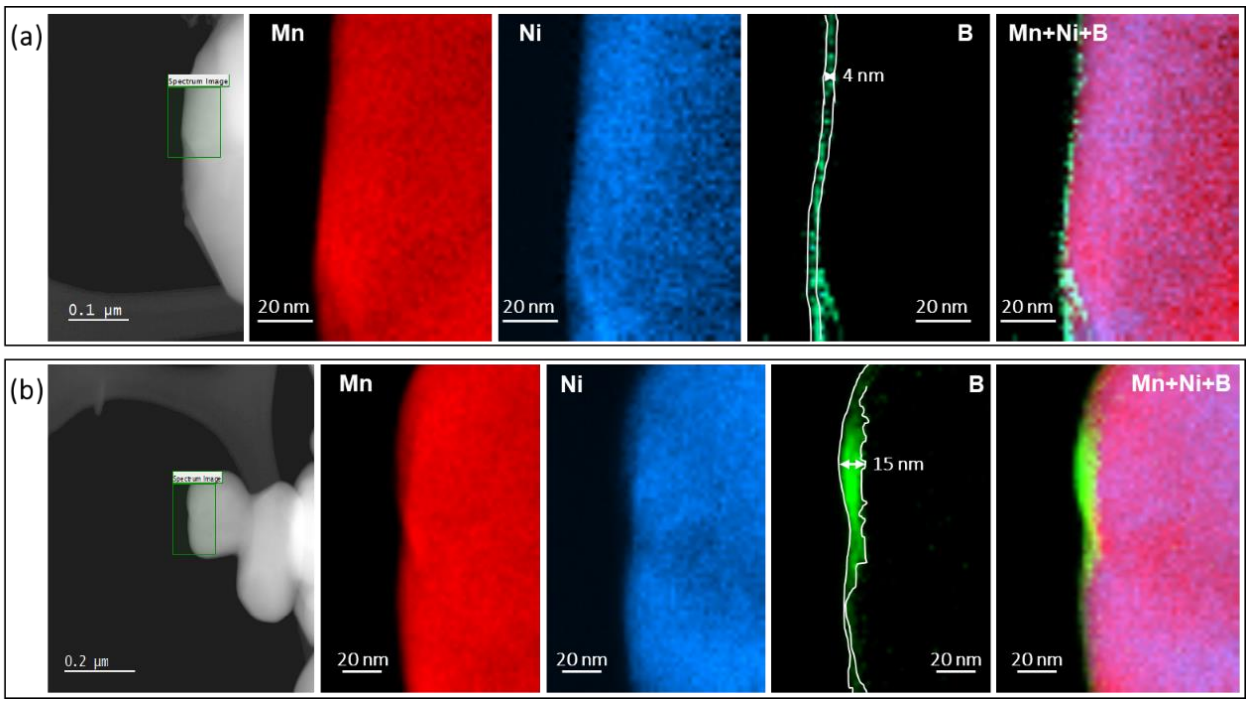

Figure 3.6: STEM-EELS mapping results of (a) 1 wt% LBO-coated LRLO and (b) 4 wt% LBO-coated LRLO.

In contrast, STEM-EELS mapping confirms that the 2 wt% LBO coating achieves optimal coverage and uniformity (**Figure 3.12 (a)**). Electrochemical evaluations were then applied to the coated samples with various weight ratios. As shown in **Figure 3.7 (a)**, the initial capacity drops for 1 wt% and 2 wt% coatings remain within acceptable values, whereas the 4 wt% coating results in a capacity loss of 17%. Moreover, during C/10 rate cycling (**Figure 3.7 (b)**), the 1 wt% LBO-coated LRLO exhibits improved capacity retention compared to uncoated LRLO; however, this improvement is not comparable with the 2 wt% sample after approximately 50 cycles, indicating that the 1 wt% of LBO coating amount is insufficient. The 4 wt% LBO-coated LRLO displays a rapid decay in discharge capacity after about 20 cycles. These results indicate that the amount of LBO coating is crucial for both initial capacity and cycling stability, with 2 wt% identified as the optimal amount.

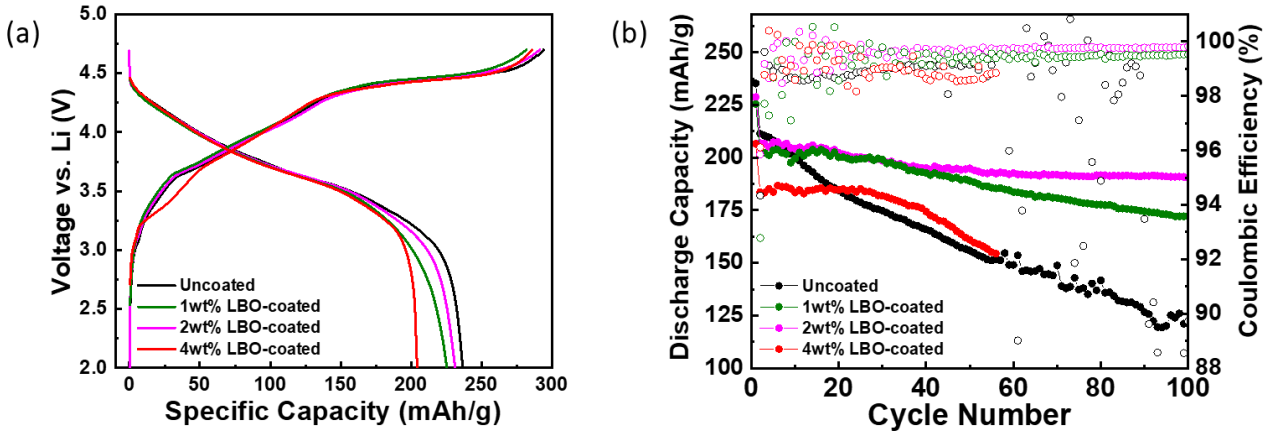

Figure 3.7: (a) Voltage profiles from uncoated and various wt% LBO-coated LRLO/graphite full cell. (b) Full cells cycling performances in the 2.0–4.55 V window at a current rate of C/10.

We confirmed that there was no reduction in electrical conductivity at the electrode level after the surface modification. This is supported by 2-point probe analysis of electrode conductivity with the areal loading of 3 mAh/cm^2 (**Table 3.1**).

Table 3.1: Electrode conductivity of uncoated and LBO-coated LRLO cathode through 2-point probe analysis.

Sample	V	A	I	t	ρ	**σ**	Error
	[V]	[cm^2]	[mA]	[um]	[Ω cm]	**[S/cm]**	[S/cm]
Uncoated LRLO	0.1	1.27	23.2	108	5.06E+02	**1.98E-03**	±5.00E-04
LBO-coated LRLO	0.1	1.27	48.5	111	2.36E+02	**4.25E-03**	±9.00E-04

Cross-sectional SEM-EDS (Scanning Electron Microscopy with Energy Dispersive X-ray Spectroscopy) analysis in **Figure 3.8** has also confirmed that there is no difference in the distribution of conducting carbon additives with and without the LBO surface modification.

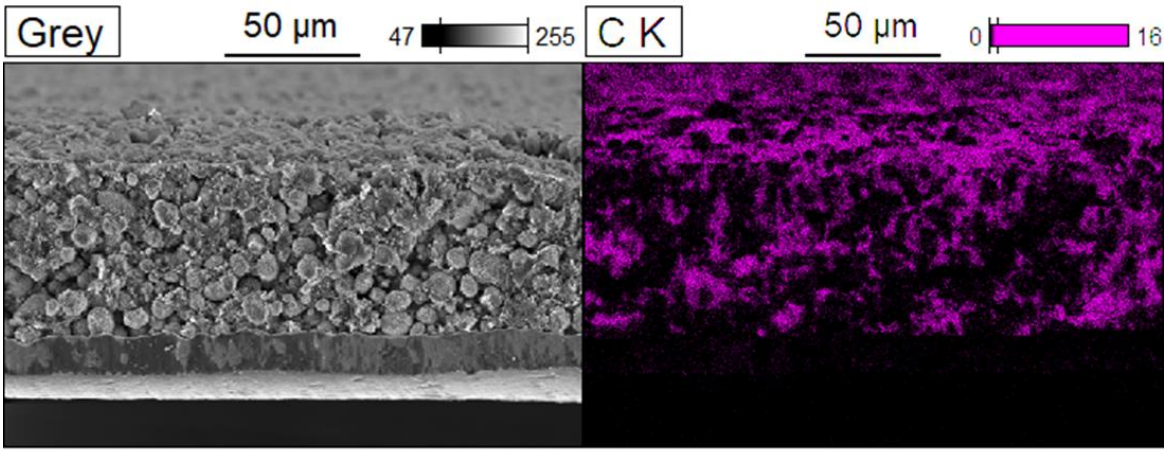

Uncoated LRLO electrode

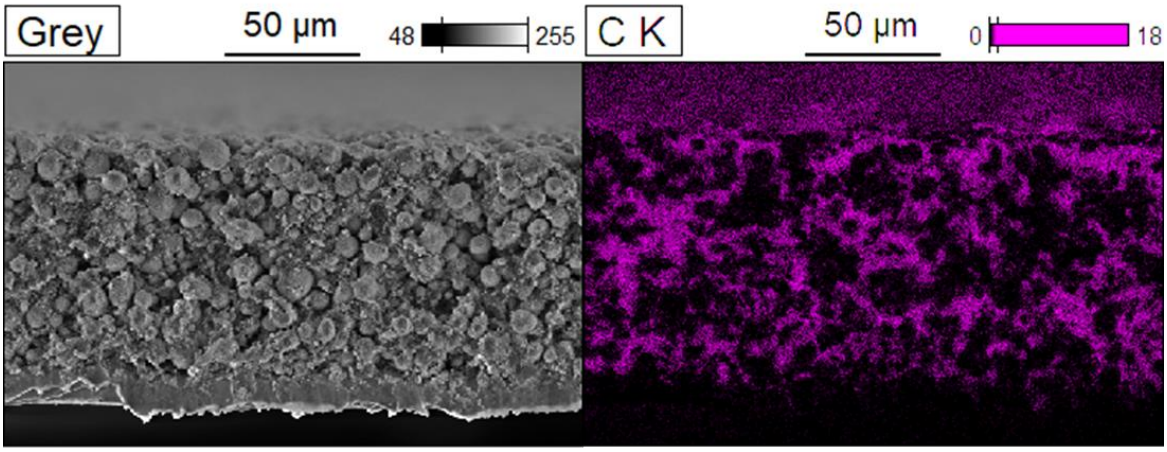

LBO-coated LRLO electrode

Figure 3.8: SEM-EDS analysis of uncoated and LBO-coated LRLO cathode with the cross-sectional view.

The similarity in electrical conductivity, combined with the uniformly distributed carbon additives, suggests that the percolation behavior of the electrical conducting agent is nearly identical.

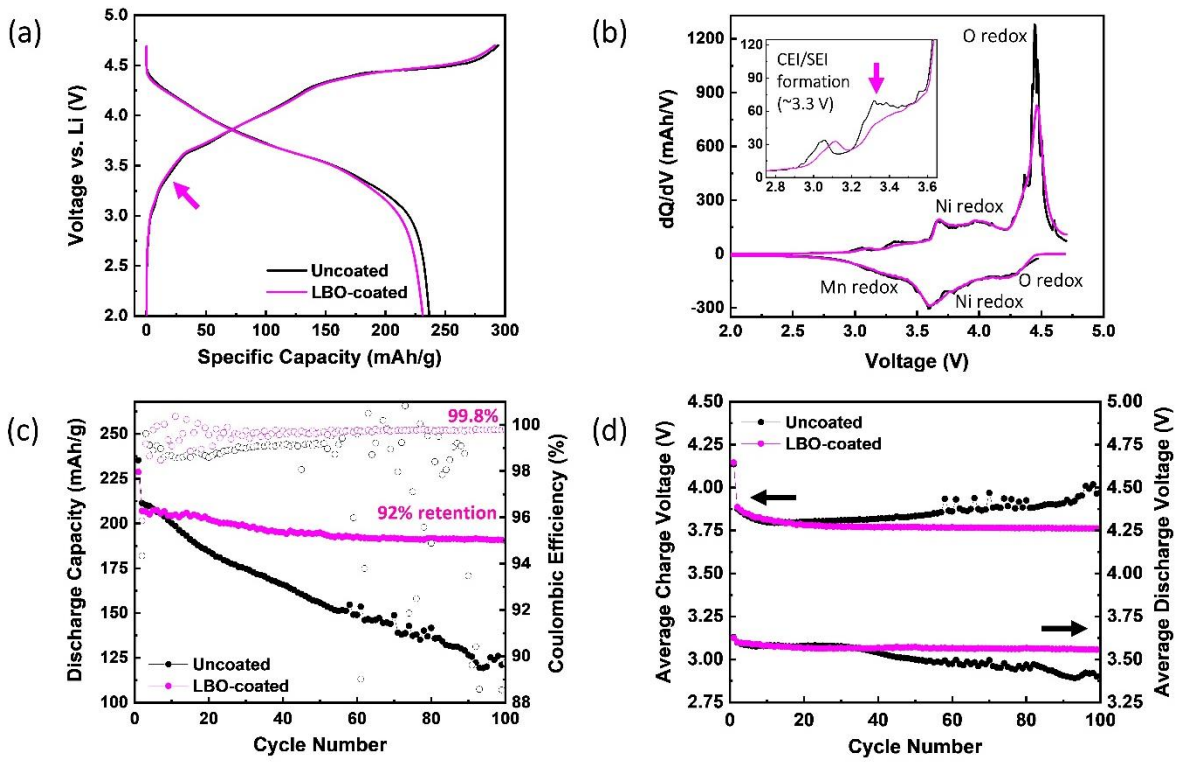

Figure 3.9. (a) Voltage profiles from uncoated and LBO-coated LRLO/graphite full cell with (b) the corresponding dQ/dV plot. The voltage window of both full cells is 2.0–4.7 V at a current rate of C/20 for the formation cycle (1 C = 270 mAh/g). (c) Full cells cycling performances with (d) the average charge and discharge voltage in the 2.0–4.55 V window at a current rate of C/10.

The LBO-coated LRLO exhibits a similar voltage profile (**Figure 3.9 (a)**) with little capacity loss compared with the uncoated cathode during the formation cycle in a full cell. The dQ/dV plots reveal a lower peak intensity for LBO-coated LRLO in the voltage range associated with electrode/electrolyte interphase formation, around 3.3 V (inset of **Figure 3.9 (b)**). Uncoated LRLO shows a continuous decrease in capacity from the beginning of the cycling (**Figure 3.9 (c)**). In contrast, LBO-coated LRLO demonstrates approximately 92% capacity retention after 100 cycles in full cell. The average charge and discharge voltage plot (**Figure 3.9 (d)**) substantiates the role of LBO surface modification on LRLO not only in improving capacity retention but also in ameliorating voltage decay. LBO surface modification enhances long-term cycling performances.

Figure 3.10 shows that the capacity retention of the uncoated LRLO improved from approximately 26% after 500 cycles to around 63% with just the LBO surface modification.

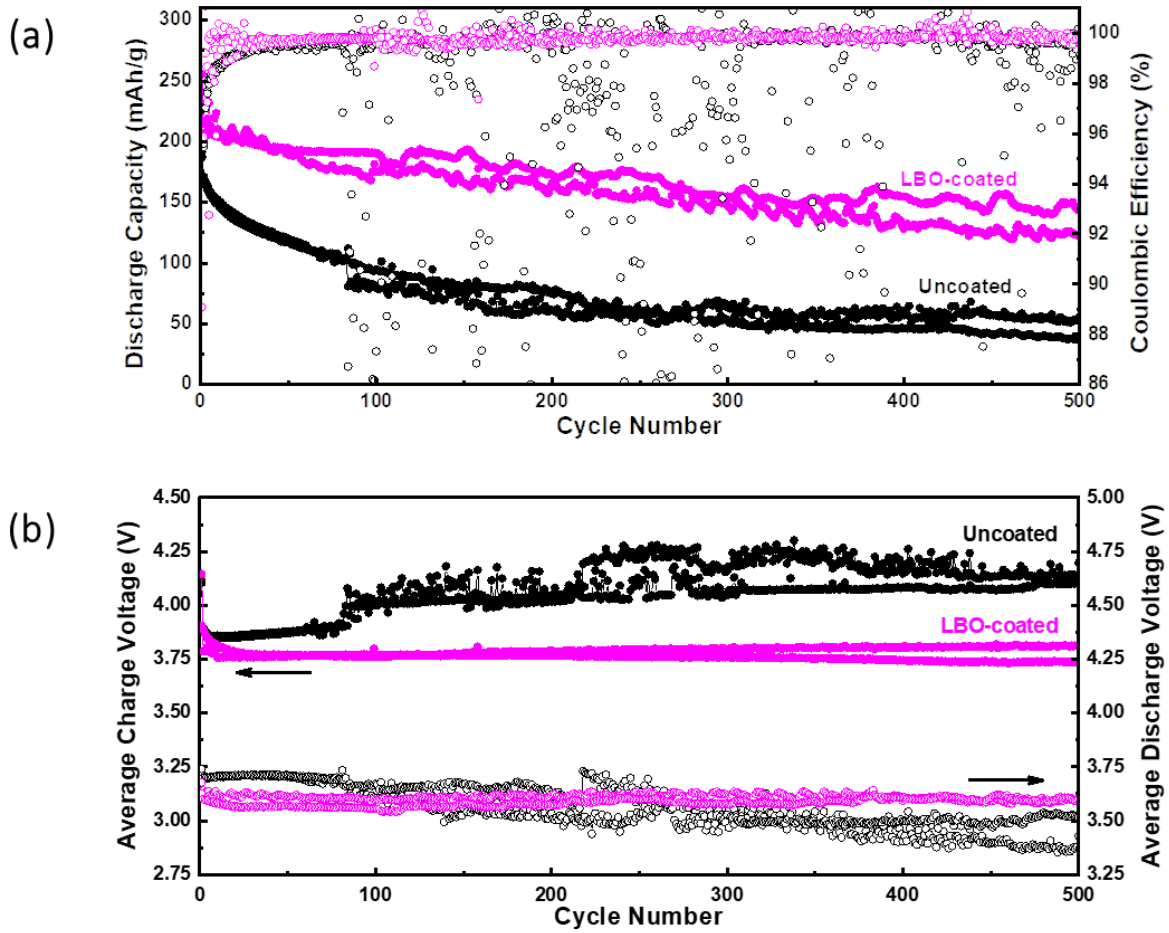

Figure 3.10: (a) Full cells cycling performance comparison with (b) the corresponding average charge and discharge voltage in the 2.0–4.55 V window at a current rate of C/10.

3.3.2 LBO coating chemistry and durability

The electrochemical assessment confirmed the effect of the surface modification. To further validate these results, an examination of the presence of boron on the cathode surface was conducted. Mixing LRLO and LBO precursors confirms the presence of relatively lighter material

on the cathode surface (**Figure 3.11 (b)**). After calcination, both high-magnification views of the cathode surface (**Figure 3.11 (c)**) and overall observations at low magnification (**Figure 3.11 (e)**) did not exhibit evidence of the coating materials.

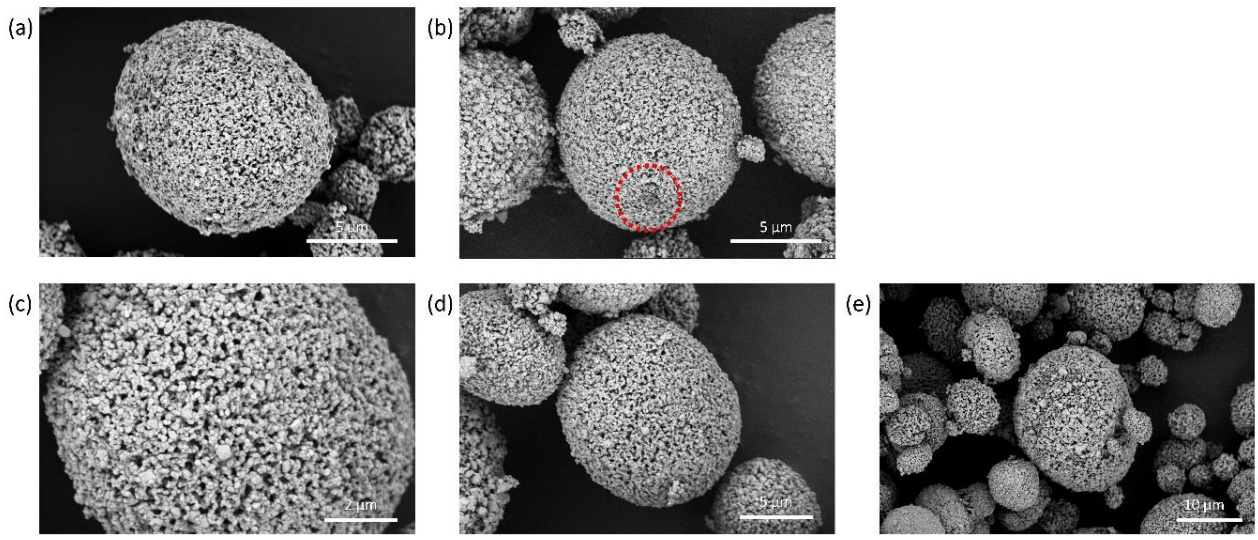

Figure 3.11: SEM/BSE images of (a) pristine LRLO (b) after mixing with LBO at 1000 rpm for 10 min (c, d, e) after calcination at 600 ℃ for 10 hrs.

This observation strongly suggests that the surface modification material, LBO, has undergone a reaction with the cathode surface or beyond. Due to LRLO's polycrystalline nature, assessing coating uniformity in SEM-backscattered electrons (BSE) mode posed challenges. In particular, boron chemistry makes it difficult to confirm the coating uniformity using EDS analysis. The boron layer was then distinctly discerned on the cathode surface through STEM-EELS analysis (**Figure 3.12 (a)**). Elemental mapping verified the partial diffusion of elements toward the cathode subsurface. This observation indicates a modification in the chemical environment between transition metals and boron, suggesting their influence on improving electrochemical performances.

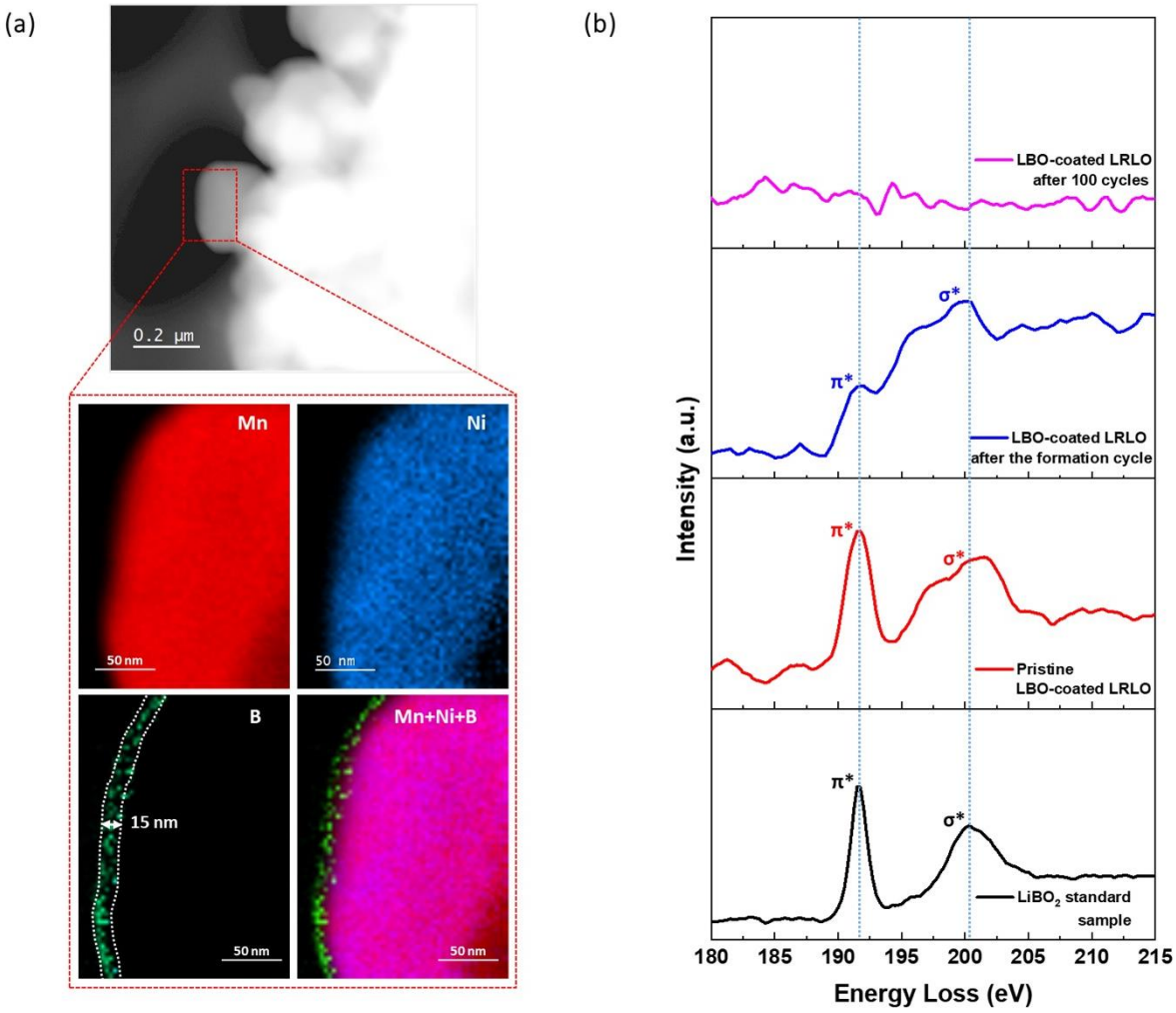

Figure 3.12: STEM-EELS mapping results of (a) LBO-coated LRLO obtained with the optimal dry coating parameters. (b) STEM-EELS spectra of boron K-edge for examining the changes in LBO under different electrochemical states and $LiBO_2$ standard sample for comparison.

To check the durability of the LBO coating layer and understand its chemical environment, STEM-EELS analysis was conducted on the cathode after the first formation cycle in the full cell. The boron coating layer was still present on the cathode surface after the formation cycle (**Figure 3.13**), albeit in a different chemical environment.

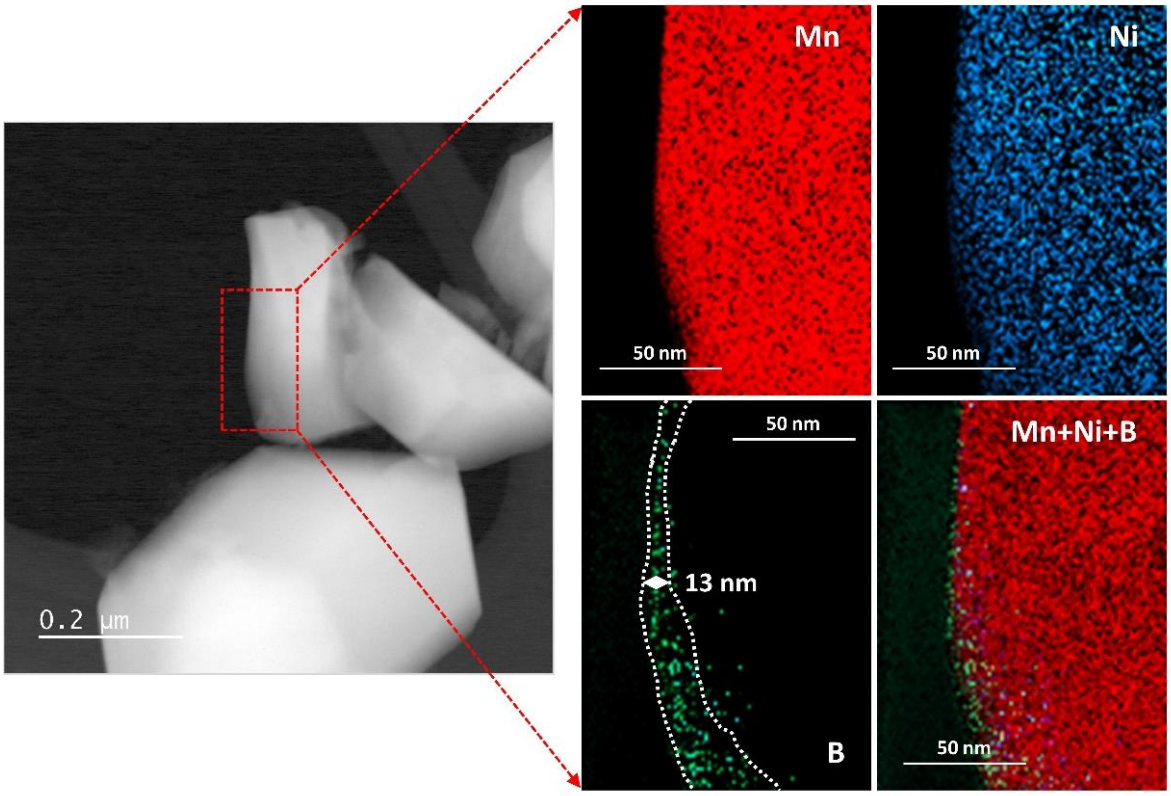

Figure 3.13: STEM-EELS mapping for manganese, nickel, and boron on LBO-coated LRLO after the formation cycle.

Figure 3.12 (b) compares the EELS spectra of the B K-edge from the surface of the LBO-coated cathode before and after electrochemical cycling. The measured near-edge structure for the $LiBO_2$ standard sample is characterized by a sharp peak at 192 eV associated with transitions to antibonding π* orbitals, and a broad feature at ~ 201 eV originated from σ* orbitals. At the pristine state, the LBO coating layer closely matches the spectrum from the $LiBO_2$ standard sample, while after the formation cycle, the change in the relative peak intensity is observed. Prior literature [25, 26] suggests that the presence of elements such as Ni, Co, and Zn as impurities in boron-based glass can affect the relative peak intensity. Therefore, boron may further diffuse into the transition metal layers during the formation process, which is confirmed through the boron K-edge EELS mapping in **Figure 3.14**. Following 100 cycles, no boron signal is detected in the boron K-edge

spectrum, implying the absence of LBO species on the cathode surface and their reactivity with the electrolyte.

To gain a clear mechanism understanding of the improved full cell performance, tracking boron is essential not only on the cathode but also on the graphite anode. As shown in **Figure 3.14 (a)**, the presence of a boron layer on the graphite surface with a thickness of up to 15 nm was confirmed after the formation cycle. The layer is thin but uniform and clearly present across the entire surface of the anode, as further confirmed by STEM-EELS spectra analysis (**Figure 3.14 (b)**). The peak positions and intensity ratios observed on the anode surface were identical to those observed on the cathode surface after the formation cycle. These observations indicate that the boron initially present on the cathode surface migrates through the electrolyte and deposits on the anode surface. This process contributes to the formation of the SEI layer, as evidenced by the change in peak intensity around 3.3 V in dQ/dV plots (**Figure 3.9 (b)**). After 100 cycles, like the cathode surface, there is an absence of any observable boron signal on the graphite anode surface. This reinforces that the LBO species can gradually undergo reactions with the electrolyte during extended cycling periods.

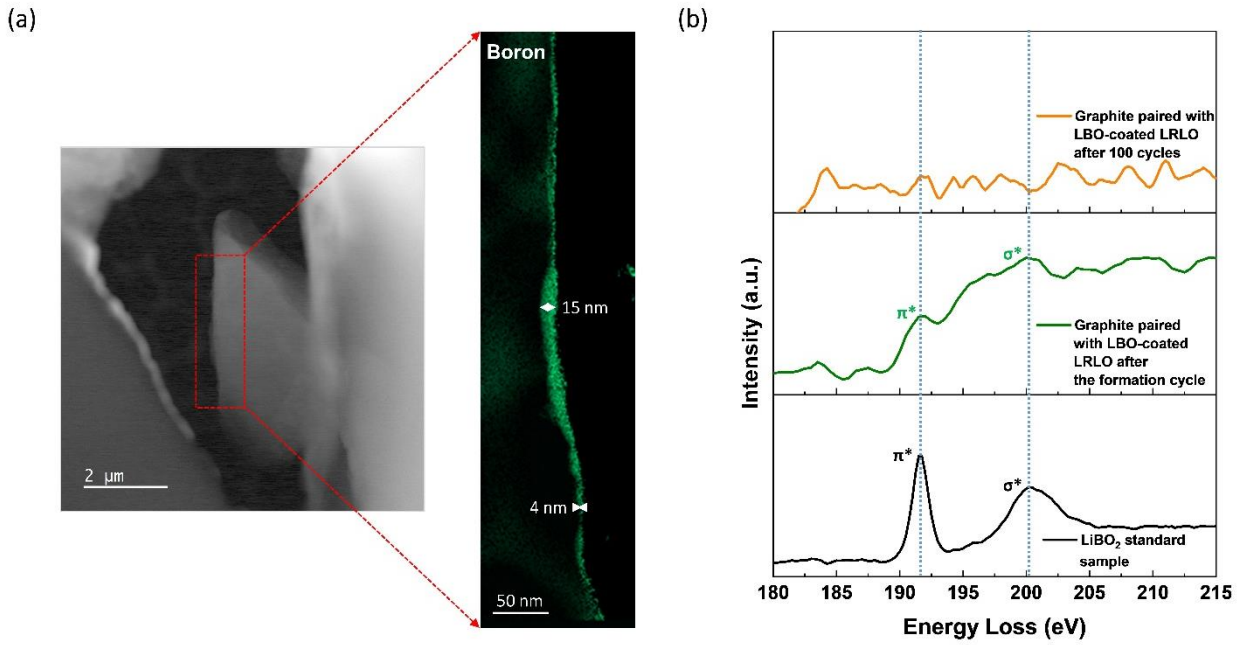

Figure 3.14: (a) STEM-EELS mapping results of graphite paired with LBO-coated LRLO after the formation cycle in the full cell. (b) EELS spectra of boron K-edge for cycled graphite and $LiBO_2$ standard sample for comparison.

3.3.3 LBO Reactivity with Electrolyte for Performance Improvement

The results obtained from STEM-EELS pinpoint the crucial factor of LBO reactivity with electrolyte for the improvement of overall cell performance. Due to insufficient electrolyte amount at the coin cell level, single-layer pouch cells were then assembled for cycling evaluation and electrolyte analysis. The uncoated LRLO pouch cell delivers a capacity retention of 79.9% after 70 cycles at a current rate of C/10. In contrast, the LBO-coated LRLO demonstrates a higher retention of 87.4% with a stabilized discharge capacity from around 40 cycles (**Figure 3.15 (a)**). Additionally, the charge and discharge voltage plot in **Figure 3.15 (b)** shows that the uncoated LRLO pouch cell has a voltage hysteresis of 0.37 V, while the LBO-coated LRLO reduces the voltage hysteresis to 0.18 V. To avoid excessive electrolyte consumption with prolonged cycling,

the pouch cells were stopped at 70 cycles, at which point a clear difference in gas generation (**Figure 3.15 (c)**) was observed.

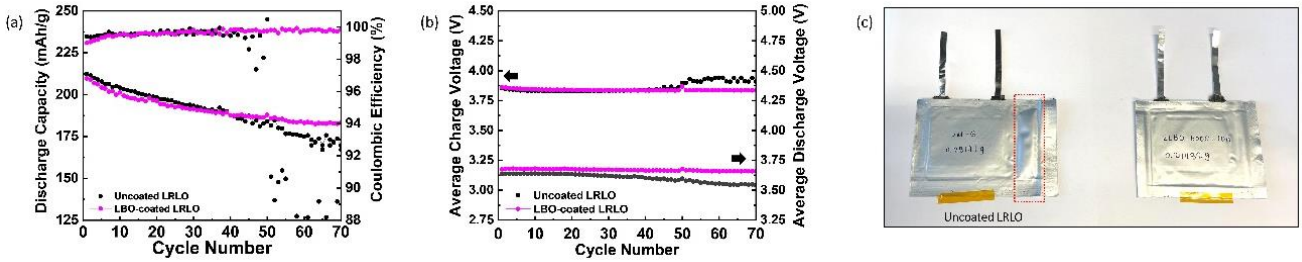

Figure 3.15: (a) Single layer pouch cell performance in the 2.0–4.55 V window at a current rate of C/10 (1 C = 270 mAh/g) with baseline electrolyte. (b) The average charge and discharge voltage. (c) Photos of pouch cells with uncoated LRLO and LBO-coated LRLO as the cathode.

The LRLO pouch cell without LBO coating exhibits evident swelling. This observation underscores the potential of LBO surface modification in reducing the gas generation which arises from the parasitic reactions in the cycled electrolyte at high voltage [27]. Pouch cells of uncoated LRLO and LBO-coated LRLO were disassembled after the formation cycle and after 70 cycles. Centrifuge tubes were utilized to efficiently extract the electrolyte through rotation at 2000 rpm. The extracted electrolyte was then analyzed by ^{19}F-NMR techniques (**Figure 3.16**).

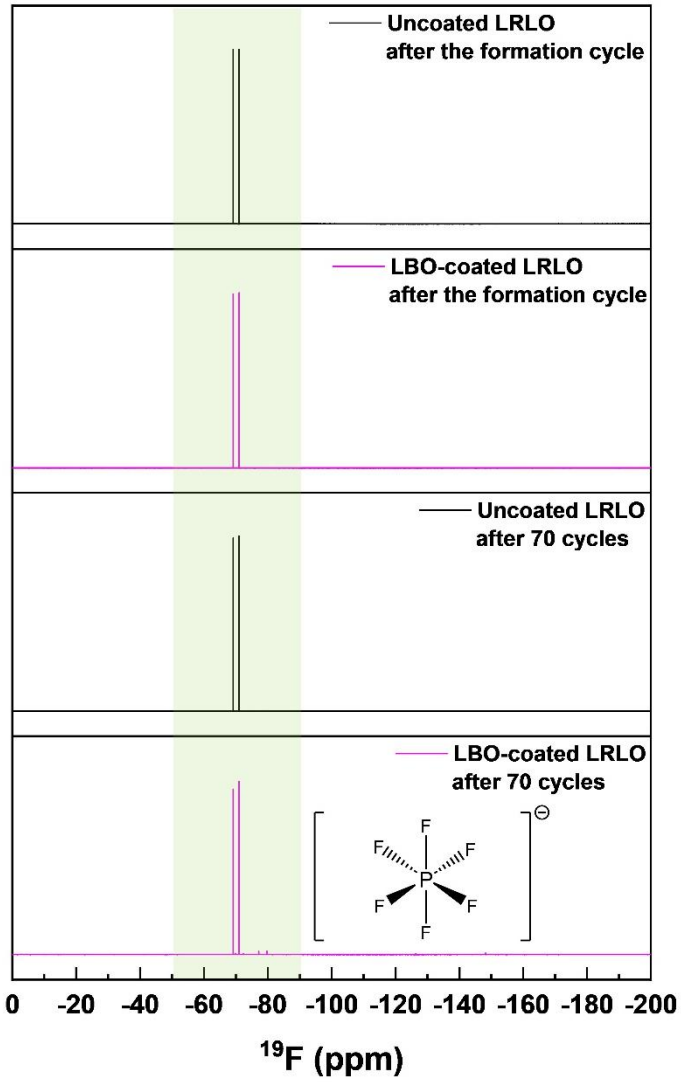

Figure 3.16: ^{19}F-NMR from different electrolyte samples, including cycled electrolytes from uncoated/LBO-coated LRLO after the formation cycle and 70 cycles in single layer pouch cell.

The presence of BF_4^- anions (**Figure 3.17 (a)**) is exclusively confirmed in the electrolyte after 70 cycles with LBO-coated LRLO. The formation of BF_4^- is absent even in the initial stage of the LBO-coated LRLO pouch cell, which implies that boron primarily contributes to forming the CEI/SEI layer during the formation cycle. As cycling progresses, boron progressively dissolves into the electrolyte, leading to the formation of the B-F environment. This observation aligns with STEM-EELS results, revealing the absence of boron on the cathode surface after 100 cycles.

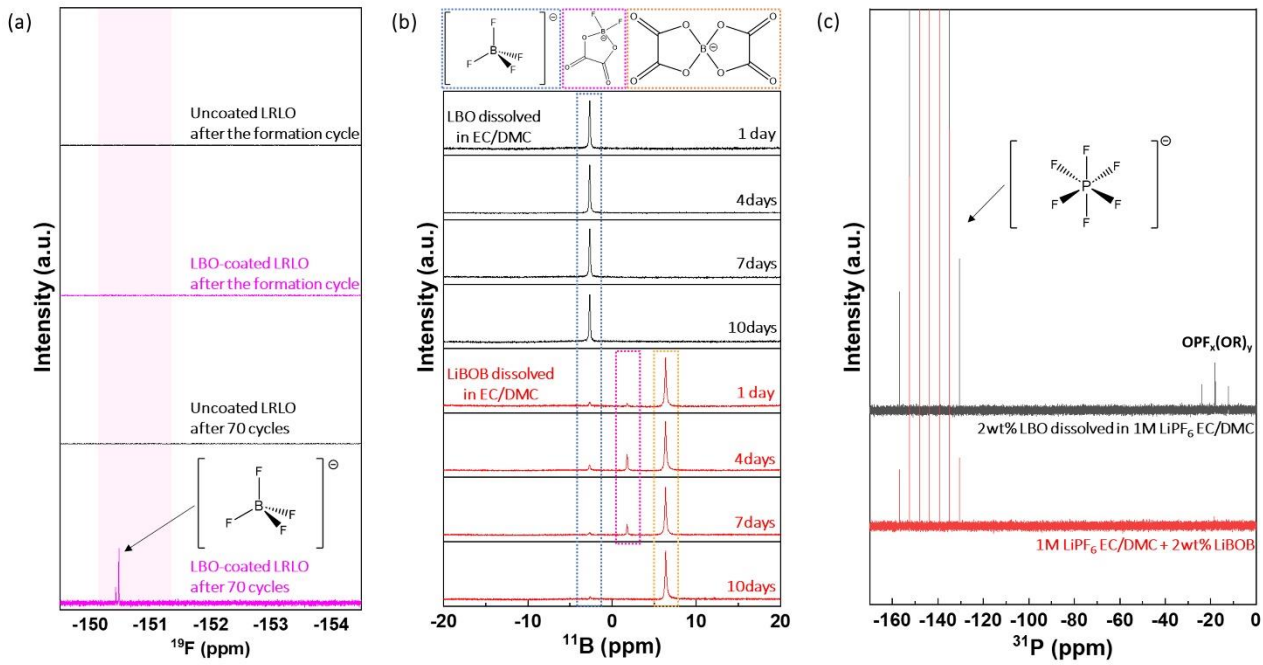

Figure 3.17: (a) ^{19}F-NMR from different electrolyte samples, including cycled electrolytes from uncoated LRLO and LBO-coated LRLO after the formation cycle and 70 cycles. (b) ^{11}B-NMR and (c) ^{31}P-NMR from different electrolyte samples, including LBO and LiBOB dissolved into carbonate baseline electrolyte.

To further investigate the reactivity of LBO, an electrolyte comprising 2 wt% LBO powder dissolved in 1M $LiPF_6$ EC/DMC 3:7 (v%) was examined. For comparison, another electrolyte containing 2 wt% LiBOB additive was also prepared in the same carbonate baseline electrolyte. In our previous study [28], the B-F environment was also present in the cycled electrolyte with LiBOB additive, which comes from the reaction between LiBOB and HF acid generated from electrolyte decomposition. Both electrolytes were stored for 1-, 4-, 7-, and 10-days post-preparation, followed by ^{11}B-NMR analysis to trace boron species (**Figure 3.17 (b)**). The findings reveal the rapid presence of BF_4^- anions within a day of LBO dissolution. After 10 days, no other boron species, apart from BF_4^-, are detected. This observation implies an immediate reaction of

LBO with the fluorine source (PF_6^- anion in the $LiPF_6$ salt) upon dissolution, leading to the formation of the B-F environment. In contrast, when LiBOB is utilized as an electrolyte additive, even after 10 days, a significant portion of the boron persists in the form of BOB^-. The emergence of a small quantity of BF_4^- and $DFOB^-$ in the LiBOB electrolyte after the storage is attributed to the disproportionation reaction between fluoride ligands on phosphorus and oxalato ligands on boron (in LiBOB) [29]. The considerably higher reactivity of LBO with the carbonate baseline electrolyte is further confirmed by ^{31}P-NMR analysis (**Figure 3.17 (c)**). The peak corresponding to PF_6^- in the -160 to -130 ppm range is evident in both electrolytes. However, distinctive peak features around -18 ppm associated with the $OPF_x(OR)_y$ organic compounds are observed solely in the electrolyte containing the LBO additive [30]. These organic compounds arise as byproducts of the reaction between LBO and PF_6^- anions in the electrolyte. The distinction in the reaction pathway leading to the formation of the B-F environment between LBO and LiBOB additives is crucial in elucidating the mechanism underlying performance improvement, as detailed below.

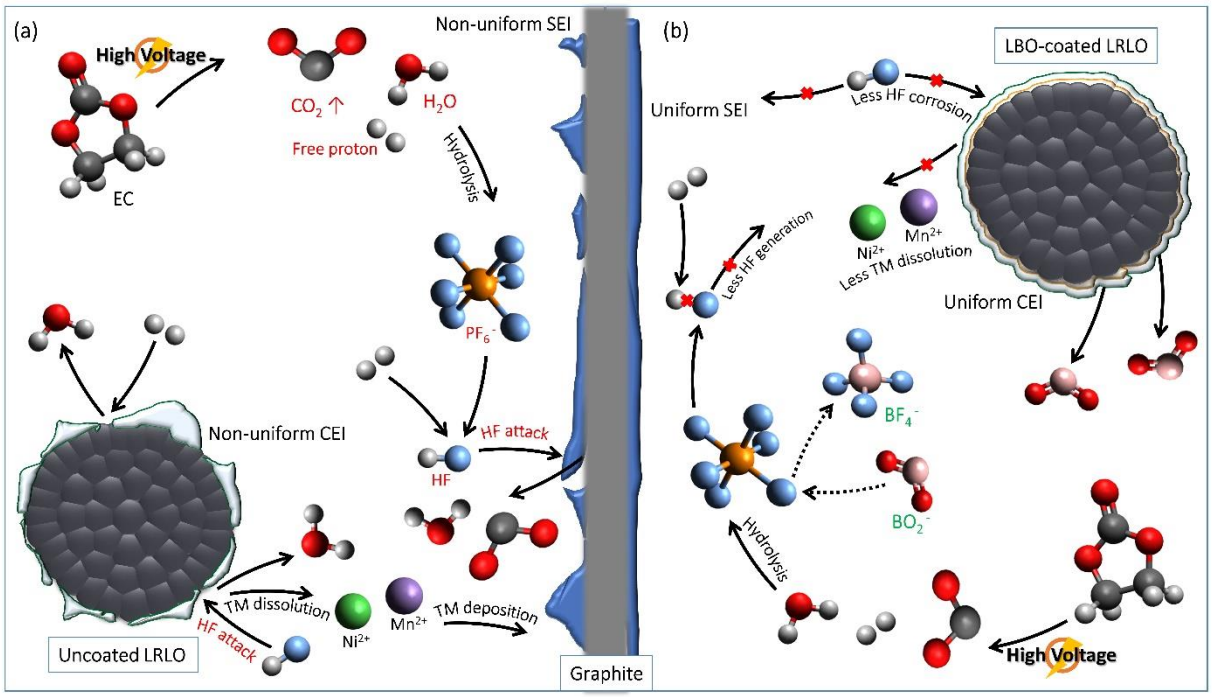

Figure 3.18: Schematics of performance improvement by LBO-coated LRLO in LRLO/graphite full cell. Reaction pathway for (a) uncoated LRLO/graphite full cell and (b) LBO-coated LRLO/graphite full cell with carbonate baseline electrolyte.

Based on all the above findings, the cycling performance improvement of LBO-coated LRLO in full cell is summarized in **Figure 3.18**. Cycling under high voltage, the ethylene carbonate (EC) component of the carbonate-based electrolyte undergoes ring opening process (**Figure 3.18 (a)**) [31]. Carbonate solvents oxidize and decompose, leading to the release of protons. The liberated protons are highly reactive on the cathode surface, binding with the oxygen and generating H_2O. This H_2O then reacts with $LiPF_6$ salt to form HF acid, which is highly corrosive to the cathode and anode surfaces [32]. On the cathode surface, the attack of HF acid causes the dissolution of transition metal, which subsequently redeposits on the anode surface through the electrolyte.

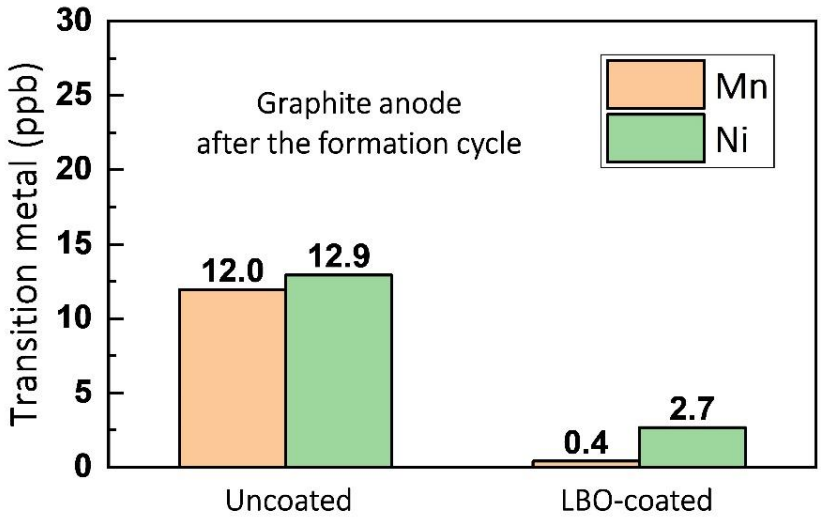

Figure 3.19: ICP-MS for transition metal (Mn and Ni) of graphite paired with uncoated and LBO-coated after the formation cycle.

The inductively coupled plasma mass spectrometry (ICP-MS) soaking test in **Figure 3.19** reveals a significantly higher concentration of Ni and Mn in the graphite when paired with the uncoated LRLO electrode after the formation cycle. The High-angle annular dark-field (HAADF) image (**Figure 3.20**) of uncoated LRLO is provided for the analysis of the CEI layer after the formation cycle.

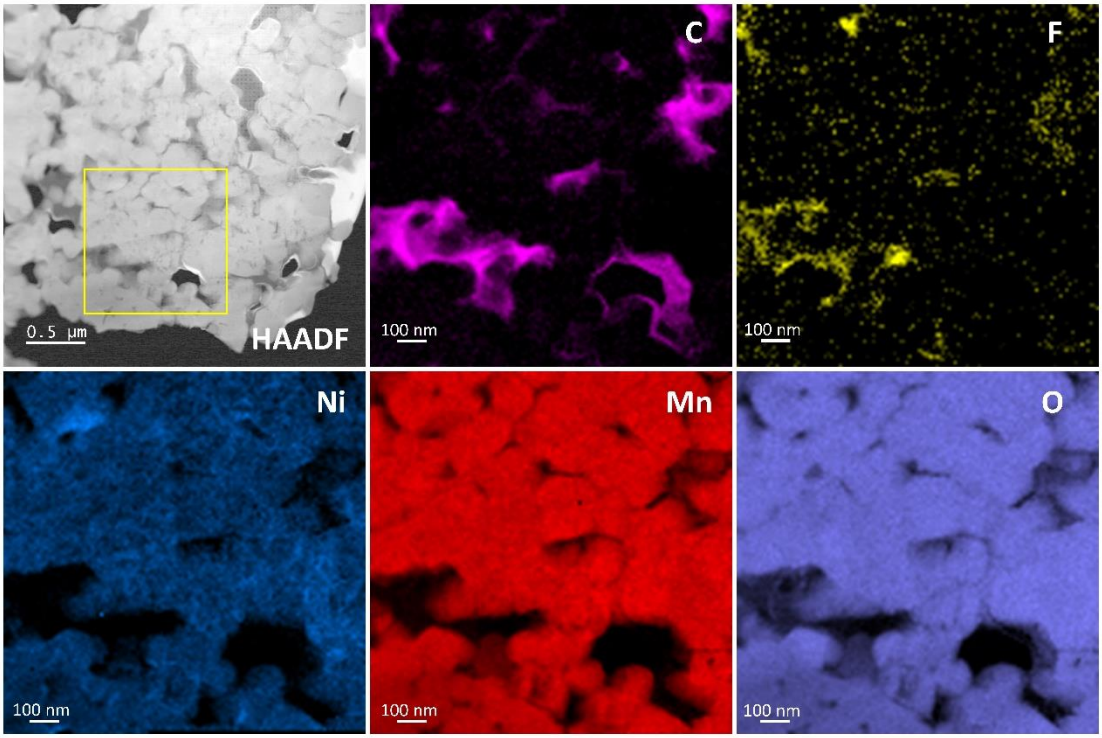

Figure 3.20: STEM-EELS carbon, fluorine, nickel, manganese, and oxygen mapping of uncoated LRLO after the formation cycle.

STEM-EELS mapping reveals a distinct clustering of carbon and fluorine, indicating a non-uniform distribution along the surface of primary particles. This observation aligns with the STEM-EDS data presented in **Figure 3.21**, confirming a similar non-uniform distribution of the SEI layer. Another noteworthy observation is the clear detection of manganese and nickel on the anode surface even after the formation cycle. This indicates that the dissolution and redeposition of transition metals occur even during the formation cycle.

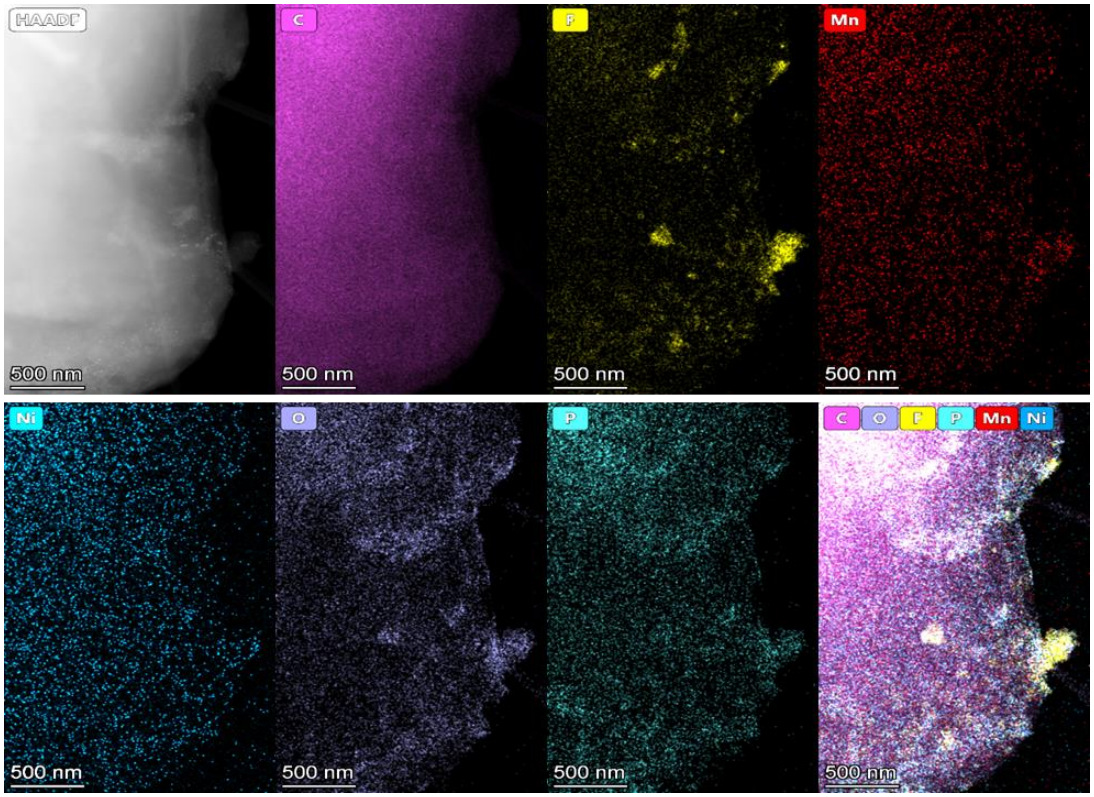

Figure 3.21: STEM-EDS mapping of SEI layer on graphite anode paired with uncoated LRLO after the formation cycle.

On the other hand, the LBO coating layer on the cathode surface engages in a competitive reaction compared to the $LiPF_6$ hydrolysis process (**Figure 3.18 (b)**). As confirmed by ^{31}P-NMR, LBO reacts with PF_6^- to form $LiBF_4$ or phosphorus fluorine oxide species. Given that the reaction between $LiPF_6$ and H_2O occurs simultaneously with the competitive interaction involving LBO, the reaction with H_2O is comparatively suppressed, thereby mitigating HF generation. The comparison of formation energies shows that the generation of B–F species is thermodynamically advantageous. The formation energy of BF_4^- (-1710 kJ mol^{-1}) [33] is much lower than that of HF (-273 kJ mol^{-1}) [34], making this reaction more favorable. Moreover, the B-F bond possesses a significantly higher bond energy (613 kJ mol^{-1}) than both H–F (565 kJ mol^{-1}) and P-F (490 kJ

mol^{-1}), indicating greater stability of the B–F bond over H–F and P–F bonds [35]. This finding is consistent with the literature, which reports that $LiBF_4$ is more stable than $LiPF_6$ [36].

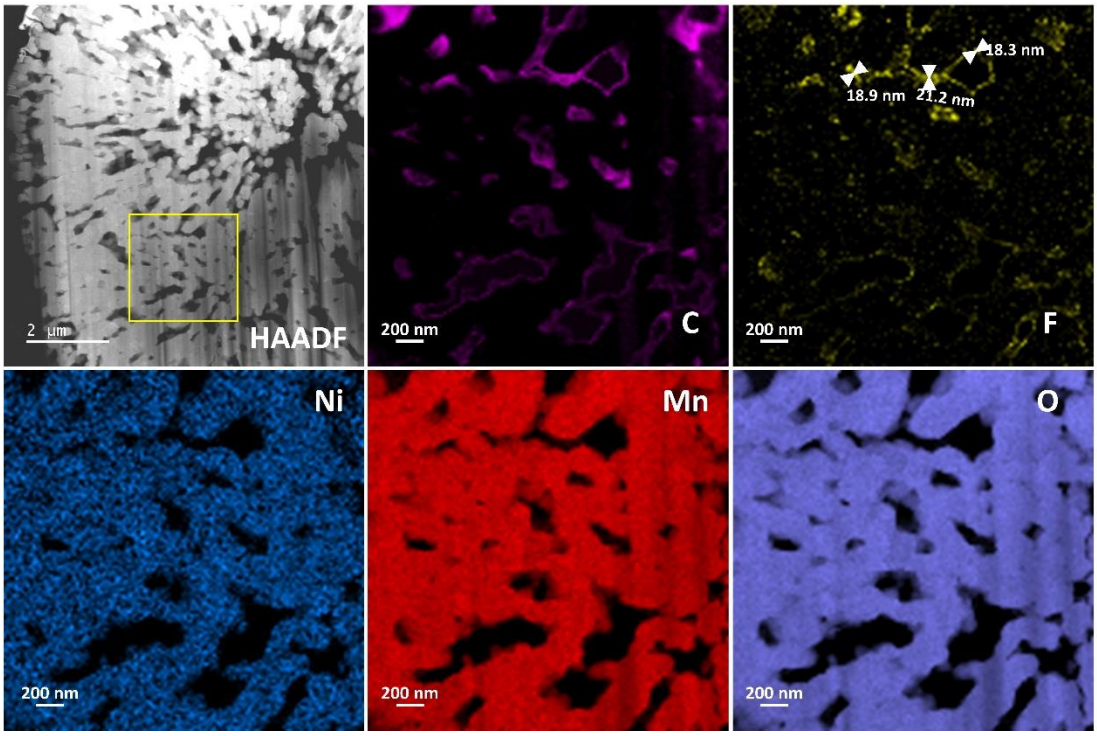

Figure 3.22: STEM-EELS carbon, fluorine, nickel, manganese, and oxygen mapping of LBO-coated LRLO after the formation cycle.

Consequently, in contrast to the uncoated LRLO case, LBO-coated LRLO exhibits a more uniform CEI layer with approximately 20 nm in thickness (**Figure 3.22**), indicating the relative attenuation of severe HF acid attacks during cycling. The STEM-EDS data in **Figure 3.23** also illustrates a uniform SEI layer, approximately 80 nm thick on the graphite anode paired with LBO-coated LRLO after the formation cycle. Transition metals were also detected in this graphite, highlighting that LBO surface modification cannot completely prohibit the dissolution and redeposition of transition metals. However, it is crucial to emphasize that the LBO surface

modification plays a significant role in mitigating these effects, as indicated by the results from the ICP-MS analysis (**Figure 3.19**).

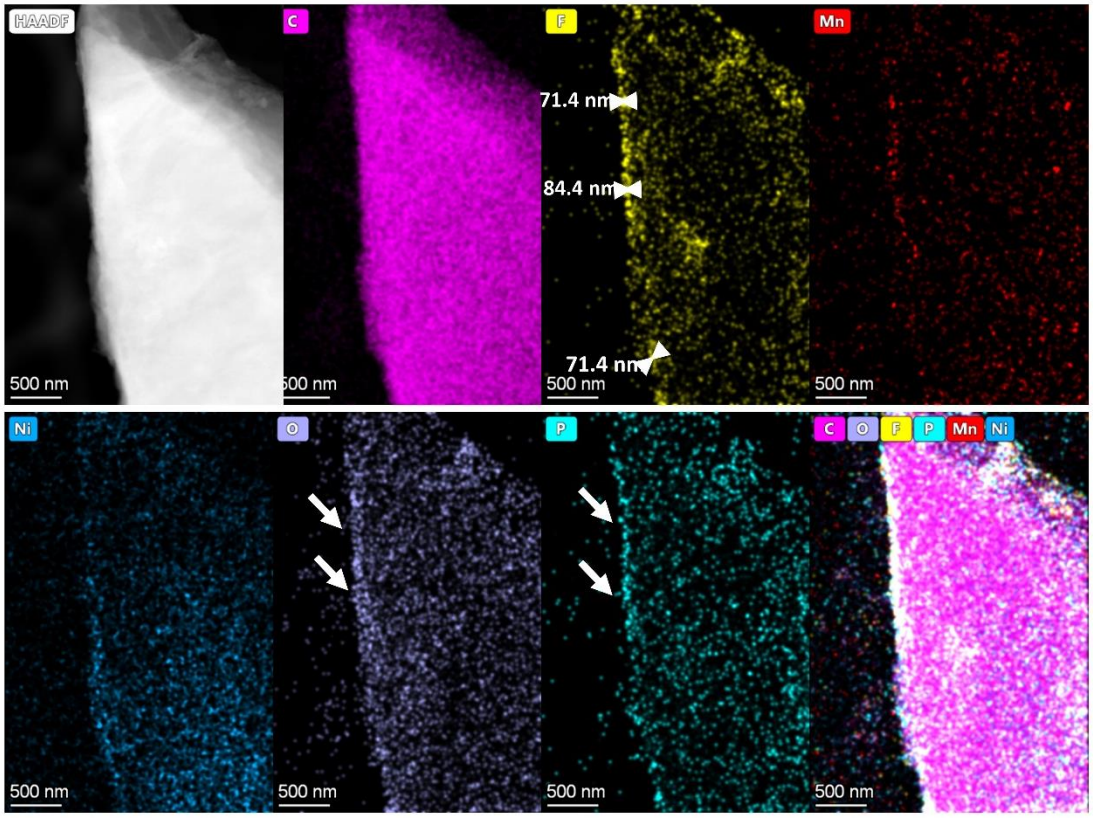

Figure 3.23: STEM-EDS mapping of SEI layer on graphite anode paired with LBO-coated LRLO after the formation cycle.

The LBO coating cannot prevent the generation of H_2O, which is the intrinsic issue of the EC solvent under a highly oxidative environment [37]; however, the continuous production of HF by PF_6^- can be reduced through the competitive reaction between LBO and PF_6^-. In our previous study [28], LiBOB was confirmed to serve as the scavenger for the generated HF acid. To completely prevent HF corrosion to the active materials and their interphase, we explore the synergy effect of employing both approaches: incorporating LBO-coated LRLO as the cathode material and introducing LiBOB as the electrolyte additive.

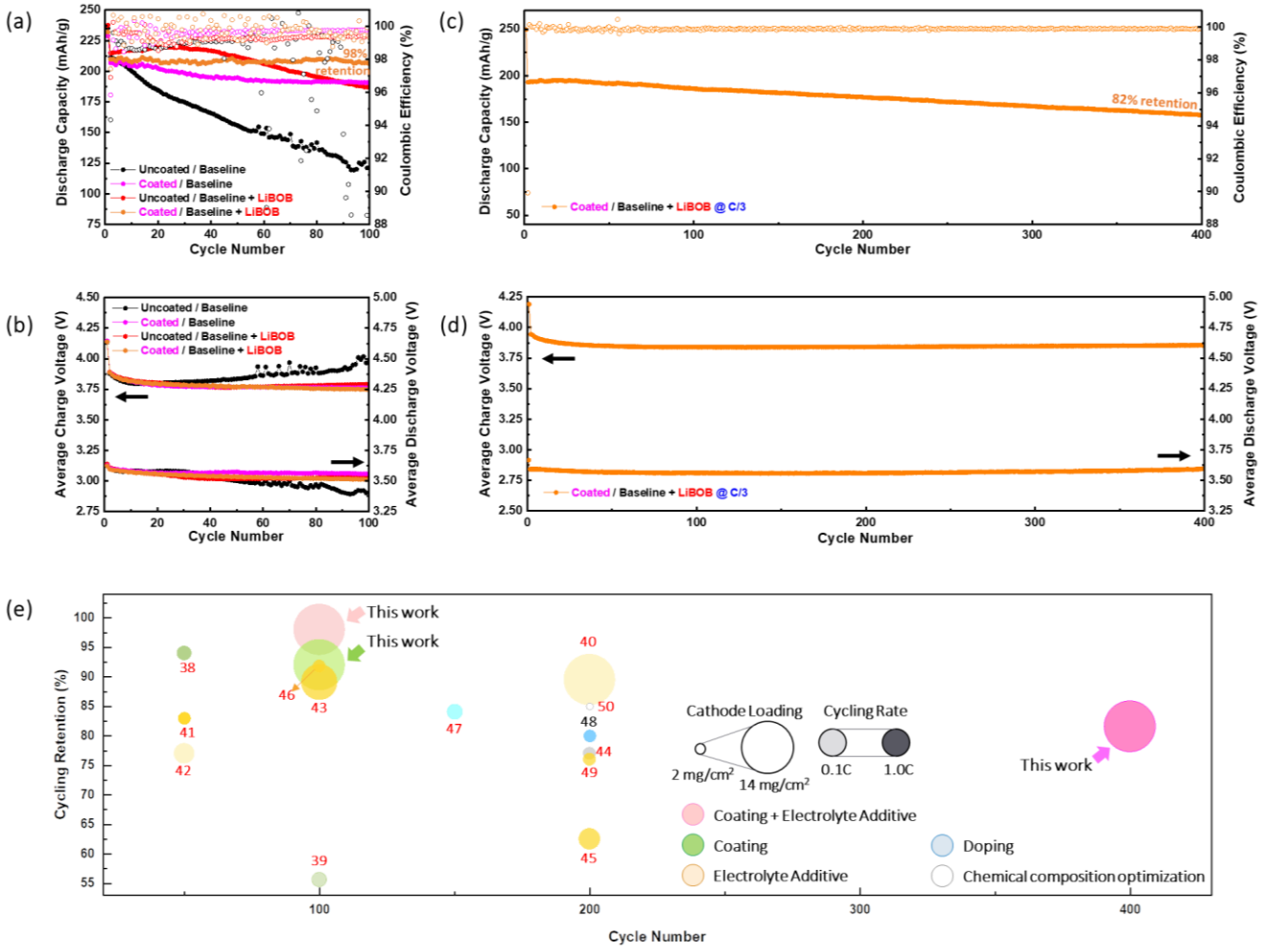

Figure 3.24. (a) Full cells cycling performance comparison with (b) the corresponding average charge and discharge voltage in the 2.0–4.55 V window at a current rate of C/10. (c) cycling performance comparison with (d) the corresponding average charge and discharge voltage in the 2.0–4.55 V window at a current rate of C/3. (e) LRLO/graphite full cell performance summary plot. (The numbers refer to the entries in **Table 3.2**. Additionally, red numbers indicate Co-containing LRLO cathode materials, while black numbers indicate Co-free LRLO cathode materials.)

Table 3.2: LRLO/graphite full cell performance summary.

		Chemical composition	Cathode loading ($mg \cdot cm^{-2}$)	Working Voltage (V)	Rate ($1C=270mA \cdot g^{-1}$)	Cycle (No.)	Retention after cycles (%)	Notice
This work	Coating + E/A	**$Li_{1.222}Ni_{0.349}Mn_{0.651}O_2$**	**14.0**	4.55-2.0	0.1C	100	98.0	2wt% LBO coating + 2wt% LiBOB
This work		**$Li_{1.222}Ni_{0.349}Mn_{0.651}O_2$**	**14.0**	4.55-2.0	**0.3C**	**400**	**81.9**	2wt% LBO coating + 2wt% LiBOB
This work	Coating	**$Li_{1.222}Ni_{0.349}Mn_{0.651}O_2$**	**14.0**	4.55-2.0	0.1C	100	92.0	2wt% LBO
38		$Li_{1.2}Mn_{0.55}Ni_{0.15}Co_{0.1}O_2$	3.5	4.6-2.2	0.3C	50	94.0	ALD 5wt% alumina
39		$0.4Li_2MnO_3 \cdot 0.6LiNi_{1/3}Co_{1/3}Mn_{1/3}O_2$	4.2	4.5-1.8	0.7C	100	55.6	Graphene oxide + Hydrazine, 60℃
40	Electrolyte Additive (E/A)	$Li_{1.144}Ni_{0.136}Co_{0.136}Mn_{0.544}O_2$	14.0	4.55-2.0	0.2C	200	89.5	2wt% LiBOB
41		$Li_{1.2}Mn_{0.54}Ni_{0.13}Co_{0.13}O_2$	N/A	4.8-2.0	0.5C	50	83.0	0.5wt% TMSPi
42		$Li_{1.13}Mn_{0.463}Ni_{0.203}Co_{0.203}O_2$	3.2	4.7-2.5	0.2C	50	77.0	DFDEC-VC
43		$0.5Li_2MnO_3 \cdot 0.5LiNi_{0.4}Co_{0.2}Mn_{0.4}O_2$	8.5	4.5-2.0	0.5C	100	89.1	5% TMSOM
44		$Li_{1.2}Mn_{0.55}Ni_{0.15}Co_{0.1}O_2$	N/A	4.8-2.0	0.5C	200	77.0	1% BTMSC
45		$Li_{1.17}Ni_{0.17}Mn_{0.5}Co_{0.17}O_2$	5.0	4.7-2.0	0.5C	200	62.5	1% LiDFOB
46		$Li_{1.13}Mn_{0.517}Ni_{0.256}Co_{0.097}O_2$	N/A	4.7-2.0	0.5C	100	91.8	0.5% TMSP + 0.5% HTCN
47	Doping	$Li_{1.2}Ni_{0.13}Co_{0.13}Mn_{0.54}B_{0.0125}O_2$	2.5	4.5-2.0	0.5C	150	84.1	LBO
48		$Li_{1.2}Mn_{0.585}Ni_{0.185}Fe_{0.03}O_2$	2.0	4.6-2.3	1.0C	200	80.0	3at% Fe
49	Optimal chemical composition	$Li_{1.2}Mn_{0.54}Ni_{0.13}Co_{0.13}O_2$	N/A	4.7-2.2	0.1C	200	76.0	-
50		$Li_{1.2}Mn_{0.54}Ni_{0.13}Co_{0.13}O_2$	2.0	4.7-2.2	0.1C	200	85.0	-

3.3.4 LBO Coating and LiBOB Additive for Long-term Cycling Stability

Irrespective of the use of electrolyte additives or surface modification, it shows no obvious capacity degradation during the formation cycle (**Figure 3.25 (a)**). The derivative of the capacity to the cell voltage was then plotted to compare the lithiation/delithiation processes for different cases. Apart from the peak at 3.3 V (corresponding to the CEI/SEI formation), there is no noticeable difference in the dQ/dV vs. plots (**Figure 3.25 (b)**). When LiBOB was used as an electrolyte additive or when the surface was modified with LBO, the intensity of the 3.3 V peak in the dQ/dV vs. plots decreased (**Figure 3.25 (c)**).

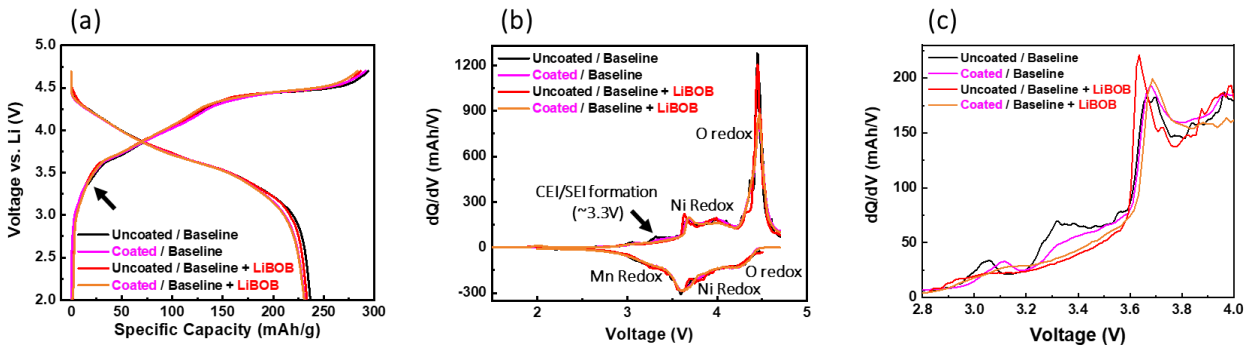

Figure 3.25: (a) Voltage profiles from uncoated and LBO-coated LRLO/graphite full cells with different electrolytes with (b) the corresponding dQ/dV plot. (c) dQ/dV plot within the CEI/SEI formation voltage range. The voltage window of full cells is 2.0–4.7 V at a current rate of C/20 for the formation cycle (1 C = 270 mAh/g).

To assess the synergy effect, a practical-level long-term cycling was conducted. Under the challenging conditions of high voltage, high loading electrode (3 mAh/cm^2), and a high current rate (C/3), the LBO-coated LRLO/graphite full cell with LiBOB electrolyte additive exhibits excellent performance, with a capacity retention of 82% after 400 cycles (**Figure 3.24 (c)**). Furthermore, even under high current rate conditions, a minimal voltage decay of 0.019 V was observed for the discharge process up to 400 cycles (**Figure 3.24 (d)**). Based on the performance summary from the published results of the LRLO/graphite full cell (**Table 3.2**), our investigation highlights the optimum cycle performance achieved with Co-free chemical composition and the highest cathode loading (**Figure 3.24 (e)**). Notably, this synergistic effect persists even under elevated temperatures. The high-temperature (45℃) testing results are presented in **Figure 3.26**.

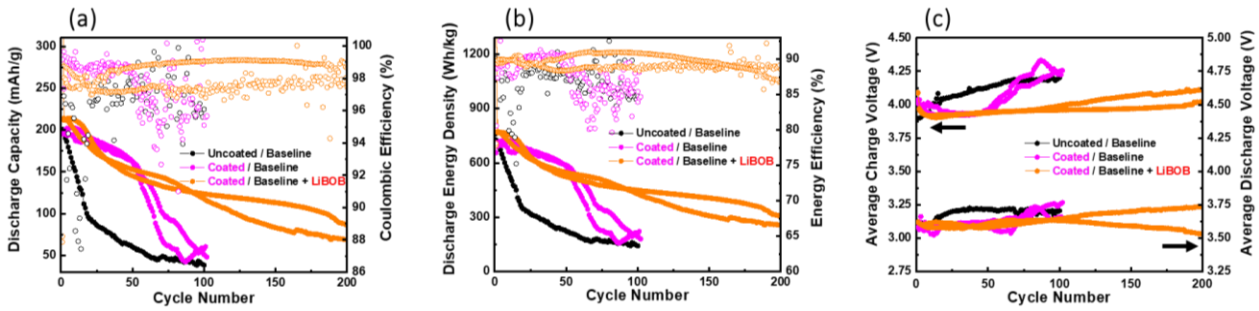

Figure 3.26: (a) Full cells cycling performances with the corresponding (b) energy density performances and (c) the average charge and discharge voltage at high temperature (45℃). The voltage window is 2.0–4.6 V at a current rate of C/3 (1 C = 270 mAh/g).

In contrast to the immediate capacity drop of the full cell with the uncoated LRLO cathode (black line), LBO surface modification alone exhibits the capacity to endure for approximately 60 cycles (pink line). The inclusion of a 2 wt% LiBOB electrolyte additive extends the cycling capability beyond 200 cycles. This observation underscores the potential to surmount the challenges associated with cycling at elevated temperatures, another obstacle that has impeded the practical application of LRLO, through strategic utilization of boron chemistry.

3.4 Conclusion

The oxygen redox products in LRLO, including radical anion complexes, readily engage with carbonate-based electrolytes, causing parasitic side reactions that compromise the cathode material's lattice structure and result in a rapid deterioration of electrochemical performance. This investigation employs boron chemistry to design a strategy for stabilizing the electrode-electrolyte interphase, proving effective in alleviating capacity and voltage decay. The LBO precursor is synthesized using a polyol process, enabling dry coating on the LRLO surface. Under optimized

conditions, a uniform LBO coating layer of 15 nm thickness is achieved, contributing to enhanced cycling stability in LRLO/graphite full cells.

The improved full-cell performance is attributed to the surface modification by LBO, which protects LRLO's lattice oxygen, and reacts with PF_6^- anions to suppress HF acid generation. This mechanistic understanding is supported by the observed reduction in transition metal dissolution and mitigated interphase corrosion in LBO-coated LRLO. The further incorporation of LiBOB additive, acting as an HF scavenger, results in promising battery performance for industrial-level applications. The full cell with LBO-coated LRLO cathode demonstrates an impressive 82% capacity retention after 400 cycles at a current rate of C/3, with an average discharge voltage drop of 0.019 V. This minimal voltage decay presents a significant opportunity for engineering LRLO materials towards achieving long-term cycling stability.

3.5 Acknowledgement

Chapter 3, in full, is a reprint of the material as it appears in "Park, N. R., Zhang, M., Han, B., Li, W., Qian, K., Nguyen, H., Kumakura, S., & Meng, Y. S. (2024). Understanding Boron Chemistry as the Surface Modification and Electrolyte Additive for Co-Free Lithium-Rich Layered Oxide. *Advanced Energy Materials*." The dissertation author was the first author of this paper.

3.6 References

[1] Armand, M., Axmann, P., Bresser, D., Copley, M., Edström, K., Ekberg, C., Guyomard, D., Lestriez, B., Novák, P., Petranikova, M., Porcher, W., Trabesinger, S., Wohlfahrt-Mehrens, M., & Zhang, H. (2020). Lithium-ion batteries – Current state of the art and anticipated developments. *Journal of Power Sources*, *479*. https://doi.org/10.1016/j.jpowsour.2020.228708

[2] Radin, M. D., Hy, S., Sina, M., Fang, C., Liu, H., Vinckeviciute, J., Zhang, M., Whittingham, M. S., Meng, Y. S., & van der Ven, A. (2017). Narrowing the Gap between Theoretical and Practical Capacities in Li-Ion Layered Oxide Cathode Materials. In *Advanced Energy Materials* (Vol. 7, Issue 20). Wiley-VCH Verlag. https://doi.org/10.1002/aenm.201602888

[3] Wu, F., Kim, G. T., Diemant, T., Kuenzel, M., Schür, A. R., Gao, X., Qin, B., Alwast, D., Jusys, Z., Behm, R. J., Geiger, D., Kaiser, U., & Passerini, S. (2020). Reducing Capacity and Voltage Decay of Co-Free $Li_{1.2}Ni_{0.2}Mn_{0.6}O_2$ as Positive Electrode Material for Lithium Batteries Employing an Ionic Liquid-Based Electrolyte. *Advanced Energy Materials*, *10*(34). https://doi.org/10.1002/aenm.202001830

[4] Zhang, B., Wang, L., Wang, X., Zhou, S., Fu, A., Yan, Y., Wang, Q., Xie, Q., Peng, D., Qiao, Y., & Sun, S. G. (2022). Sustained releasing superoxo scavenger for tailoring the electrode-electrolyte interface on Li-rich cathode. *Energy Storage Materials*, *53*, 492–504. https://doi.org/10.1016/j.ensm.2022.09.032

[5] Zhang, M., Liu, H., Liu, Z., Fang, C., & Meng, Y. S. (2018). Modified Coprecipitation Synthesis of Mesostructure-Controlled Li-Rich Layered Oxides for Minimizing Voltage Degradation. *ACS Applied Energy Materials*, *1*(7), 3369–3376. https://doi.org/10.1021/acsaem.8b00545

[6] Heng, Y.-L., Gu, Z.-Y., Guo, J.-Z., Yang, X.-T., Zhao, X.-X., & Wu, X.-L. (2022). Research progress on the surface/interface modification of high-voltage lithium oxide cathode materials. *Energy Materials*, *2*(3). https://doi.org/10.20517/energymater.2022.18

[7] Zhang, M., Kitchaev, D. A., Lebens-Higgins, Z., Vinckeviciute, J., Zuba, M., Reeves, P. J., Grey, C. P., Whittingham, M. S., Piper, L. F. J., van der Ven, A., & Meng, Y. S. (2022). Pushing the limit of 3d transition metal-based layered oxides that use both cation and anion redox for energy storage. In *Nature Reviews Materials* (Vol. 7, Issue 7, pp. 522–540). Nature Research. https://doi.org/10.1038/s41578-022-00416-1

[8] Singer, A., Zhang, M., Hy, S., Cela, D., Fang, C., Wynn, T. A., Qiu, B., Xia, Y., Liu, Z., Ulvestad, A., Hua, N., Wingert, J., Liu, H., Sprung, M., Zozulya, A. v., Maxey, E., Harder, R., Meng, Y. S., & Shpyrko, O. G. (2018). Nucleation of dislocations and their dynamics in layered oxide cathode materials during battery charging. *Nature Energy*, *3*(8), 641–647. https://doi.org/10.1038/s41560-018-0184-2

[9] Li, Y., Zuba, M. J., Bai, S., Lebens-Higgins, Z. W., Qiu, B., Park, S., Liu, Z., Zhang, M., Piper, L. F. J., & Meng, Y. S. (2021). Regeneration of degraded Li-rich layered oxide materials through heat treatment-induced transition metal reordering. *Energy Storage Materials*, *35*, 99–107. https://doi.org/10.1016/j.ensm.2020.11.013

[10] Hy, S., Liu, H., Zhang, M., Qian, D., Hwang, B. J., & Meng, Y. S. (2016). Performance and design considerations for lithium excess layered oxide positive electrode materials for lithium ion batteries. In *Energy and Environmental Science* (Vol. 9, Issue 6, pp. 1931–1954). Royal Society of Chemistry. https://doi.org/10.1039/c5ee03573b

[11] Zhao, T., Chen, S., Chen, R., Li, L., Zhang, X., Xie, M., & Wu, F. (2014). The positive roles of integrated layered-spinel structures combined with nanocoating in low-cost Li-rich cathode $Li[Li_{0.2}Fe_{0.1}Ni_{0.15}Mn_{0.55}]O_2$ for lithium-ion batteries. *ACS Applied Materials and Interfaces*, *6*(23), 21711–21720. https://doi.org/10.1021/am506934j

[12] Zhang, X., Belharouak, I., Li, L., Lei, Y., Elam, J. W., Nie, A., Chen, X., Yassar, R. S., & Axelbaum, R. L. (2013). Structural and electrochemical study of Al_2O_3 and TiO_2 Coated $Li_{1.2}Ni_{0.13}Mn_{0.54}Co_{0.13}O_2$ cathode material using ALD. *Advanced Energy Materials*, *3*(10), 1299–1307. https://doi.org/10.1002/aenm.201300269

[13] Kim, S. Y., Park, C. S., Hosseini, S., Lampert, J., Kim, Y. J., & Nazar, L. F. (2021). Inhibiting Oxygen Release from Li-rich, Mn-rich Layered Oxides at the Surface with a Solution Processable Oxygen Scavenger Polymer. *Advanced Energy Materials*, *11*(30). https://doi.org/10.1002/aenm.202100552

[14] Park, N. R., Li, Y., Yao, W., Zhang, M., Han, B., Mejia, C., Sayahpour, B., Shimizu, R., Bhamwala, B., Dang, B., Kumakura, S., Li, W., & Meng, Y. S. (2023). Understanding the Role of Lithium Borate as the Surface Coating on High Voltage Single Crystal $LiNi_{0.5}Mn_{1.5}O_4$. *Advanced Functional Materials*. https://doi.org/10.1002/adfm.202312091

[15] Zheng, J., Gu, M., Xiao, J., Polzin, B. J., Yan, P., Chen, X., Wang, C., & Zhang, J. G. (2014). Functioning mechanism of AlF_3 coating on the Li- and Mn-rich cathode materials. *Chemistry of Materials*, *26*(22), 6320–6327. https://doi.org/10.1021/cm502071h

[16] Wu, F., Zhang, X., Zhao, T., Li, L., Xie, M., & Chen, R. (2015). Multifunctional $ALPO_4$ coating for improving electrochemical properties of low-cost $Li[Li_{0.2}Fe_{0.1}Ni_{0.15}Mn_{0.55}]O_2$ cathode materials for lithium-ion batteries. *ACS Applied Materials and Interfaces*, *7*(6), 3773–3781. https://doi.org/10.1021/am508579r

[17] Shi, S. J., Tu, J. P., Tang, Y. Y., Zhang, Y. Q., Liu, X. Y., Wang, X. L., & Gu, C. D. (2013). Enhanced electrochemical performance of LiF-modified $LiNi_{1/3}Co_{1/3}Mn_{1/3}O_2$ cathode materials for Li-ion batteries. *Journal of Power Sources*, *225*, 338–346. https://doi.org/10.1016/j.jpowsour.2012.10.065

[18] Jo, C. H., Cho, D. H., Noh, H. J., Yashiro, H., Sun, Y. K., & Myung, S. T. (2015). An effective method to reduce residual lithium compounds on Ni-rich $Li[Ni_{0.6}Co_{0.2}Mn_{0.2}]O_2$

active material using a phosphoric acid derived Li_3PO_4 nanolayer. *Nano Research*, *8*(5), 1464–1479. https://doi.org/10.1007/s12274-014-0631-8

[19] Jiang, J., Li, Y., Liu, J., Huang, X., Yuan, C., & Lou, X. W. (2012). Recent advances in metal oxide-based electrode architecture design for electrochemical energy storage. In *Advanced Materials* (Vol. 24, Issue 38, pp. 5166–5180). https://doi.org/10.1002/adma.201202146

[20] Wang, W., Yin, Z., Wang, J., Wang, Z., Li, X., & Guo, H. (2015). Effect of heat-treatment on Li_2ZrO_3-coated $LiNi_{1/3}Co_{1/3}Mn_{1/3}O_2$ and its high voltage electrochemical performance. *Journal of Alloys and Compounds*, *651*, 737–743. https://doi.org/10.1016/j.jallcom.2015.08.114

[21] Zhou, L., Yin, Z., Tian, H., Ding, Z., Li, X., Wang, Z., & Guo, H. (2018). Spinel-embedded and Li_3PO_4 modified $Li[Li_{0.2}Mn_{0.54}Ni_{0.13}Co_{0.13}]O_2$ cathode materials for High-Performance Li-Ion battries. *Applied Surface Science*, *456*, 763–770. https://doi.org/10.1016/j.apsusc.2018.06.114

[22] Liu, W., Oh, P., Liu, X., Myeong, S., Cho, W., & Cho, J. (2015). Countering Voltage Decay and Capacity Fading of Lithium-Rich Cathode Material at 60 ℃by Hybrid Surface Protection Layers. *Advanced Energy Materials*, *5*(13). https://doi.org/10.1002/aenm.201500274

[23] Zhou, L. J., Yin, Z. L., Ding, Z. Y., Li, X. H., Wang, Z. X., & Guo, H. J. (2018). CeO_2 coating to improve the performance of $Li[Li_{0.2}Mn_{0.54}Ni_{0.13}Co_{0.13}]O_2$. *Ionics*, *24*(9), 2533–2542. https://doi.org/10.1007/s11581-017-2387-0

[24] Liu, H., Qian, D., Verde, M. G., Zhang, M., Baggetto, L., An, K., Chen, Y., Carroll, K. J., Lau, D., Chi, M., Veith, G. M., & Meng, Y. S. (2015). Understanding the Role of NH_4F and Al_2O_3 Surface Co-modification on Lithium-Excess Layered Oxide $Li_{1.2}Ni_{0.2}Mn_{0.6}O_2$. *ACS Applied Materials and Interfaces*, *7*(34), 19189–19200. https://doi.org/10.1021/acsami.5b04932

[25] Sauer, H., Brydson, R., Rowley, P. N., Engel, W., & Thomas, J. M. (1993). Determination of coordinations and coordination-specific site occupancies by electron energy-loss spectroscopy: an investigation of boron-oxygen compounds Dedicated to Professor Elmar Zeitler on the occasion of his 65th birthday. In *Ultramicroscopy* (Vol. 49).

[26] Lelong, G., Cormier, L., Hennet, L., Michel, F., Rueff, J. P., Ablett, J. M., & Monaco, G. (2017). Lithium borate crystals and glasses: How similar are they? A non-resonant inelastic X-ray scattering study around the B and O K-edges. *Journal of Non-Crystalline Solids*, *472*, 1–8. https://doi.org/10.1016/j.jnoncrysol.2017.06.012

[27] Yao, W., Chouchane, M., Li, W., Bai, S., Liu, Z., Li, L., Chen, A. X., Sayahpour, B., Shimizu, R., Raghavendran, G., Schroeder, M. A., Chen, Y. T., Tan, D. H. S., Sreenarayanan, B., Waters, C. K., Sichler, A., Gould, B., Kountz, D. J., Lipomi, D. J., Zhang,

M., & Meng, Y. S. (2023). A 5 V-class cobalt-free battery cathode with high loading enabled by dry coating. *Energy and Environmental Science*, *16*(4), 1620–1630. https://doi.org/10.1039/d2ee03840d

[28] Li, Y., Li, W., Shimizu, R., Cheng, D., Nguyen, H. N., Paulsen, J., Kumakura, S., Zhang, M., & Meng, Y. S. (2022). Elucidating the Effect of Borate Additive in High-Voltage Electrolyte for Li-Rich Layered Oxide Materials. *Advanced Energy Materials*, *12*(11). https://doi.org/10.1002/aenm.202103033

[29] Xiao, A., Yang, L., & Lucht, B. L. (2007). Thermal reactions of $LiPF_6$ with added LiBOB. *Electrochemical and Solid-State Letters*, *10*(11), 241–244. https://doi.org/10.1149/1.2772084

[30] Dong, Y., Demeaux, J., Zhang, Y., Xu, M., Zhou, L., MacIntosh, A. D., & Lucht, B. L. (2017). Improving the Performance at Elevated Temperature of High Voltage Graphite/$LiNi_{0.5}Mn_{1.5}O_4$ Cells with Added Lithium Catechol Dimethyl Borate. *Journal of The Electrochemical Society*, *164*(2), A128–A136. https://doi.org/10.1149/2.0331702jes

[31] Metzger, M., Strehle, B., Solchenbach, S., & Gasteiger, H. A. (2016). Hydrolysis of Ethylene Carbonate with Water and Hydroxide under Battery Operating Conditions. *Journal of The Electrochemical Society*, *163*(7), A1219–A1225. https://doi.org/10.1149/2.0411607jes

[32] Li, W., Cheng, D., Shimizu, R., Li, Y., Yao, W., Raghavendran, G., Zhang, M., & Meng, Y. S. (2022). Artificial cathode electrolyte interphase for improving high voltage cycling stability of thick electrode with Co-free 5 V spinel oxides. *Energy Storage Materials*, *49*, 77–84. https://doi.org/10.1016/j.ensm.2022.04.002

[33] Aravindan, V., Gnanaraj, J., Madhavi, S., & Liu, H. K. (2011). Lithium-ion conducting electrolyte salts for lithium batteries. In *Chemistry - A European Journal* (Vol. 17, Issue 51, pp. 14326–14346). https://doi.org/10.1002/chem.201101486

[34] J. D. Cox, D. D. Wagman, V. A. Medvedev, CODATA Key Values for Thermodynamics, Hemisphere Publishing Corp., New York 1989.

[35] T. L. Cottrell, The Strengths of Chemical Bonds, Butterworths Scientific Publications, London 1958.

[36] Ellis, L. D., Hill, I. G., Gering, K. L., & Dahn, J. R. (2017). Synergistic Effect of $LiPF_6$ and $LiBF_4$ as Electrolyte Salts in Lithium-Ion Cells. *Journal of The Electrochemical Society*, *164*(12), A2426–A2433. https://doi.org/10.1149/2.0811712jes

[37] Liu, M., Vatamanu, J., Chen, X., Xing, L., Xu, K., & Li, W. (2021). Hydrolysis of $LiPF_6$-Containing Electrolyte at High Voltage. *ACS Energy Letters*, *6*(6), 2096–2102. https://doi.org/10.1021/acsenergylett.1c00707

[38] Bettge, M., Li, Y., Sankaran, B., Rago, N. D., Spila, T., Haasch, R. T., Petrov, I., & Abraham, D. P. (2013). Improving high-capacity $Li_{1.2}Ni_{0.15}Mn_{0.55}Co_{0.1}O_2$-based lithium-ion cells by modifiying the positive electrode with alumina. *Journal of Power Sources*, *233*, 346–357. https://doi.org/10.1016/j.jpowsour.2013.01.082

[39] Oh, P., Ko, M., Myeong, S., Kim, Y., & Cho, J. (2014). A novel surface treatment method and new insight into discharge voltage deterioration for high-performance $0.4Li_2MnO_3$-$0.6LiNi_{1/3}Co_{1/3}Mn_{1/3}O_2$ cathode materials. *Advanced Energy Materials*, *4*(16). https://doi.org/10.1002/aenm.201400631

[40] Li, Y., Li, W., Shimizu, R., Cheng, D., Nguyen, H. N., Paulsen, J., Kumakura, S., Zhang, M., & Meng, Y. S. (2022). Elucidating the Effect of Borate Additive in High-Voltage Electrolyte for Li-Rich Layered Oxide Materials. *Advanced Energy Materials*, *12*(11). https://doi.org/10.1002/aenm.202103033

[41] Zhu, Y., Luo, X., Xu, M., Zhang, L., Yu, L., Fan, W., & Li, W. (2016). Failure mechanism of layered lithium-rich oxide/graphite cell and its solution by using electrolyte additive. *Journal of Power Sources*, *317*, 65–73. https://doi.org/10.1016/j.jpowsour.2016.03.090

[42] Pham, H. Q., Hwang, E. H., Kwon, Y. G., & Song, S. W. (2016). Understanding the interfacial phenomena of a 4.7V and 55 ℃ Li-ion battery with Li-rich layered oxide cathode and graphite anode and its correlation to high-energy cycling performance. *Journal of Power Sources*, *323*, 220–230. https://doi.org/10.1016/j.jpowsour.2016.05.038

[43] Lim, S. H., Cho, W., Kim, Y. J., & Yim, T. (2016). Insight into the electrochemical behaviors of 5V–class high–voltage batteries composed of lithium–rich layered oxide with multifunctional additive. *Journal of Power Sources*, *336*, 465–474. https://doi.org/10.1016/j.jpowsour.2016.11.002

[44] Lan, J., Zheng, Q., Zhou, H., Li, J., Xing, L., Xu, K., Fan, W., Yu, L., & Li, W. (2019). Stabilizing a High-Voltage Lithium-Rich Layered Oxide Cathode with a Novel Electrolyte Additive. *ACS Applied Materials and Interfaces*, *11*(32), 28841–28850. https://doi.org/10.1021/acsami.9b07441

[45] Cha, J., Han, J. G., Hwang, J., Cho, J., & Choi, N. S. (2017). Mechanisms for electrochemical performance enhancement by the salt-type electrolyte additive, lithium difluoro(oxalato)borate, in high-voltage lithium-ion batteries. *Journal of Power Sources*, *357*, 97–106. https://doi.org/10.1016/j.jpowsour.2017.04.094

[46] Zhao, J., Liang, Y., Zhang, X., Zhang, Z., Wang, E., He, S., Wang, B., Han, Z., Lu, J., Amine, K., & Yu, H. (2021). In Situ Construction of Uniform and Robust Cathode–Electrolyte Interphase for Li-Rich Layered Oxides. *Advanced Functional Materials*, *31*(8). https://doi.org/10.1002/adfm.202009192

[47] Sun, Z., Xu, L., Dong, C., Zhang, H., Zhang, M., Liu, Y., Zhou, Y., Han, Y., & Chen, Y. (2019). Enhanced cycling stability of boron-doped lithium-rich layered oxide cathode

materials by suppressing transition metal migration. *Journal of Materials Chemistry A*, *7*(7), 3375–3383. https://doi.org/10.1039/C8TA10786F

[48] Wu, F., Kim, G. T., Kuenzel, M., Zhang, H., Asenbauer, J., Geiger, D., Kaiser, U., & Passerini, S. (2019). Elucidating the Effect of Iron Doping on the Electrochemical Performance of Cobalt-Free Lithium-Rich Layered Cathode Materials. *Advanced Energy Materials*, *9*(43). https://doi.org/10.1002/aenm.201902445

[49] Silvestri, L., Celeste, A., Tuccillo, M., & Brutti, S. (2023). Li-Rich Layered Oxides: Structure and Doping Strategies to Enable Co-Poor/Co-Free Cathodes for Li-Ion Batteries. In *Crystals* (Vol. 13, Issue 2). MDPI. https://doi.org/10.3390/cryst13020204

[50] Celeste, A., Brescia, R., Gigli, L., Plaisier, J., Pellegrini, V., Silvestri, L., & Brutti, S. (2023). Unravelling structural changes of the $Li_{1.2}Mn_{0.54}Ni_{0.13}Co_{0.13}O_2$ lattice upon cycling in lithium cell. Materials Today Sustainability, 21. https://doi.org/10.1016/j.mtsust.2022.100277

Chapter 4 Summary and Perspective

4.1 Addressing High-Voltage Cathode Challenges

Advancing lithium-ion battery technology requires innovative strategies to address challenges associated with high-voltage cathodes, such as capacity fade, voltage decay, and interfacial instability. In this study, we explored boron-based surface engineering as a means to stabilize electrode-electrolyte interphases and improve the long-term performance of full cells employing single-crystal LNMO and LRLO cathodes. The LBO coatings demonstrated significant benefits in mitigating degradation mechanisms and enhancing cycling stability.

The LBO precursor was synthesized through a scalable polyol process, achieving uniform nano-sized coatings and partial doping on cathode surfaces. Electrochemical testing revealed that LBO coatings effectively reduced transition metal dissolution, minimized lattice oxygen degradation, and suppressed the generation of HF acid by reacting with PF_6^- anions. The dissolution of LBO during cycling formed $LiBF_4$, which prevented electrolyte decomposition and contributed to stable cathode-electrolyte interphases. The incorporation of the LiBOB additive further amplified these benefits, acting as an HF scavenger to improve electrolyte stability. As a result, full cells with LBO-coated LRLO demonstrated remarkable performance, achieving 82% capacity retention after 400 cycles at C/3 with minimal voltage decay. Similarly, coated LNMO showed superior cycling stability, highlighting the broad applicability of this approach.

4.2 Mechanistic Insights into Boron-Based Stabilization

From a mechanistic perspective, the study provided key insights into the role of boron species in stabilizing the interphase. The coatings not only acted as a protective barrier but also interacted with electrolyte components to mitigate cross-talk between cathodes and anodes.

Characterization techniques such as STEM-EELS, ^{19}F-NMR, and ICP-MS confirmed the uniformity of the coatings and elucidated the changes in chemical species during cycling, supporting the proposed mechanisms of degradation suppression.

These findings offer a promising pathway for enhancing high-voltage lithium-ion batteries and accelerating their commercialization. Future research should focus on optimizing boron-based coatings for various cathode materials, exploring their compatibility with next-generation electrolytes, and scaling up these approaches for industrial applications. By leveraging the dual functionalities of surface protection and electrolyte stabilization, this work contributes to the development of robust, high-performance energy storage systems suitable for long-term use in electric vehicles and grid storage.

4.3 Future Directions and Reflections on Cathode Research

Cathode materials remain an enduring subject of research. Over a decade ago, many believed that cathode development had already reached its peak. Yet, even today, they continue to be the most critical and enigmatic component of lithium-ion batteries. My journey into the exploration of cathode materials began with surface treatment studies on LCO and has since expanded through NCM523, NCM622, NCA, NCMA, and NCM811, progressing to advanced systems like LNMO, LRLO, and LMFP (Lithium Manganese Iron Phosphate). However, there is still a vast frontier of work ahead, spanning precursor synthesis, optimization of heat treatment conditions, surface coating and doping strategies, and fine-tuning chemical compositions.

Cathode materials are critical components in batteries, directly influencing various performance metrics such as energy density, stability, cost, and cycle performance. Beyond the research areas discussed earlier, studies on cost-competitive LMFP and next-generation sodium-

based cathode materials represent significant opportunities for cathode researchers. Considering this, the following specific research directions are proposed:

1. Enhancing conductivity of LMFP: LMFP is renowned for its exceptional stability and safety relative to cost; however, its low electrical conductivity and limited ionic diffusion remain key challenges. Researchers can address these issues through the following approaches:
    - Surface coating and doping strategies: Applying carbon-based coatings, incorporating conductive additives, or introducing metal ion doping can improve conductivity and expand the electrochemical active volume.
    - Optimization of microstructure: Nanostructuring LMFP to shorten ion diffusion pathways and increase active surface areas should guide the design of the synthesis process.
    - Innovative electrode design: Developing electrode compositions and current collector designs that maintain high conductivity while maximizing LMFP's inherent properties is crucial.

2. Development of Na-Based cathode materials: Na-ion batteries offer a promising alternative to overcome the limitations of Li resources, particularly for low-cost energy storage systems. However, Na cathode materials face challenges such as lower energy density and performance stability compared to Li counterparts. Key research objectives include:
    - Exploration of High-Voltage Sodium-Based cathodes: Surface treatments are necessary to address voltage fading issues in Na_xMO_2 systems, such as $NaNi_{1/3}Mn_{1/3}Co_{1/3}O_2$.

- Utilization of Cost-effective materials like $NaFePO_4$: Na-based iron-phosphate cathodes offer significant cost advantages, necessitating optimized synthesis processes and enhanced conductivity.
- Stabilization of Cathode-Electrolyte interfaces: Addressing unique challenges such as electrolyte decomposition and interface instability in Na-ion batteries through electrolyte additives and interface engineering is essential.

3. Ensuring environmental friendliness and sustainability: Next-generation cathode material research must prioritize not only performance improvements but also environmental sustainability and resource efficiency.
    - Development of recyclable cathode materials: Designing materials that are easy to recycle or improving recycling efficiency for existing materials is essential.
    - Minimization of hazardous materials: Efforts should focus on reducing reliance on cobalt and other toxic elements, replacing them with environmentally non-toxic elements like iron and manganese.

4. Balancing battery performance and cost
    - Optimizing cost efficiency: Maximizing the economic viability of cathode materials by simplifying precursor synthesis and manufacturing processes is critical. For example, cost-effective compounds should be leveraged to produce high-performance cathode materials.

- Analyzing the correlation between electrochemical properties and manufacturing costs: Data-driven approaches should be adopted to identify the optimal balance between electrochemical performance and cost.

5. Compatibility with Next-Generation battery technologies
    - Suitability for Solid-State Batteries (SSB): Developing cathode materials that perform stably in solid electrolyte environments is indispensable.
    - Integration with various chemical systems: Exploring cathode materials compatible with next-generation systems such as lithium-sulfur and lithium-air batteries is essential.

6. Industrialization and mass production
    - To translate laboratory successes into practical applications, scalable synthesis techniques and automated production processes must be developed.

Now is a pivotal time to reflect on the technologies we have developed and to prepare for the next leap forward. This reflection not only allows us to consolidate our achievements but also positions us to address new challenges in cathode innovation.

This work serves as a stepping stone toward the development of next-generation cathode materials, contributing to the advancement of energy storage technologies. By building on the foundation laid by prior studies and incorporating innovative approaches such as AI-based technologies, we can continue to push the boundaries of what is possible in lithium-ion battery research and realize a more sustainable and efficient energy future for our next generation.